# Synthetic strategies for control of structure from individual macromolecules to nanoscale materials to networks

by

Deborah J.C. Ehrlich

B.S., Chemistry
University of Massachusetts Amherst, 2013

Submitted to the Department of Chemistry
in partial fulfillment of the requirements for the degree of

Doctor of Philosophy in Chemistry

at the

MASSACHUSETTS INSTITUTE OF TECHNOLOGY

June 2019



Signature redacted

Author ..... .....
Department of Chemistry
May 09, 2019

Signature redacted

Certified by..... .....
Jeremiah A. Johnson
Associate Professor of Chemistry
Thesis Supervisor

Signature redacted

Accepted by ..... .....
Robert W. Field
Haslam and Dewey Professor of Chemistry
Chair, Department Committee on Graduate Students

This doctoral thesis has been examined by a Committee of the Department of Chemistry as follows:

Signature redacted

Professor Timothy M. Swager.....

Chairman, Thesis Committee

John D. MacArthur Professor of Chemistry

Signature redacted

Professor Jeremiah A. Johnson.....

Thesis Supervisor

Associate Professor of Chemistry

Signature redacted

Professor Darrell Irvine.....

Member, Thesis Committee

Professor of Materials Science and Engineering & Biological Engineering

# Synthetic strategies for control of structure from individual macromolecules to nanoscale materials to networks

by

Deborah J.C. Ehrlich

Submitted to the Department of Chemistry
on May 09, 2019, in partial fulfillment of the
requirements for the degree of
Doctor of Philosophy in Organic Chemistry

## Abstract

Chapter 1. Aqueous self-assembly of prodrug macromonomers

A series of highly tunable micelles for drug delivery were made from norbornene based poly(ethylene glycol) macromonomers with covalently linked drugs. A total of five macromonomers were made using three different drugs (telmisartan, paclitaxel, and SN-38) and three different drug loadings. Combinations of these macromonomers were then allowed to self assemble into micellar aggregates. The size, stability, and shape of these micellar aggregates were controlled with the highly versatile structure.

Chapter 2. Post micellization modification of norbornene-containing prodrug macromonomers

Highly tunable micelles for drug delivery were functionalized after their self-assembly. Post-micellization inverse electron demand Diels-Alder reactions of norbornenes and tetrazines were used to signal changes in micelle size and stability through the addition of either hydrophilic or hydrophobic tetrazines. Thiol-ene additions reactions were used to increase micelle size and form chemically crosslinked nanoparticles. These modifications of norbornene-containing prodrug macromonomer assemblies illustrate their versatility.

Chapter 3. Synthesis of polymers by iterative exponential growth

A scalable synthetic route that enables absolute control over polymer sequence and structure has remained a key challenge in polymer chemistry. Here, we report an iterative exponential growth plus side-chain functionalization (IEG+) strategy for the production of macromolecules with defined sequence, length, and stereoconfiguration. Each IEG+ cycle begins with the azide opening of an enantiopure epoxide,

followed by side chain functionalization, alkyne deprotection, and copper-catalyzed azide-alkyne cycloaddition (CuAAC). These cycles have been conducted to form unimolecular macromolecules with molar masses of over 6,000 g/mol. Subsequent modifications to IEG+ allow for the functionalization of monomers prior to the IEG+ cycle, expanding the library of compatible side chain chemistries.

Chapter 4. Introduction to elastomer toughening strategies

Silicone elastomers are ubiquitous. Here, silicone elastomers are discussed in terms of network structure, the impact of network structure upon physical properties, and modifications of network structure in order to achieve desired physical properties. Fillers, the standard toughening strategy, are discussed in conjunction with entanglement density. Focus is placed on the impact of entanglement density on material properties. Topological networks are discussed and noted for their stress dissipative properties.

Chapter 5. Topology modification of polydimethylsiloxane elastomers through loop formation

Topological networks are well known for their stress dissipation through the pulley effect leading to soft, extensible materials. Combining these properties with a traditionally crosslinked network to produce a hybrid material allows for enhanced extensibility without a loss in modulus. Here, such hybrid networks were made with poly(dimethyl siloxane) polymers of a range of molecular weights. Side-loop polymer brushes were synthesized and then crosslinked to create hybrid networks with the statistical formation of topological bonds. These materials were characterized through tensile testing. Elastomers formed with the same molecular weight polymer in both side-loops and network formation did not show mechanical properties that depended upon the fraction of networks used for brush formation. Elastomers made with long polymers in brush formation and shorter polymers for network formation resulted in highly extensible systems without significant loss in modulus.

Thesis Supervisor: Jeremiah A. Johnson
Title: Associate Professor of Chemistry

# Acknowledgments

I am so thankful to have had the support of a multitude of wonderful people throughout my time at graduate school. I am extremely grateful to you all.

I'd like to begin by thanking my PhD adviser, Professor Jeremiah Johnson, for the opportunity to work in his lab with so many talented researchers. I deeply appreciate his advice and support over the years, and his constant efforts to keep the Johnson Group a wonderful place to work. I do not have the words to express my gratitude.

My thanks to my thesis committee chair, Professor Timothy Swager, for his advice over the years, and for his generosity towards the Johnson group. Working in the basement laboratory connected to the Swager lab has been a great opportunity to share with and learn from members of the Swager group.

To my thesis committee member, Professor Darrell Irvine, my thanks for his support and his guidance.

My deepest appreciation to past and present members of the Johnson group: graduate students, postdoctorates, undergrads, visiting students, and visiting researchers. I have loved talking with you about science, life, and pets and getting to know each and every one of you.

My special thanks to Shannon Wagner, Brian Pretti, and Tyler Brezler for all the work that keeps the group running. I would have been lost without you.

It was a joy to have Buddy and Ellory around the offices and at group events for their constant cheer and enthusiasm for play. Thank you to Dr. Michelle MacLeod and Prof. Junpeng Wang for bringing them into the offices.

My thanks to the basement offices for the research discussed, cookies shared, fish mourned, and time together in the last few years. Thank you to the upstairs office for your love of dogs and for putting up with me when I came to steal your food and enjoy the sunlight.

To Angela Gao, Molly Sowers, Alexandra Cok, and Dr. Longyan Liao: during my first few months in graduate school, I was amazed by the sense of community in the Johnson group. Although we did not overlap for very long, I'd like to thank

you for helping me get a start in the lab. More specifically, I'd like to thank Angela Gao for taking the time during her transition out of graduate school to show me the basics of the IEG project, Molly Sowers for her heartfelt advice and good cheer, and Alexandra Cok and Dr. Longyan Liao for answering all of my silly questions day in and day out.

My thanks to Dr. Jenny Liu and Dr. Michelle MacLeod for being the best role models I could ask for. To Dr. Alex Zhukhovitskiy and Dr. Ken Kawamoto (and Dr. Jenny Liu and Dr. Michelle MacLeod) for making the time to help me with all my questions throughout the years.

I am sure that the following people have noticed by now that I generally show my appreciation through baked goods, care packages, and candy left on desks in the middle of the night without a note. It seems impossible to thank you all for the impact you have made upon my life, so I've chosen to mention specific things that make me smile.

To Yuwei Gu, for his appreciation of tacos and willingness to discuss science no matter how busy he was; Hung Nguyen for his constant supply of sour patch kids, backup stockpiles of useful reagents, and willingness to share synthesized compounds; and Yivan Jiang for never giving up while learning to whistle and keeping the lab supplied with bulk reagents. To Julia Zhao for listening to my complaints and my nonsense, for working to improve the department through ChemREFS, the organic retreat, and innumerable other events, and for keeping the Johnson group safe. To Peter Qin (and Martin Henriksen) for the adventures to the electronics waste. To Wencong Wang for her kindness and for organizing bubble tea delivery. To Matthew Pearson for joining Julia and me in keeping the lab safe, and for the beautiful commemorative mug. To Sachin Bhagchandani, for his enthusiasm in joining group events even before officially becoming a group member. To Keith Husted for keeping us out of the deep snow filled ditches in Michigan. To Gihan Hewage for somehow managing to be a dear friend to each group member even after leaving graduate school. To David Lundberg, Michael Stolberg, and Alexandra Sourakov, and the rest of the Johnson Group – my best wishes for the time ahead!

To Prof. Matthew Golder for his sensibility, Dr. Manuel Hartweg for his good cheer, Dr. Samantha Kristufek for her fresh perspective, Dr. Jessica Lamb for being exactly what the Johnson group needed with her powers of organization, Dr. Nate Oldenhuis for the coffee, Dr. Bo Qiao for planning so many wonderful group events, Dr. Peyton Shieh for his enthusiasm, Dr. Farrukh Vohidov for his kindness, Dr. Wenxu Zhang for somehow turning the group into a pack of runners. To Prof. Mingjiang Zhong for always making the time to help out group members, Dr. Qixian Chen for the aquatic community he maintained, and Prof. Junpeng Wang for bringing in Ellory so often. To Prof. Yufeng Wang, Prof. Mao Chen, Dr. Yoshiki Shibuya, Dr. Eileen Burke, Dr. Nolan Gallagher, Prof. Mingjun Huang, Prof. Jonathan Barnes, Dr. Teruhiko Saito, Dr. Masamichi Shirakura, Johanna Ertl, Alan Enciso, Yongsheng Gao, Prof. Ellane Park, Julian Grundler, Gabriela Alvaradejo, Shuto Mochizuki, Prof. Masahiro Yoshizawa-Fujita, Prof. Xiaojuan Liau, and Zhihao Huang, thank you for the camaraderie over the years.

To Naomi Bright for her assistance over these last few years of graduate school and Erica Zhao for her help during the first few years.

Prof. E. Bryan Coughlin gave me the opportunity to join his group as an undergraduate: I'd like to thank him for the opportunity to learn what it meant to work in a lab. Thank you to Prof. Elizabeth Sterner for her outstanding mentorship while I was an undergraduate, the level to which I now aspire. To Dr. Brian Cromer, Dr. Wenxu Zhang, Dr. Kinkini Roy, Dr. Piril Ertem, Dr. Xiaohui Liu, Dr. Connor Evans, Dr. Huseyin Tas, Dr. Tsung Han Tsai, Dr. Katherine Williams, Dr. Patrick Homyak, and Dr. Haomiao Yuan: thank you for making me a part of the UMass PSE community.

Prof. Ramanathan Nagarajan gave me the opportunity to work with him at the Natick Soldier Research Development & Engineering Center. My thanks to him for giving me my first taste of research. To Prof. Sree Srinivasan for showing me that you can attend seminars regardless of departmental affiliation, and Melissa Roth for her company. To Patricia Bremner for helping me find the confidence to apply in the first place.

To my friends in graduate school: I am so thankful to have shared this experience with you, and have been amazed to see my own experience reflected in my friends across the country and in different disciplines. To my friends outside of graduate school: Thank you for keeping me connected to the outside world.

To my family for always being there for me.

To my husband, Alex Haugland, for his unwavering support.

# Contents

# Preface

This thesis has been adapted from the following articles:

Barnes, J. C.; **Ehrlich, D.J.C.**; Gao, A. X.; Leibfarth, F. A.; Jiang, Y.; Zhou, E.; Jamison, T. F.; Johnson, J. A., Iterative Exponential Growth of Stereo- and Sequence-Controlled Polymers, Nat. Chem., 2015, 7, 810– 815.

Jiang, Y.; Golder, M.R.; Nguyen, H.V.-T.; Wang, Y.; Zhong, M.; Barnes, J.C.; **Ehrlich, D.J.C.**; Johnson, J.A., Iterative Exponential Growth Synthesis and Assembly of Uniform Diblock Copolymers. JACS, 2016, 138(30), 9369-372.

Golder, M. R.; Liu, J.; Andersen, J. N.; Shipstein, M.; Vohidov, F.; Nguyen, H., V.-T.; **Ehrlich, D.J.C.**; Jin Huh, S.; Vangamudi, B.; Economides, K.; Neenan, A.; Ackley, J.; Baddour, J.; Pramisivan, S.; Brady, S.W.; Held, E.J.; Reiter, L.A.; Saucier-Sawyer, J.; Kopesky, P.; Chickering, D.; Blume-Jensen, P.; Johnson, J. A., Reduction of liver fibrosis by rationally designed macromolecular telmisartan prodrugs. Nat. Biomed. Eng. 2018, 2, 822-830

In preparation:

**Ehrlich, D. J. C.**; Bright, N. S.; Johnson, J. A., Aqueous Self-Assembly of Norbornene-PEG-branch-drug Macromonomers. 2019

# Respective Contributions

This thesis describes work that resulted from collaborative efforts of the author with other colleagues at MIT. The specific contributions of the author and collaborators are delineated below.

Chapter 1. The results presented in Chapter 1 were the result of a collaborative effort between Hung V.T. Nguyen, Naomi S. Bright, and Deborah J.C. Ehrlich. Hung V.T. Nguyen synthesized some of the doubly loaded telmisartan macromonomer and macromonomer with multi-alkyne functionality used for macromonomer synthesis. Naomi S. Bright prepared some of the solutions used to determine the critical micelle concentration.

Chapter 2. The work presented in Chapter 2 was performed by Deborah J.C. Ehrlich.

Chapter 3. The work presented in Chapter 2 was the result of a collaborative effort between Prof. Jonathan C. Barnes and Deborah J.C. Ehrlich. Prof. Jonathan C. Barnes and Deborah J.C. Ehrlich performed the research for the original IEG+ cycle together, and Prof. Jonathan C. Barnes designed several of the figures shown here.

Chapter 4. The research presented in Chapter 4 was performed by Deborah J.C. Ehrlich.

Chapter 5. The research presented in Chapter 5 was a collaborative effort between Prof. Junpeng Wang, Keith Husted, Naomi S. Bright, and Deborah J.C. Ehrlich. Naomi S. Bright prepared some of the brush polymers and ran gel swelling experiments.

# Abbreviations and Acroynms

| | |
|---|---|
| $^{13}$C-NMR | Carbon- 13 nuclear magnetic resonance |
| $^{1}$H-NMR | Proton nuclear magnetic resonance |
| $a$ | Surface area per monomer |
| Acetal-XL | Acetal crosslinker |
| Az | Azide |
| BASP | Brush-arm star polymer |
| BPTZ | 3,6-Di-2-pyridyl-1,2,4,5-tetrazine |
| CuAAC | Copper (I) - catalyzed alkyne-azide cycloaddition |
| CuOAc | Copper (I) acetate |
| DCIF | MIT Department of Chemistry Instrument Facility |
| DCM | Dichloromethane |
| DIPEA | N,N-Diisopropylethylamine |
| DLS | Dynamic light scattering |
| DMAP | 4-dimethylaminopyridine |
| DMF | N,N-dimethylformamide |
| DMSO | Dimethyl sulfoxide |
| dn/dc | Refractive index increment |
| DP | Degree of polymerization |
| DSC | Dynamic Scanning Calorimetry |
| DTT | Dithiothreitol |
| EDC-HCl | N-(3-Dimethylaminopropyl)-N'-ethylcarbodiimide hydrochloride |

| | |
|---|---|
| EDTA | Ethylenediaminetetraacetic acid |
| Et2O | Diethyl ether |
| EtOAc | Ethyl acetate |
| G3 | Grubbs 3rd generation catalyst with pyridine ligands |
| GPC-MALLS | Gel permeation chromatography with multi-angle light scattering detection |
| HPLC | High-performance liquid chromatography |
| IEG | Iterative exponential growth |
| IEG+ | Iterative exponential growth plus side chains |
| LCMS | Liquid chromatography mass spectrometry |
| LS | Light scattering |
| m | Ratio of MM to G3 in brush synthesis (ie. DP of brush polymer) |
| MALDI-TOF | Matrix-assisted laser desorption ionization time-of-flight |
| MeCN | Acetonitrile |
| MeOH | Methanol |
| min | Minutes |
| MM | Macromonomers |
| MMw | Micellar molecular weight |
| Mn | Number average molar mass (number average molecular weight) |
| MW | Mass average molar mass (weight average molecular weight) |
| N | Crosslinker equivalents in star polymer synthesis |
| $N_{agg}$ | Aggregation number |
| NHS | N-hydroxysuccinimide |
| PDI | polydispersity index |
| PDMS | Polydimethylsiloxane |
| PEG | Polyethylene glycol |

| | |
|---|---|
| PEO | Polyethylene glycol |
| PTX | Paclitaxel |
| PTX-1 | PTX functionalized MM |
| RI | Refractive Index |
| ROMP | Ring opening metathesis polymerization |
| rt | Room temperature |
| RuAAC | Ruthenium catalyzed alkyne-azide cycloaddition |
| SN-38 | 7-Ethyl-10-hydroxy-camptothecin |
| SN38-1 | SN-38 functionalized MM |
| TBAF | Tetra-n-butylammonium fluoride |
| TEG | Triethylene glycol |
| TEL | Telmisartan |
| TEL-1 | TEL functionalized MM |
| TEL-2 | Functionalized MM with two TEL units |
| TEL-3 | Functionalized MM with three TEL units |
| TEM | Transmission electron microscopy |
| TET-PEG | PEG 3k functionalized BPTZ |
| TFA | Trifluoroacetic acid |
| TGA | Thermal gravimetric analysis |
| THF | Tetrahydrofuran |
| UV-Vis | Ultraviolet-visible spectroscopy |
| XL | Crosslinker |

# Chapter 1

# Aqueous self-assembly of prodrug macromonomers

## 1.1 Introduction

Micelles are drug delivery carriers with a number of attractive features. Several micelle-based drug formulations either approved or currently under investigation by the FDA.[1,2] Although the synthesis and theoretical understanding of micelles have been well understood for decades,[3] their development as clinically translatable drug delivery systems is still an active area of investigation. Micelles are an excellent option for drug delivery due to their ability to solubilize drugs and shield them from degradation, and their potential to passively accumulate in tumor tissue. Polymeric micelles, which are micelles derived from polymeric components rather than small molecule surfactants, benefit in particular from enhanced circulation time leading to a greater therapeutic response.[4]

The theories describing self-assembly explain that the driving force for micelle formation results from the decrease in free energy upon minimizing interactions between hydrophobic domains and water through aggregation.[3] The relative quantities and identities of the hydrophobic and hydrophilic sections of the constituent amphiphile determine the enthalpic and entropic energies associated with micelle formation, thus determining particle stability, shape, and size.[5] As advances in polymer synthesis facilitated the design and synthesis of highly controlled and structurally diverse macromolecules,[6,7] it became possible to study the impact of amphiphile structural changes upon micelle properties.[8,9] The Amir group has shown that increasing the length of the hydrophilic chain, in this case polyethylene glycol (PEG), decreases the stability of micelles correlating to a faster enzymatic degradation rate, while increasing the number of hydrophobic end groups has the opposite effect.[10–12] The Columbus group has used binary mixtures of common detergents to systematically tune the shape and size of micelles.[13] As size and shape play a critical role in the circulation and uptake of particles, the ability to control these features can significantly impact micellar efficacy as drug delivery agents.[14–19]

A rough estimate of aggregate shape can come from amphiphile geometry. In order to minimize interfacial surface area without creating void spaces amphiphiles

will form the aggregate with the largest surface curvature possible with the given ratio of hydrophobic to hydrophilic segments.[20] The higher the ratio of hydrophobic to hydrophilic segments, the lower the surface curvature observed in the final aggregate. When comparing a series of amphiphiles based on the ratio of hydrophobic to hydrophilic segments, it is possible to estimate relative aggregate surface curvatures, and thus relative sizes.

Norbornene-terminated PEG branched macromonomers with covalently linked drugs have been previously utilized by the Johnson group to form bottlebrush polymers and brush-arm star polymers (BASPs) for drug delivery, self-assembly, and imaging applications.[21–25] These macromonomers are highly versatile and can be readily modified to alter the drug identity and loading. The ring-opening metathesis polymerization (ROMP) used to polymerize and crosslink macromonomers to form BASPs is a highly robust and functional group tolerant polymerization that allowed the synthesis of sterically hindered bottlebrush and star poly(norbornene)s.[24,26,27] However, ROMP relies upon initiation by metal complexes that can be difficult to fully remove from the final product.[28] In addition, the covalent cross-links used to form particles slow drug release by reducing enzymatic access to the particle core.[29,30] Herein, we present a strategy to use these highly adaptable macromonomers for the formation of micelles. With variation of the macromonomer drug loading, it is possible to tune the properties of these micelles.

A series of norbornene-based PEG branched macromonomers were synthesized as previously reported.[23,31,32] To test the impact of drug loading on micelle properties while minimizing structural changes, three different norbornene based poly(ethylene glycol) macromonomers were synthesized, with one, two, or three alkyne functionalities. A series of azide-functionalized drugs were synthesized containing telmisartan, paclitaxel, or SN-38. The aforementioned azides and alkynes were coupled using copper-catalyzed azide-alkyne cycloaddition (CuAAC) to produce five different macromonomers; a singly loaded SN-38 macromonomer (SN38-1), a singly loaded paclitaxel macromonomer (PTX-1), and each of the singly, doubly, and triply loaded telmisartan macromonomers (TEL-1, TEL-2, TEL-3), showing the applicability of

this system to multiple drugs.[31,33] Each conjugated azide included a hydrolyzable ester for drug release, and a short linker to facilitate both conjugation and release.[34] Combinations of these macromonomers were used to tune micelle size, shape, and stability.

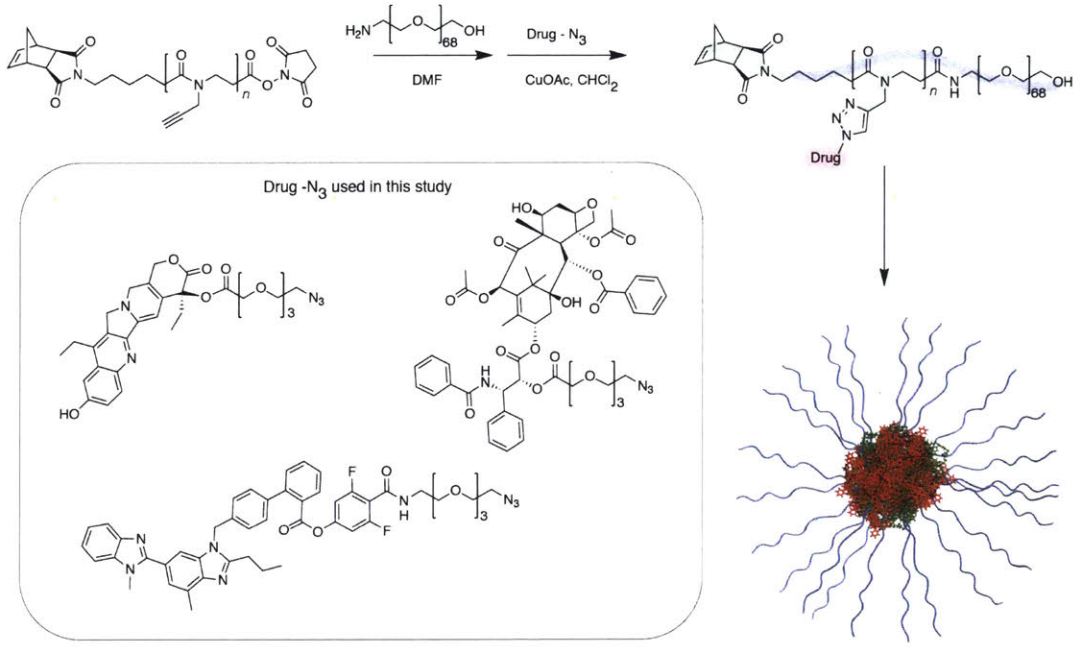


**Figure 1-1:** Chemical structures of the synthesis of norbornene-based PEG branched macromonomers and the formation of micelles from these macromonomers are shown here. Three norbornene alkyne macromonomers, with $n = 1$, 2, or 3, were each functionalized with 0.95 eq 3k PEG amine in dimethyl formamide (DMF), then purified via precipitation three times in diethyl ether. CuAAC with 4 equivalents of copper(I)acetate in dichloromethane under a nitrogen atmosphere at ambient temperature was used to attach drug azides of telmisartan, paclitaxel, and SN-38 to the alkyne macromonomers shown. Purification was carried out on a chloroform preparatory GPC. In this manner, five norbornene functionalized macromonomers were produced, a singly loaded telmisartan ($n = 1$), doubly loaded telmisartan ($n = 2$), triply loaded telmisartan ($n = 3$), singly loaded paclitaxel ($n = 1$), and singly loaded SN-38 ($n = 1$). Each macromonomer has the potential to self-assemble in aqueous environments due to the hydrophobic nature of the drugs chosen as well as the norbornene substituent.

## 1.2 Results and Discussion

We expected that as the drug loading per monomer increased, the particle size would increase due to the changed geometric requirements of the macromolecule leading to reduced surface curvature. The additional hydrophobic content would result in an increased driving force for aggregation. Consequently, both a decrease in the surface area per monomer in the aggregate ($a$) and a decrease in the CMC were anticipated.

The singly loaded telmisartan macromonomer (TEL-1) formed particles with $8 \pm 1$ nm diameter as measured by dynamic light scattering (DLS, Table 1) whereas the doubly loaded telmisartan macromonomer (TEL-2) and triply loaded telmisartan macromonomer (TEL-3) formed particles of $15 \pm 1$ nm and $18 \pm 1$ nm diameters, respectively, correlating with drug loading as anticipated. Transmission electron microscopy (TEM) images of the micelles showed slightly larger particle sizes than those seen by the DLS, likely due to both minor aggregation during sample preparation and difficulty visualizing the smaller particles. A decrease in $a$ was seen with increased drug loading, suggesting that the reduction of surface tension outweighed entropic concerns.

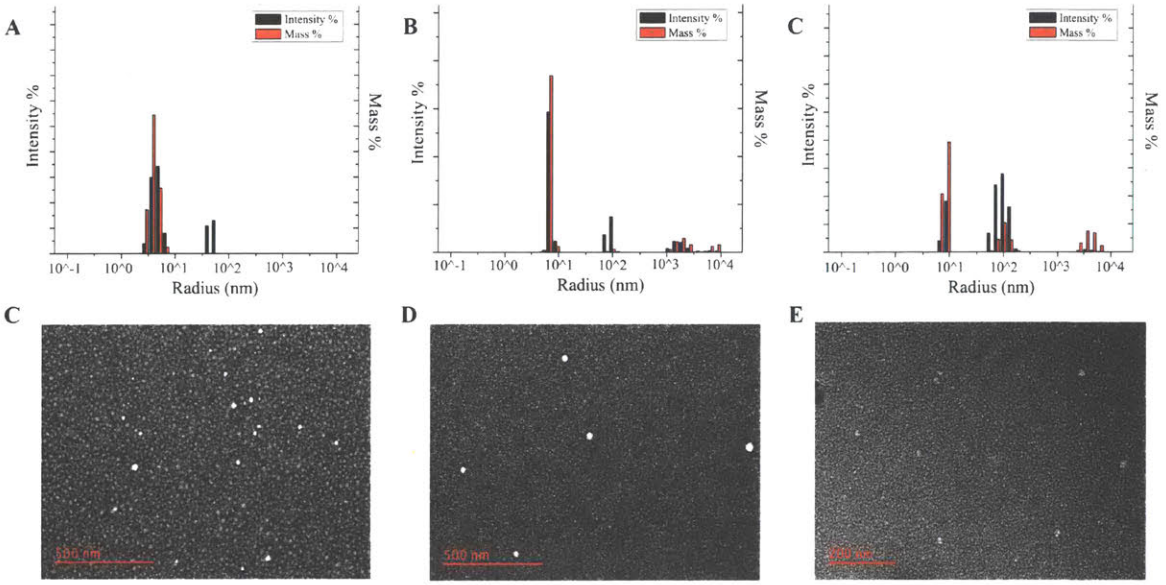


**Figure 1-2:** A) DLS histogram of micelles formed from TEL-1, B) DLS histogram of micelles formed from TEL-2, C) DLS histogram of micelles formed from TEL-3, C) TEM image of micelles formed from TEL-1, 1 mg/ml, stained with uranyl acetate. The particles have an average diameter of $18 \pm 5$ nm (ImageJ analysis). D) TEM image of micelles formed from TEL-2, 1 mg/ml, stained with uranyl acetate. The particles have an average diameter of $19 \pm 5$ nm (ImageJ analysis). E) TEM image of micelles formed from TEL-3, 1 mg/ml, stained with uranyl acetate. The particles have an average diameter of $18 \pm 4$ nm (ImageJ analysis).

Particle stability was evaluated through determination of the CMC of the particles. Thermodynamically stable particles have low CMC values, indicating a large driving force for particle formation,[20] which suggests the particles will remain intact for longer in the body. Particles with high CMC values may not remain stable during circulation in the bloodstream.[35] As seen in Table 1, the CMC of these micelles decreased from 52 $\mu$M to 8$\mu$M as the macromonomer drug loading increased. A decrease in CMC also indicates that the increased drug loading shifted the equilibrium between aggregate and monomer towards the aggregate, which results in a slower drug release.[30] The relative sizes of micelles and the CMCs for corresponded to expectations based on chemical structure.

| Sample | Drug Loading (wt%) | Particle Diameter (nm) | MMw (kDa) | $N_{agg}$ | a($\frac{nm^2}{unit}$) | CMC ($\mu$M) |
|---|---|---|---|---|---|---|
| TEL-1 | 12 | $8 \pm 1$ | 67 | 16 | 3 | 52 |
| TEL-2 | 20 | $15 \pm 1$ | 602 | 113 | 0.8 | 9.5 |
| TEL-3 | 25 | $18 \pm 1$ | 1075 | 172 | 0.7 | 7.7 |
| SN38-1 | 10 | $9 \pm 3$ | 128 | 32 | 1.7 | 15 |
| PTX-1 | 20 | $6 \pm 1$ | 26 | 6 | 6 | 100 |

**Table 1.1:** Particle diameters and the micelle molecular weight (MMw) of the aggregates formed from macromonomers shown in Figure 1 were determined from DLS. The aggregation number ($N_{agg}$) and surface area per monomer in $nm^2$ per macromonomer ($a$) followed mathematically. The CMC was determined with a nile red assay.

From the results with micelles formed from TEL-1, TEL-2, and TEL-3, it seemed reasonable that mixed micelle systems would have intermediate properties. We created three sets of mixed micelles, one from combinations of TEL-1 and TEL-2, one from combinations of TEL-2 and TEL-3, and one from combinations of TEL-1 and TEL-3. Here, premixing the macromonomers in a good solvent prior to micelle formation was essential to the formation of a narrowly dispersed system. As seen in Figure 2, particle diameter increased linearly as a function of overall drug loading, regardless of the macromonomer combination used. $N_{agg}$ and $a$ followed the same trends as the unmixed systems, showing that these systems can be easily tuned for the desired physical properties.

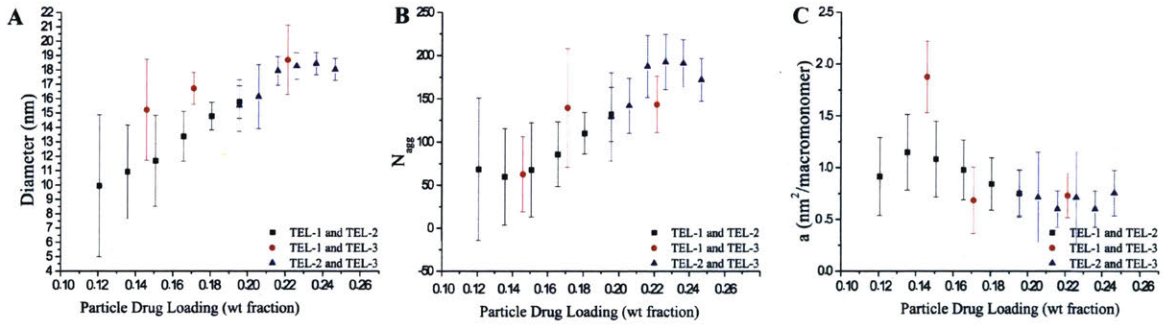


**Figure 1-3:** DLS data was used to determine the micelle diameter, aggregation number ($N_{agg}$), and surface area per monomer ($a$) for all aggregates. A) Micelle diameter, as determined from DLS, increases with the drug loading, regardless of the combination of TEL-1, TEL-2, and TEL-3 used. B) Aggregation number, as determined from DLS, increased with drug loading, regardless of the combination of TEL-1, TEL-2, and TEL-3 used. C) Surface area per macromonomer, as determined from DLS, did not strongly correlate with drug loading.

Although all systems discussed thus far self-assembled into spherical micelles, it seemed possible that the geometric differences between TEL-1 and TEL-3 could lead to aggregates with non-spherical geometries.[13,36] Indeed, by doping the TEL-3 with TEL-1 thus introducing a species with a higher surface curvature, worm-like micelles could form. As seen in Figure 3, it is probable that the end caps of these worms are rich in TEL-1 due to the high surface curvature it prefers, while the main body of the worm is rich in TEL-3. After the initial observation of these worm-like micelles, we created a series of samples to determine whether the average aggregate length correlated to TEL-1 content. By decreasing the percentage of TEL-1 used from 10% to 1%, the worms grew in average length from $31 \pm 10$ nm to $55 \pm 12$ nm. However, at 10%, the same spherical micelles observed at higher percentages were seen in addition to worms, suggesting a limit over which spheres are the preferred geometry. CryoTEM confirmed the results seen in Figure 1-4.

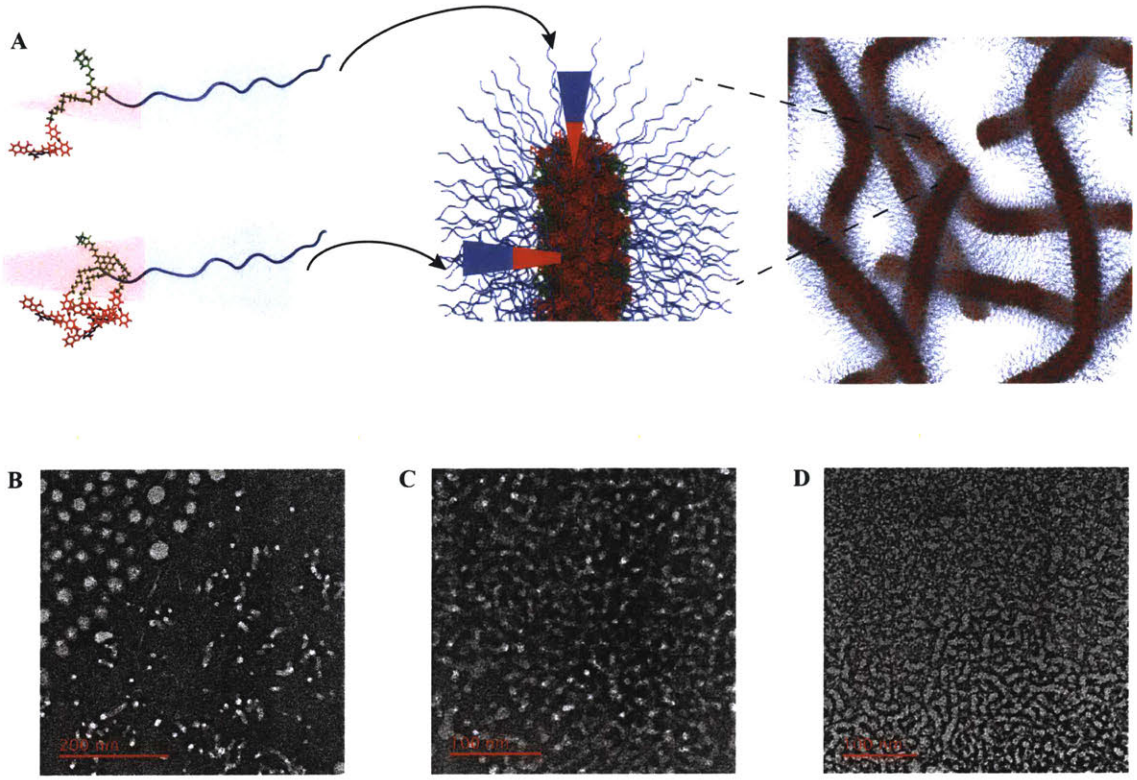


**Figure 1-4:** A) In this graphical representation, TEL-1 and TEL-3 were combined to create worm-like micelles. As the surface curvature of particles formed by TEL-1 is higher than that of TEL-3, the TEL-1 would be preferentially found on the end caps of the worms, in regions of increased surface curvature. By increasing the percentage of TEL-1, it is possible to introduce more regions of increased curvature and to decrease the average worm length. B) TEM image of a mixture of 10% TEL-1 and 90% TEL-3, 1 mg/ml, stained with uranyl acetate. Both worms and spherical micelles were seen throughout this sample. Worms were $31 \pm 10$ nm in length. C) TEM image of a mixture of 5% TEL-1 and 95% TEL-3, 1 mg/ml, stained with uranyl acetate. Worms were $47 \pm 14$ nm in length. D) TEM image of a mixture of 1% TEL-1 and 99% TEL-3, 1 mg/ml, stained with uranyl acetate. Worms were $55 \pm 12$ nm in length.

## 1.3 Conclusions

Norbornene-PEG-*branch*-drug macromonomers form micellar aggregates that can be tuned in terms of size, shape, and stability through drug loading. Micelle size correlated with drug loading for both unmixed and mixed systems. The CMC of these micelles, an indicator of particle stability, decreased as the macromolecular drug loading increased. Geometric differences between the macromonomers led to non-spherical aggregates, with the particle size controlled by the percentage of TEL-1 present in the system. Moving forward, the reactivity of the norbornene component of these aggregates can be used to trigger specific functions (see Chapter 2).

## 1.4 Experimental Methods

### 1.4.1 Materials and General Methods

All reagents were purchased from commercial sources and used without further purification unless stated otherwise.

#### Instrumentation

Liquid chromatography-mass spectrometry (LC-MS) was performed on an Agilent 1260 instrument with an Agilent 6130 single quadrupole mass spectrometer and an Advanced Materials Technology Halo C18 (HALO) column using a binary solvent system of acetonitrile and 0.1% acetic acid in water.

Gel permeation chromatography was performed on an Agilent 1260 instrument with two Agilent PLGel mixed C columns in series, a 0.025 M lithium bromide in dimethylformamide mobile phase run at 60 celsius, a Wyatt Optilab T-rEX detector, and a Wyatt Heleos II detector.

Column chromatography was carried out on silica gel 60F (EMD Millipore, 0.040-0.063 mm).

$^{1}$H nuclear magnetic resonance ($^{1}$H-NMR) and $^{13}$C nuclear magnetic resonance ($^{13}$C-NMR) spectra were recorded on Bruker AVANCE-400 NMR spectrometers in the Department of Chemistry Instrumentation Facility at MIT. Chemical shifts are reported in ppm relative to the signals corresponding to residual non-deuterated solvents: $CDCl_3$: $\delta$H = 7.26 ppm, DMSO-d6: $\delta$H = 2.50 ppm. Spectra were analyzed on MestReNova NMR software.

Matrix-assisted laser desorption/ionization-time of flight (MALDI-TOF) mass spectra were measured on a Bruker model MicroFlex instrument using $\alpha$-cyano-4-hydroxycinnamic acid as the matrix.

Transmission electron microscopy (TEM) was performed on a FEI Tecnai Multi-purpose TEM at 120 kV with carbon coated copper TEM grids, CF200-CU-UL from

Electron Microscopy Sciences.

Dynamic Light Scattering (DLS) was conducted with a Wyatt Möbius with a 660 nm laser. The average hydrodynamic diameter and aggregate molecular weight of a set of 20 readings was calculated with a regularization algorithm from Dynamics 7.3.1.15.

Fluorimetry was performed on SPEX Fluorolog- $\tau 2$ fluorometer (model f13-21, 450 W. Xenon lamp).

UV-Vis absorption experiments were performed on a Cary 50 Scan UV-Vis Spectrophotometer.

Preparative gel permeation chromatography (prep-GPC) was performed on a JAI Preparative Recycling HPLC (LaboACE-LC-5060) system equipped with 2.5HR and 2HR columns in series (20 mm ID x 600 mm length) with ethanol stabilized chloroform as the eluent running at 10 mL/minute.

### Light Scattering Standard Operating Procedure

Dynamic Light Scattering (DLS) was taken with a Wyatt Möbius with a 660 nm laser. All samples were diluted to 1 mg/mL in nanopure water and filtered with a 0.45 $\mu$m nylon syringe filter. The average hydrodynamic diameter and aggregate molecular weight of a set of 20 readings was calculated with a regularization algorithm from Dynamics 7.3.1.15. The aggregation number and particle surface area were calculated mathematically from these results. $N_{agg}$ was determined by dividing the MMw by the polymer molecular weight. $a$ was determined by using the particle diameter to calculate surface area, assuming a sphere, and dividing the results by $N_{agg}$ to obtain the results per monomer.

### Transmission electron microscopy

Transmission electron microscopy (TEM) was performed on a FEI Tecnai Multipurpose TEM at 120 kV with carbon coated copper TEM grids, CF200-CU-UL from

Electron Microscopy Sciences. The standard sample preparations were as follows: 7 $\mu$L of a 1 mg/mL solution of particles in nanopure water was dropped onto a carbon film coated copper grid. After 15 minutes, excess aqueous solution was wicked away with the twisted corner of a Kimwipe. For negative staining, 7 $\mu$L of a 2 wt% uranyl acetate stain (Electron microscopy sciences) was dropped onto the grid. After 2 minutes, excess stain was wicked away with a Kimwipe.

### 1.4.2 Synthetic Protocols

The synthesis of norbornene based poly(ethylene glycol) macromonomers with one,[24] two,[32] or three[32] alkyne functionalities, difluorophenyl telmisartan azide,[31] SN-38 azide,[33] and paclitaxel azide[37] were conducted following previously reported procedures. CuAAC coupling chemistry to produce TEL-1, TEL-2, TEL-3, SN38-1, and PTX-1 were conducted following previously reported procedures.[24]

### 1.4.3 Micelles

#### Micelle Formation

Each macromonomer was dissolved in dimethylformamide to create a 50.0 mg/mL stock solution. These solutions were combined in molar ratios as described below and diluted with dimethylformamide to make 10 mg/mL solutions. The mixtures were briefly sonicated and then dialyzed in 1 kDa dialysis tubing (Spectrum Labs) against nanopure water to remove dimethyl formamide for 4 hours. Water was exchanged after 1 hour and 2 hours. The removed water phases were concentrated and analyzed by LC-MS to confirm negligible drug release prior to further analysis.

Note that for the singly loaded drug conjugate macromonomers no difference in micelle assembly was observed between this method or direct dissolution of the macromonomer in water followed by sonication.

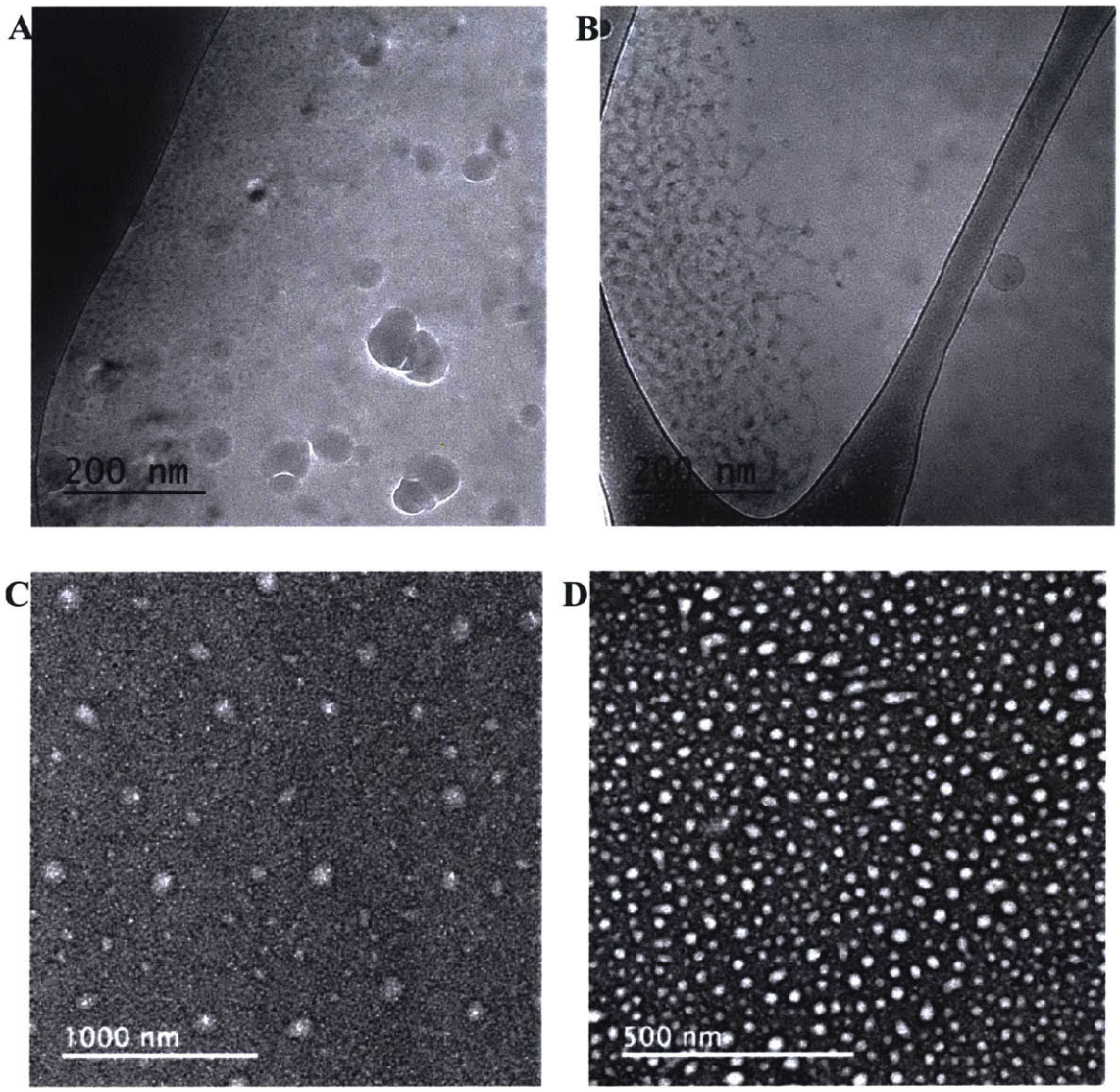


**Figure 1-5:** A) CryoTEM of 10% Tel-1 and 90% TEL-3, B) CryoTEM of 1% TEL-1 and 90% TEL-3, C) TEM of 25% TEL-1 and 75% TEL-2, 1 mg/ml stained with uranyl acetate. Although wormlike micelles were not seen for the TEL-1 and TEL-2 combination systems examined, some combinations did show nonspherical structures, D) TEM of 75% TEL-1 and 25% TEL-2, 1 mg/ml stained with uranyl acetate

### Critical Micelle Concentration (CMC)

The CMC of the macromonomers in aqueous media were determined with a nile red assay, as described by Stuart et al.[38] Samples were made for CMC determination by dissolving the macromonomer in nanopure water with an initial concentration of 10.0 mg/mL. The macromonomer solution was then diluted serially to produce 900 $\mu$L of each desired concentration, with brief sonication between each dilution. To

each solution was added 100 $\mu$L of a 200 $\mu$M aqueous nile red solution. The final samples were sonicated for 1 minute, and allowed to equilibrate overnight in order to ensure full incorporation of the nile red. Fluorescence spectra were collected over a range 600-675 nm with a 1 nm step and 550 nm excitation on a SPEX Fluorolog-$\tau$2 fluorometer (model f13-21, 450 W. Xenon lamp). The intensity was averaged over three scans, and values at 636 nm recorded for each sample. A shift in emission maximum was noted at the critical micelle concentration for all samples.

All fluorescent intensities at 636 nm were plotted against concentration. Then, two best fit lines were generated. The point at which the best fit lines overlapped was taken as the critical micelle concentration. Multiple CMC assays were run with TEL-1 to ensure reproducibility and to confirm that the concentrations of Nile Red used did not interfere with micellization.

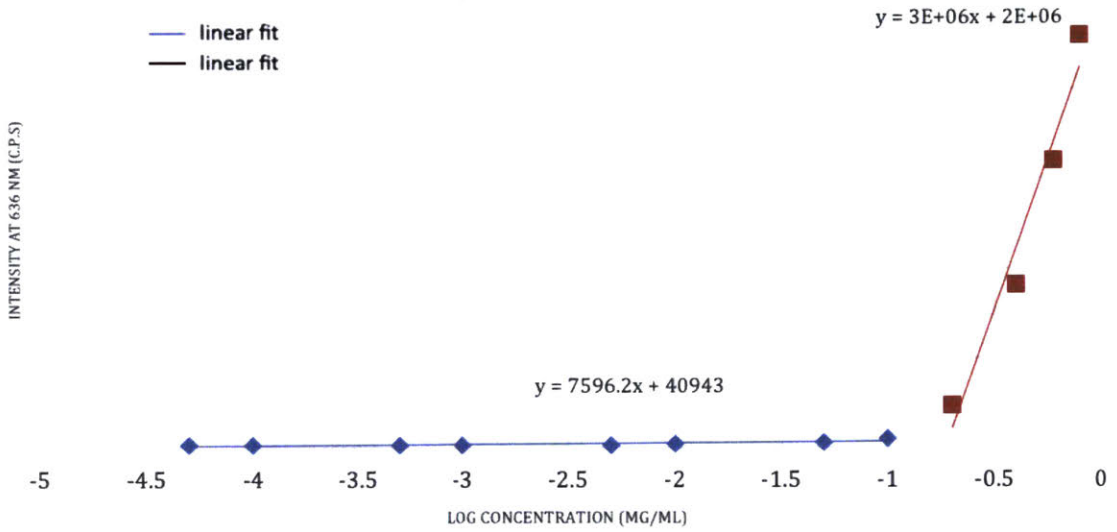


**Figure 1-6:** CMC Determination for TEL-1. The CMC was found to be 0.22 mg/mL, or 0.052 mM.

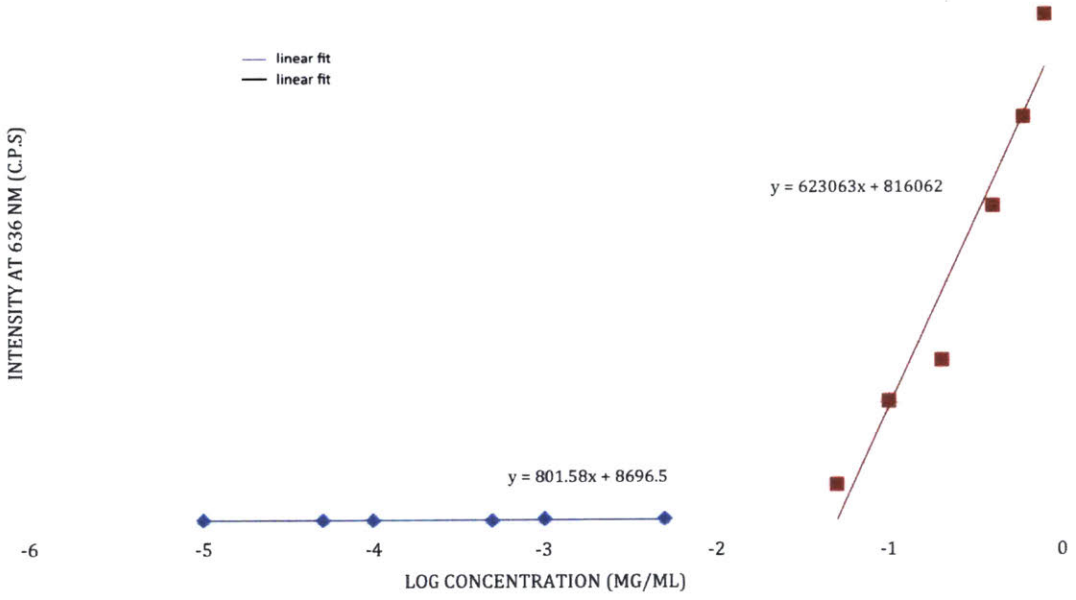


**Figure 1-7:** CMC Determination for the TEL-2. The CMC was found to be 0.050 mg/mL, or 0.010 mM.

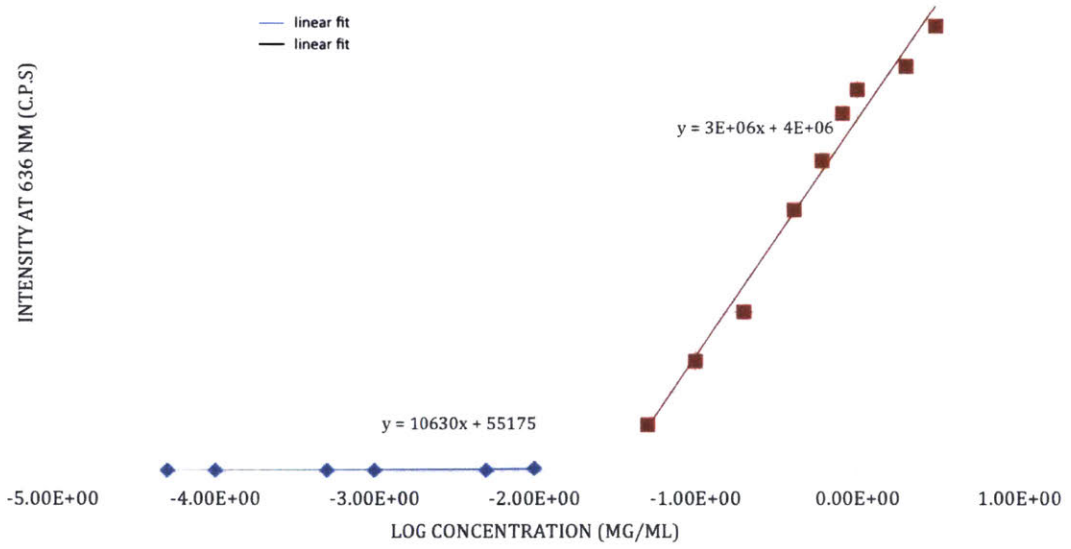


**Figure 1-8:** CMC Determination for TEL-3. The CMC was found to be 0.048mg/mL, or 0.0077mM.

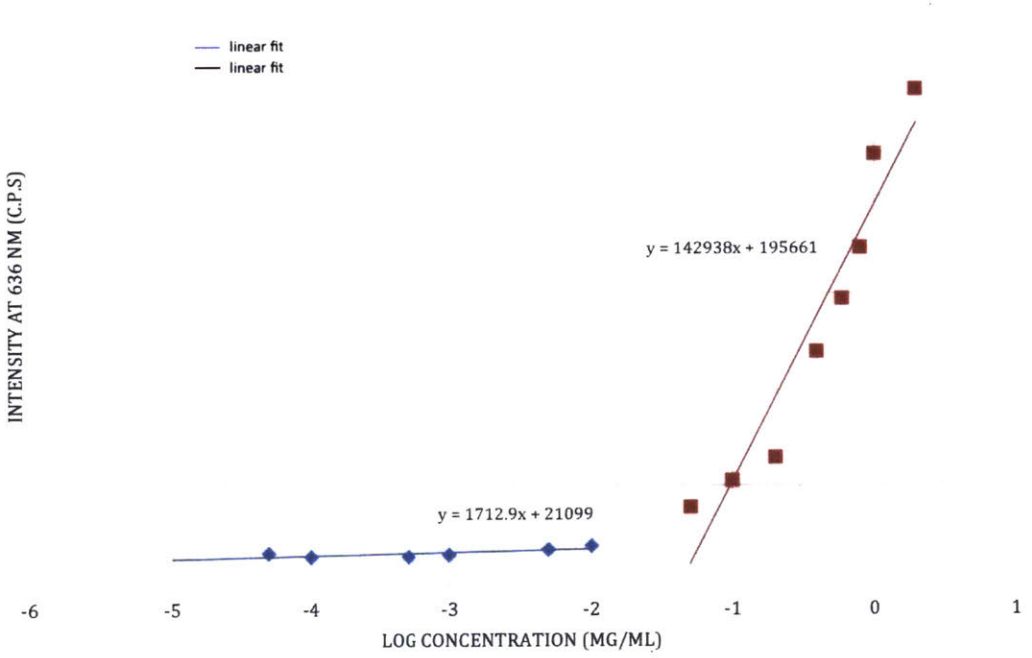


**Figure 1-9:** CMC Determination for the G2 SN-38 macromonomer. The CMC was found to be 0.06mg/mL, or 0.015mM.

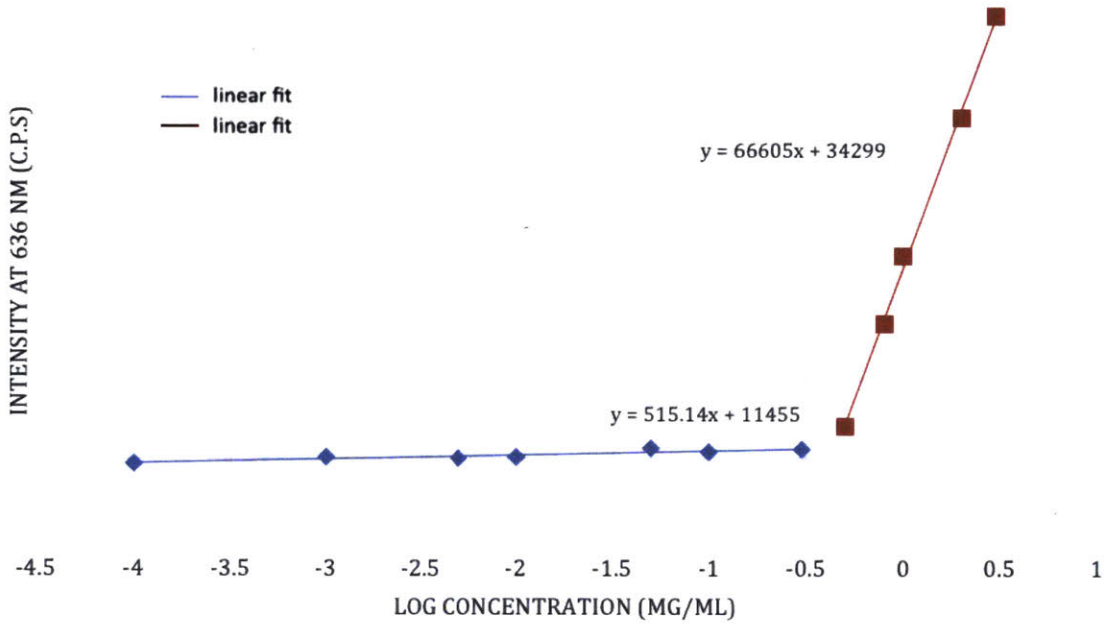


**Figure 1-10:** CMC Determination for PTX-1. The CMC was found to be 0.45 mg/mL, or 100 mM.

## 1.5 References


(1) Al-Achi, A.; Lawrence, J. Antoine Al-Achi and Jonathan Lawrence. Micelles: Chemotherapeutic Drug Delivery. Clin Pharmacol Biopharm;2(2):e114, 2013. *Clinical Pharmacology and Biopharmaceutics* **2013**, *2*, e114.

(2) Ventola, C. L. Progress in Nanomedicine: Approved and Investigational Nanodrugs. *P T* **2017**, *42*, 742–755.

(3) Israelachvili, J. N.; Mitchell, D. J.; Ninham, B. W. Theory of Self-Assembly of Hydrocarbon Amphiphiles into Micelles and Bilayers. *Journal of the Chemical Society-Faraday Transactions Ii* **1976**, *72*, 1525–1568.

(4) M.C., J.; Leroux, J. Polymeric micelles a new generation of colloidal drug carriers. *Eur. J. Pharm. Biopharm.* **1999**, 101–111.

(5) Tanford, C. Micelle Shape and Size. *J. Phys. Chem.* **1972**, *76*, 3020–&.

(6) Barnes, J. C.; Ehrlich, D. J.; Gao, A. X.; Leibfarth, F. A.; Jiang, Y.; Zhou, E.; Jamison, T. F.; Johnson, J. A. Iterative exponential growth of stereo- and sequence-controlled polymers. *Nat. Chem.* **2015**, *7*, 810–5.

(7) Gitsov, I.; Wooley, K. L.; Hawker, C. J.; Ivanova, P. T.; Frechet, J. M. J. Synthesis and Properties of Novel Linear Dendritic Block-Copolymers - Reactivity of Dendritic Macromolecules toward Linear-Polymers. *Macromolecules* **1993**, *26*, 5621–5627.

(8) Nakayama, M.; Okano, T.; Miyazaki, T.; Kohori, F.; Sakai, K.; Yokoyama, M. Molecular design of biodegradable polymeric micelles for temperature-responsive drug release. *J Control Release* **2006**, *115*, 46–56.

(9) Napoli, A.; Valentini, M.; Tirelli, N.; Müller, M.; Hubbell, J. A. Oxidation-responsive polymeric vesicles. *Nat. Mater.* **2004**, *3*, 183–189.

(10) Amir, R. Enzyme-Responsive PEG–Dendron Hybrids as a Platform for Smart Nanocarriers. *Synlett* **2015**, *26*, 2617–2622.

(11) Harnoy, A. J.; Buzhor, M.; Tirosh, E.; Shaharabani, R.; Beck, R.; Amir, R. J. Modular Synthetic Approach for Adjusting the Disassembly Rates of Enzyme-Responsive Polymeric Micelles. *Biomacromolecules* **2017**, *18*, 1218–1228.

(12) Segal, M.; Avinery, R.; Buzhor, M.; Shaharabani, R.; Harnoy, A. J.; Tirosh, E.; Beck, R.; Amir, R. J. Molecular Precision and Enzymatic Degradation: From Readily to Undegradable Polymeric Micelles by Minor Structural Changes. *J. Am. Chem. Soc.* **2017**, *139*, 803–810.

(13) Oliver, R. C.; Lipfert, J.; Fox, D. A.; Lo, R. H.; Kim, J. J.; Doniach, S.; Columbus, L. Tuning micelle dimensions and properties with binary surfactant mixtures. *Langmuir* **2014**, *30*, 13353–61.

(14) Cabral, H.; Matsumoto, Y.; Mizuno, K.; Chen, Q.; Murakami, M.; Kimura, M.; Terada, Y.; Kano, M. R.; Miyazono, K.; Uesaka, M.; Nishiyama, N.; Kataoka, K. Accumulation of sub-100 nm polymeric micelles in poorly permeable tumours depends on size. *Nat. Nanotechnol.* **2011**, *6*, 815–23.

(15) Chithrani, B. D.; Ghazani, A. A.; Chan, W. C. W. Determining the size and shape dependence of gold nanoparticle uptake into mammalian cells. *Nano Lett.* **2006**, *6*, 662–668.

(16) Geng, Y.; Dalhaimer, P.; Cai, S.; Tsai, R.; Tewari, M.; Minko, T.; Discher, D. E. Shape effects of filaments versus spherical particles in flow and drug delivery. *Nat. Nanotechnol.* **2007**, *2*, 249–55.

(17) Nagayasu, A.; Uchiyama, K.; Kiwada, H. The size of liposomes: a factor which affects their targeting efficiency to tumors and therapeutic activity of liposomal antitumor drugs. *Adv. Drug Delivery Rev.* **1999**, *40*, 75–87.

(18) Sharma, G.; Valenta, D. T.; Altman, Y.; Harvey, S.; Xie, H.; Mitragotri, S.; Smith, J. W. Polymer particle shape independently influences binding and internalization by macrophages. *J Control Release* **2010**, *147*, 408–12.

(19) Toy, R.; Peiris, P. M.; Ghaghada, K. B.; Karathanasis, E. Shaping cancer nanomedicine: the effect of particle shape on the in vivo journey of nanoparticles. *Nanomedicine (Lond)* **2014**, *9*, 121–34.

(20) Israelachvili, J. N. Intermolecular and Surface Forces, 3rd Edition. *Intermolecular and Surface Forces, 3rd Edition* **2011**, 1–674.

(21) Burts, A. O.; Liao, L. Y.; Lu, Y. Y.; Tirrell, D. A.; Johnson, J. A. Brush-first and Click: Efficient Synthesis of Nanoparticles that Degrade and Release Doxorubicin in Response to Light. *Photochem. Photobiol.* **2014**, *90*, 380–385.

(22) Gao, A. X.; Liao, L. Y.; Johnson, J. A. Synthesis of Acid-Labile PEG and PEG-Doxorubicin-Conjugate Nanoparticles via Brush-First ROMP. *ACS Macro Lett.* **2014**, *3*, 854–857.

(23) Johnson, J. A.; Lu, Y. Y.; Burts, A. O.; Lim, Y. H.; Finn, M. G.; Koberstein, J. T.; Turro, N. J.; Tirrell, D. A.; Grubbs, R. H. Core-clickable PEG-branch-azide bivalent-bottle-brush polymers by ROMP: grafting-through and clicking-to. *J. Am. Chem. Soc.* **2011**, *133*, 559–66.

(24) Johnson, J. A.; Lu, Y. Y.; Burts, A. O.; Xia, Y.; Durrell, A. C.; Tirrell, D. A.; Grubbs, R. H. Drug-Loaded, Bivalent-Bottle-Brush Polymers by Graft-through ROMP. *Macromolecules* **2010**, *43*, 10326–10335.

(25) Liao, L. Y.; Liu, J.; Dreaden, E. C.; Morton, S. W.; Shopsowitz, K. E.; Hammond, P. T.; Johnson, J. A. A Convergent Synthetic Platform for Single-Nanoparticle Combination Cancer Therapy: Ratiometric Loading and Controlled Release of Cisplatin, Doxorubicin, and Camptothecin. *J. Am. Chem. Soc.* **2014**, *136*, 5896–5899.

(26) Liu, J.; Burts, A. O.; Li, Y. J.; Zhukhovitskiy, A. V.; Ttavian, M. F.; Turro, N. J.; Johnson, J. A. "Brush-First" Method for the Parallel Synthesis of Photocleavable, Nitroxide-Labeled Poly(ethylene glycol) Star Polymers. *J. Am. Chem. Soc.* **2012**, *134*, 16337–16344.

(27) Sutthasupa, S.; Shiotsuki, M.; Sanda, F. Recent advances in ring-opening metathesis polymerization, and application to synthesis of functional materials. *Polym. J.* **2010**, *42*, 905–915.

(28) Wheeler, P.; Phillips, J. H.; Pederson, R. L. Scalable Methods for the Removal of Ruthenium Impurities from Metathesis Reaction Mixtures. *Org. Process Res. Dev.* **2016**, *20*, 1182–1190.

(29) Amir, R. J.; Zhong, S.; Pochan, D. J.; Hawker, C. J. Enzymatically Triggered Self-Assembly of Block Copolymers. *J. Am. Chem. Soc.* **2009**, *131*, 13949.

(30) Rosenbaum, I.; Avinery, R.; Harnoy, A. J.; Slor, G.; Tirosh, E.; Hananel, U.; Beck, R.; Amir, R. J. Reversible Dimerization of Polymeric Amphiphiles Acts as a Molecular Switch of Enzymatic Degradability. *Biomacromolecules* **2017**, *18*, 3457–3468.

(31) Golder, M. et al. Rationally Designed Macromolecular Telmisartan Conjugates that Reverse Liver Fibrosis. **2018**.

(32) Nguyen, H. V.; Detappe, A.; Gallagher, N. M.; Zhang, H.; Harvey, P.; Yan, C.; Mathieu, C.; Golder, M. R.; Jiang, Y.; Ottaviani, M. F.; Jasanoff, A.; Rajca, A.; Ghobrial, I.; Ghoroghchian, P. P.; Johnson, J. A. Triply Loaded Nitroxide Brush-Arm Star Polymers Enable Metal-Free Millimetric Tumor Detection by Magnetic Resonance Imaging. *ACS Nano* **2018**, *12*, 11343–11354.

(33) Liu, J. Design and development of Brush-Arm Star Polymers for applications in drug delivery., Thesis, 2017.

(34) Wei, H.; Zhuo, R.-X.; Zhang, X.-Z. Design and development of polymeric micelles with cleavable links for intracellular drug delivery. *Prog. Polym. Sci.* **2013**, *38*, 503–535.

(35) Kulthe, S. S.; Choudhari, Y. M.; Inamdar, N. N.; Mourya, V. Polymeric micelles: authoritative aspects for drug delivery. *Des. Monomers Polym.* **2012**, *15*, 465–521.

(36) Blanazs, A.; Armes, S. P.; Ryan, A. J. Self-Assembled Block Copolymer Aggregates: From Micelles to Vesicles and their Biological Applications. *Macromol. Rapid Commun.* **2009**, *30*, 267–77.

(37) Golder, M. R.; Nguyen, H. V. T.; Oldenhuis, N. J.; Grundler, J.; Park, E. J.; Johnson, J. A. Brush-First and ROMP-Out with Functional (Macro)monomers: Method Development, Structural Investigations, and Applications of an Expanded Brush-Arm Star Polymer Platform. *Macromolecules* **2018**, *51*, 9861–9870.

(38) Stuart, M. C. A.; van de Pas, J. C.; Engberts, J. B. F. N. The use of Nile Red to monitor the aggregation behavior in ternary surfactant-water-organic solvent systems. *J. Phys. Org. Chem.* **2005**, *18*, 929–934.

# Chapter 2

# Post micellization modification of norbornene-containing prodrug macromonomers

## 2.1 Introduction

Stimuli responsive micelles are popular scaffolds for drug delivery due to their small size, their resultant ability to accumulate in tumor tissues, their stabilizing and solubilizing effects on drugs, and their potential for rapid drug release.[1–5] They are generally composed of amphiphilic macromonomers that self assemble into a structure with a hydrophilic corona and a hydrophobic core that can shield a physically encapsulated payload or covalently bound agents for delivery. Inclusion in the hydrophobic core often stabilizes drugs, lowers drug toxicity, and increases circulation time.[6] For these reasons, several drug loaded polymeric micelles are currently under investigation.[7,8] Many utilize a stimulus-responsive linker to release the drug upon pH change, UV exposure, or temperature change.[9–11]

Micelles are composed of molecules with both hydrophobic and hydrophilic segments called amphiphiles that self-assemble to form structures with a hydrophobic core and a hydrophilic corona. The type, size, and stability of a micelle is based on the identity and relative sizes of each segment of the amphiphile.[12,13] Self-assembly of amphiphiles into micelles is driven by the thermodynamic benefit derived from reducing exposure of the hydrophobic block to an aqueous environment. At low concentrations, the amphiphiles exist as monomers; they do not begin to self assemble until a concentration known as the critical micelle concentration (CMC) is reached.[14] When dissolved in aqueous solution above the CMC, the amphiphiles spontaneously self-assemble into structures with both hydrophilic and hydrophobic domains. The hydrophobic domain controls the thermodynamic and kinetic stability of the micelle.[12] It is within this hydrophobic domain that lipophilic drugs can be solubilized for delivery, dramatically increasing the drug concentration that can be delivered. The hydrophilic domain, which is often comprised of a polymer such as polyethylene glycol, provides solubility and prevents opsonization thus minimizing recognition by the reticulo-endothelial system and increasing circulation time. Similar 'stealth' coatings have been approved for clinical use, although similar effects can be seen with a variety of polymers.[15,16]

The CMC values depend upon the micelle system in use, and can be taken as a measure of thermodynamic micelle stability.[17] CMC values for small molecule micelles are generally high,[7] and upon dilution such as during injection into a body these micelle dissociate into monomers. This dissociation releases any encapsulated drug rapidly. Polymeric micelles have the benefit of increased thermodynamic stability seen through a decreased CMC and relatively high kinetic stability, resulting in a longer circulation time in vivo.[18]

Generally, micelles are spherical structures although other micelle shapes do occur, as seen in Chapter 1.[19,20] The size, structure, and stability of the most stable aggregates are dependent upon the thermodynamics of micelle formation for the given system of amphiphiles.[13] These energies can be determined by understanding the chemical structure, and thus the relative geometries and interaction parameters of the hydrophobic and hydrophilic amphiphile segments.[12,13] These factors determine the CMC, which is consequently a useful parameter with which to understand micelle stability and thus drug release. Modifying the chemical structure of the micelle constituents can be used to tune micelle size and stability.

Simuli responsive micelles that release their drug load in response to an external stimulus, such as a change in pH, temperature, light, or small molecule signaling agent, change the thermodynamic stability of the micelle through modification of either the hydrophobic or hydrophilic domain to trigger drug release .[9,11,21–24]

pH sensitive micelles take advantage of the wide array of pH values found in biological tissues. Tumor tissues often have a lower pH than normal tissues, and micelles that are endocytosed experience an even lower pH of 5.0-5.5 making pH a useful trigger for tumor-specific delivery.[21,25,26] There are three common mechanisms for pH triggered drug release.[15,21] The first is a through the use of a polymer with ionizable functional groups such as poly(acrylic acid)[20] or poly(ethyleneimine). As the environmental pH changes, the thermodynamic minimum aggregate structure of amphiphiles with ionizable blocks changes as well. As the micelle undergoes structural transformation, drugs can be released. pH sensitive bonds can be used to trigger drug release concurrently with pH change.[15,21] The hydrolysis of acid labile bonds such as

esters, imines, oximes, acetals, and hydrazones is another common strategy to release a drug after a drug delivery particle has been endocytosed. Finally, amphiphiles can be designed with an acid labile linker to create a pH responsive PEG detachment system, ensuring that the delivery system will fall apart in a tumor environment and release drug.[11,27]

Temperature sensitive polymeric micelles generally contain a polymeric block that experiences a change in properties as the temperature changes.[28] Polymers with lower critical solution temperatures (LCSTs) or upper critical solution temperatures (USCTs) near biological temperatures such as poly(N-isopropylacrylamide) (PNIPAM) have been studied in depth.[27] PNIPAM experiences an LCST at 32°C, upon which it goes from being hydrophilic to hydrophobic.[29] PNIPAM containing polymers change properties above the LCST, and have been used to induce a sol-gel transition, form micelles, or deform micelles for drug delivery.[30–34]

Molecular triggers offer control over drug release from micelles, generally changing the amphiphilic hydrobic/hydrophilic ratio resulting in morphology changes.[9,35] Peroxides,[36,37] glutathione,[38] and dithiothreitol[39] have been used to trigger oxidation or reduction sensitive materials.

The previous chapter described the self-assembly of norbornene-containing prodrug macromonomers, showing how the resultant micelles could be controlled through consideration of the macromonomer drug loading. Here, we show the added functionality available as a result of the norbornene handle within the micelle. Small molecule and polymeric triggers are used to alter the morphology and stability of the drug loaded micelle. Two highly efficient "click" reactions were selected for their reactivity with norbornenes: the inverse electron demand Diels-Alder reaction and thiol-ene addition.

The inverse electron demand Diels-Alder reaction between tetrazine and alkenes has been used to induce a transition from vesicles to micelle with a concomitant increase cellular uptake and drug release.[40] This "click" reaction is of particular interest due to its speed, bioorthogonality, and biocompatibility.[41] The reaction between tetrazines and dienophiles such as norbornene is a rapid inverse electron demand

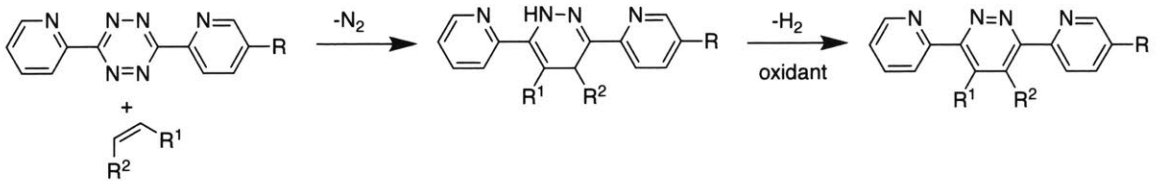


**Figure 2-1:** Chemical structures are shown for a generic inverse electron demand Diels-Alder reaction of a tetrazine and an alkene, followed by oxidation to form a pyridazine.

Diels-Alder reaction.[42] This and other bioorthogonal copper free "click" reactions[43] have been successfully used for bioconjugation[44–46] and for the formation of hydrogels.[41,47,48] The inverse electron demand Diels-Alder reaction of tetrazines and norborne is used herein to modify norbornene-containing prodrug macromonomers. By using functionalized tetrazines it is possible to change the ratio between the hydrophobic and hydrophilic segments of the macromonomer, triggering a morphological change in their micellar aggregates. Ultimately, we hope to modify micelles for drug delivery with tetrazines that trigger micelle growth, micelle dissociation, and even enable increased drug loading.

Thiol-ene addition reactions have been used to crosslink poly(norbornenes)[40] and to form thiol-norbornene networks.[49] In order to show another application of the norbornene functional handle in our micellar aggregates, these aggregates were chemically crosslinked to form nanoparticles using thiol-ene addition reactions under aqueous conditions required for micellization.

## 2.2 Results and Discussion

In this report, both tetrazine functionalization and thiol-ene crosslinking were investigated for their ability to modify micellar properties in a bio-compatible manner. Tetrazines proved to be a convenient signaling agent. The commercially available 3,6-bis(2-pyridyl)-1,2,4,5-tetrazine (BPTZ) was used to modify the G2 difluorophenyl telmisartan macromonomer (TEL-1) after aqueous self-assembly. The additional hydrophobic content provided by BPTZ was expected to increase the CMC, a measure of the additional driving force for micelle formation. Additional hydrophobic content is also expected to increase the radius of the micelle, as seen in the previous chapter. Upon the addition and subsequent reaction of BPTZ with the TEL-1, the signature magenta tetrazine color rapidly disappeared as BPTZ was taken up into the micelles. The increased local concentration within the micelle core led to rapid reaction kinetics, as studied in the experimental section.

### 2.2.1 Tetrazine

After the reaction between TEL-1 micelles and BPTZ, a dramatic increase was seen in the particle size (Figure 2-4), from ~8 nm particle diameters to aggregates ranging from 100-1000 nm in size. In the previous chapter, we saw that nearly tripling the hydrophobic content of the aqueously self assembled aggregates increased the particle diameter from $8 \pm 1$ nm to $18 \pm 1$ nm. The increase in particle diameter due to the addition of BPTZ is more than anticipated from the hydrophobic addition alone based on previous results, suggesting that the change in macromolecular structure is significant. However, the critical micelle concentration did not change significantly, from 52 $\mu$M to 54 $\mu$M, implying minimal change to particle stability.

A highly hydrophilic PEG 3k functionalized tetrazine (TET-PEG), was made in the hopes that the addition of significant hydrophilic content would shift the unimer-aggregate equilibrium to the unimer, increasing drug release rates, or even allowing individual unimers to dissolve directly in aqueous environments, disassembling the aggregates entirely. The reaction of TET-PEG with the TEL-1 micelles resulted in

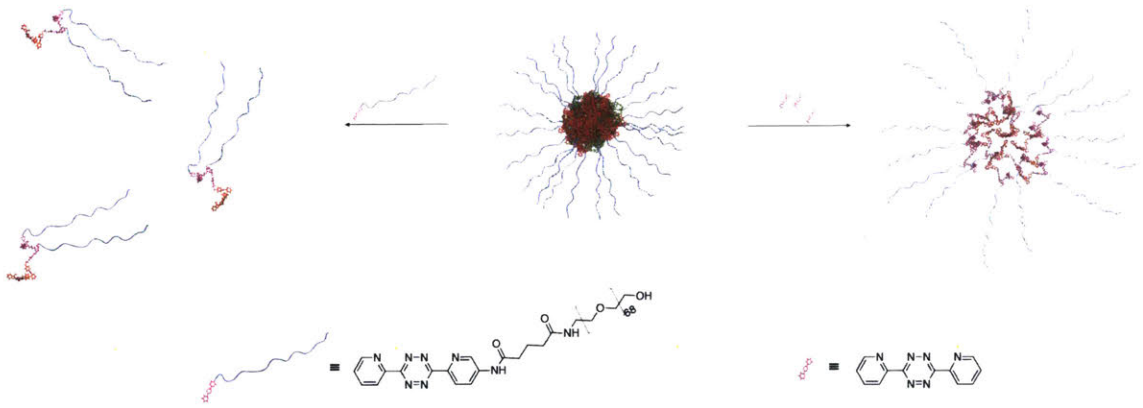

**Figure 2-2:** A TEL-1 based micelle is shown at the center of the above figure. To the left is shown the reaction of the aggregate with a PEG3k functionalized tetrazine (TET-PEG), creating highly soluble drug loaded polymers. To the right is shown the reaction of this aggregate with a small molecule tetrazine, 3,6-bis(2-pyridyl)-1,2,4,5-tetrazine (BPTZ), increasing the size of the aggregate through the addition of hydrophobic content.

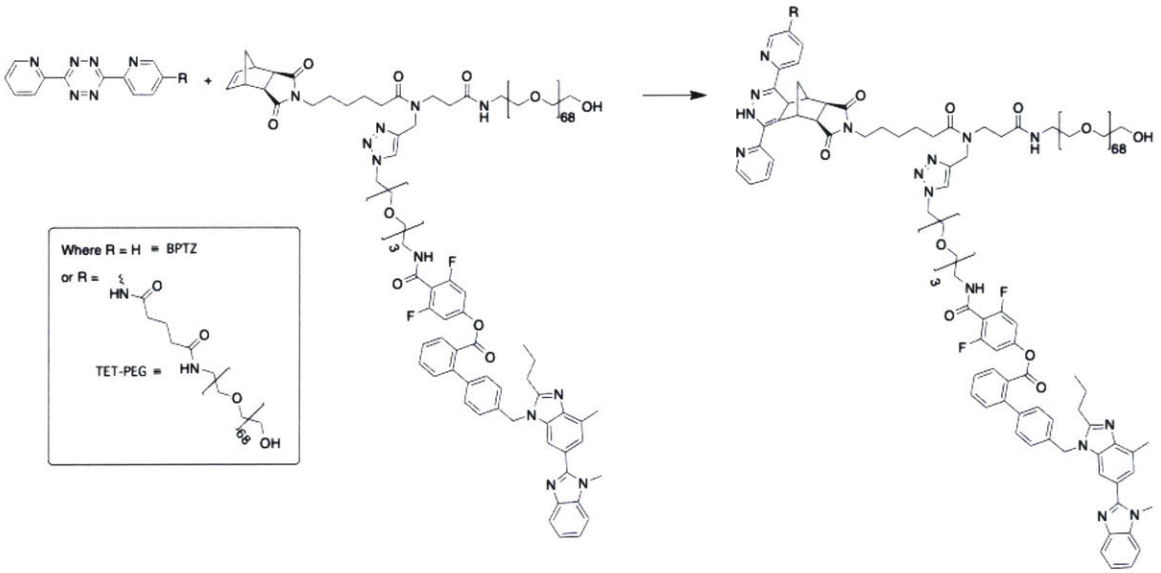


**Figure 2-3:** Tetrazine functionalizations of the TEL-1, G2 difluorophenyl telmisartan macromonomer were conducted under both aqueous and organic conditions.

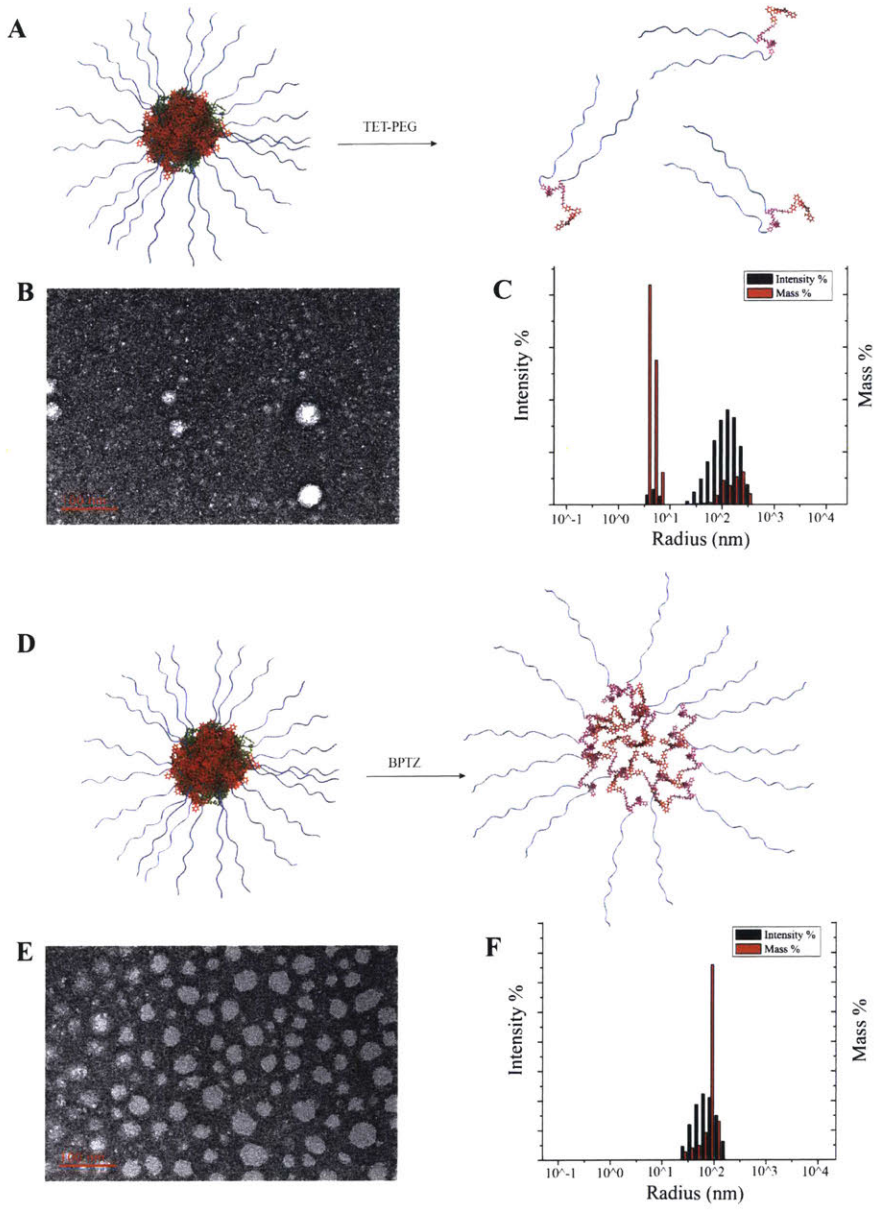


**Figure 2-4:** TEL-1 micelles were exposed to both BPTZ and TET-PEG. A) Upon reaction with the PEG 3k functionalized BPTZ, the micelles appeared to break apart into smaller units perhaps indicative of monomers or small aggregates. B) TEM image of TEL-1 micelles after reaction with TET-PEG, 1 mg/ml, stained with uranyl acetate. Few large aggregates are visible by TEM. C) DLS histogram of TEL-1 micelles after reaction with TET-PEG D) Upon reaction with BPTZ (right) the micelles enlarged, which can be attributed to the additional hydrophobic content of btpz. E) TEM image of TEL-1 micelles after reaction with BPTZ, 1 mg/ml, stained with uranyl acetate.After reaction with BPTZ, the micelles are irregular in shape with multiple distributions, perhaps the result of larger particles breaking down under TEM sample preparation conditions. F) DLS histogram of TEL-1 micelles after reaction with BPTZ.

| Sample Name | Molecular Weight (g/mol) | CMC (mg/mL) | CMC ($\mu$M) |
|---|---|---|---|
| TEL-1 | 4260 | 0.22 | 52 |
| BPTZ + TEL-1 | 4410 | 0.24 | 54 |

**Table 2.1:** Molecular weight and critical micelle concentrations of both TEL-1 and BPTZ functionalized TEL-1. Although a molecular weight change of only 3.6% resulted in a dramatically different aggregate size, the critical micelle concentration did not change notably.

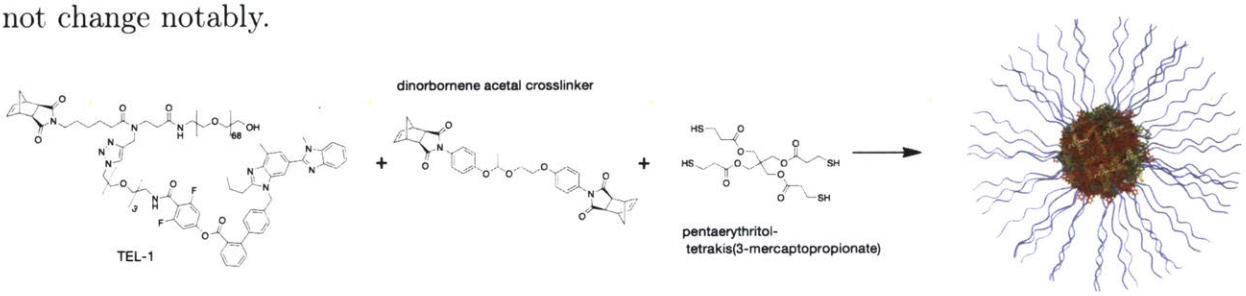


**Figure 2-5:** A commercially available tetrafunctional thiol (pentaerythritol tetrakis(3-mercaptopropionate) was used in conjunction with a dinorbornene acetal crosslinker to crosslink TEL-1 aggregates

the formation of two particle distributions at ~7.5 nm and ~128 nm. These particles were not stable under TEM sample preparation conditions, forming $20 \pm 3$ nm as determined by ImageJ analysis. These post-micellization functionalizations show that micelle systems formed from norbornene-drug-macromonomers are not only highly tunable, but sensitive to bio-orthogonal signaling as well.

### 2.2.2 Thiol-ene

Thiol-ene "click" chemistry was used to crosslink the macromonomers. Here, a commercially available tetrafunctional thiol (pentaerythritol tetrakis(3-mercaptopropionate) was used in conjunction with a dinorbornene acetal crosslinker to create covalently structured nanoparticles. As with the tetrazine functionalizations, the addition of these hydrophobic components strongly influenced micelle size. Micelle diameter correlated with the quantity of crosslinker used until greater than 5 equivalents of crosslinker were used, upon which the entire system began to gel. These crosslinkers form permanent nanoparticles, disrupting the unimer to aggregate equilibrium,

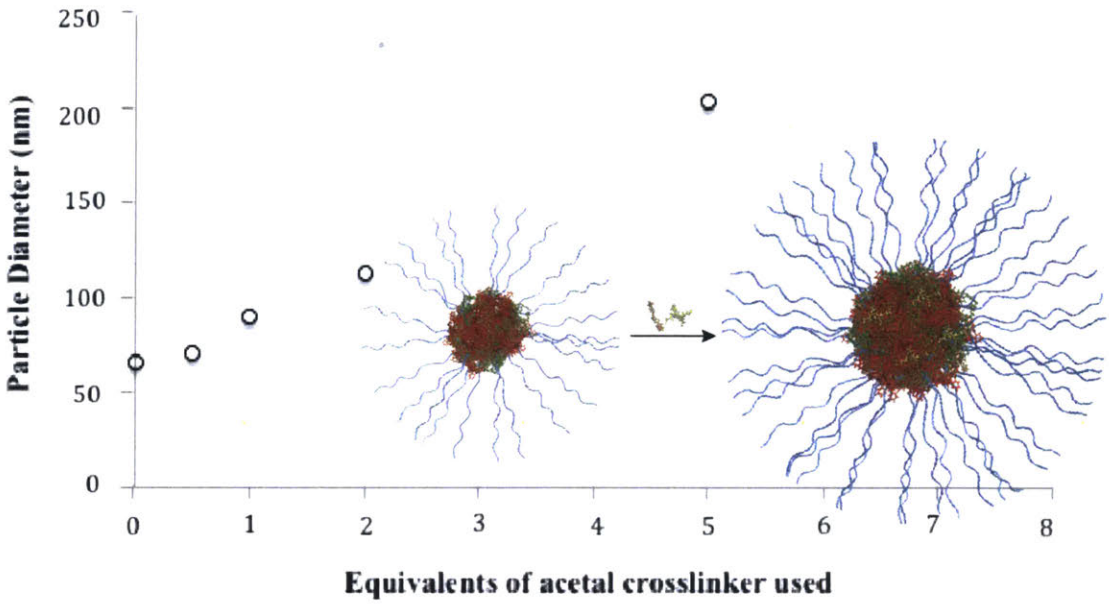


**Figure 2-6:** Particle diameter as a function of acetal crosslinker used. As the equivalents of acetal crosslinker increased, the particle diameter did as well.

and thus decreasing potential drug release. The use of this chemistry provides a method to increase particle stability far beyond that of a micelle without sacrificing the versatility of the system.

### 2.2.3 Conclusions

Aqueously assembled norbornene-PEG-branch-drug macromonomers form tunable aggregates that can be functionalized after the formation of aggregates. Particle size can be controlled through the addition of functionalized tetrazines. The CMC of these micelles, an indicator of particle stability, does not necessarily change with tetrazine functionalization. Post-micellization tetrazine "click" chemistry can be used to induce an in situ response, further modifying the properties of these particles. Thiol-ene "click" chemistry can be used to form large nanoparticles without the potential for disassembly.

## 2.3 Experimental

### 2.3.1 Materials and General Methods

All reagents were purchased from commercial sources and used without further purification unless stated otherwise.

Liquid chromatography mass spectrometry (LC-MS) tandem was performed on an Agilent 1260 instrument with an Agilent 6130 single quadrupole mass spectrometer and an Advanced Materials Technology Halo C18 (HALO) column using a binary solvent system of acetonitrile and 0.1% acetic acid in water.

Gel permeation chromatography was performed on an Agilent 1260 instrument with two Agilent PLGel mixed C columns in series, a 0.025M lithium bromide in dimethyl formamide mobile phase run at 60 celsius, a Wyatt Optilab T-rEX detector, and a Wyatt Heleos II detector.

Column chromatography was carried out on silica gel 60F (EMD Millipore, 0.040-0.063 mm).

$^{1}$H nuclear magnetic resonance ($^{1}$H-NMR) and $^{13}$C nuclear magnetic resonance ($^{13}$C-NMR) spectra were recorded on Bruker AVANCE-400 NMR spectrometers in the Department of Chemistry Instrumentation Facility at MIT. Chemical shifts are reported in ppm relative to the signals corresponding to residual non-deuterated solvents: $CDCl_3$: $\delta$H = 7.26 ppm, DMSO-d6: $\delta$H = 2.50 ppm. Spectra were analyzed on MestReNova NMR software.

Matrix-assisted laser desorption/ionization-time of flight (MALDI-TOF) mass spectra were measured on a Bruker model MicroFlex instrument using $\alpha$-cyano-4-hydroxycinnamic acid as the matrix.

Transmission electron microscopy (TEM) was performed on a FEI Tecnai Multipurpose TEM at 120 kV with carbon coated copper TEM grids, CF200-CU-UL from Electron Microscopy Sciences. For typical TEM sample preparation, 7 $\mu$L of

a 1 mg/mL solution of particles in nanopure water was dropped onto a carbon film coated copper grid. After 15 minutes, excess aqueous solution was wicked away with the twisted corner of a Kimwipe. For negative staining, 7 $\mu$L of a 2 wt% uranyl acetate stain (Electron microscopy sciences) was dropped onto the grid. After 2 minutes, excess stain was wicked away with a Kimwipe.

Dynamic Light Scattering (DLS) was taken with a Wyatt Möbius with a 660 nm laser. The average hydrodynamic diameter of a set of 20 samples was calculated with a proprietary regularization algorithm from Dynamics 7.3.1.15.

Fluorimetry was performed on SPEX Fluorolog-$\tau$2 fluorometer (model f13-21, 450 W. Xenon lamp).

UV Vis absorption experiments were performed on a Cary 50 Scan UV-Vis Spectrophotometer.

### 2.3.2 Synthetic Protocols

All reagents were purchased from commercial sources and used without further purification unless stated otherwise.

5-oxo-5-((6-(6-(pyridin-2-yl)-1,2,4,5-tetrazin-3-yl)pyridin-3-yl)amino)pentanoic acid (TET-COOH) was synthesized according to literature procedures.[50]

2,5-dioxopyrrolidin-1-yl 5-oxo-5-((6-(6-(pyridin-2-yl)-1,2,4,5-tetrazin-3-yl)pyridin-3-yl)amino) pentanoate [Tet-NHS] was synthesized according to literature procedures.[50]

N1-(poly(ethyleneglycol))-N5-(6-(6-(pyridin-2-yl)-1,2,4,5-tetrazin-3-yl)pyridin-3-yl)glutaramide [T PEG] was synthesized based on to literature procedures.[50]

Dinorbornene acetal cross linker was synthesized based on to literature procedures.[51]

**Tet-PTX**

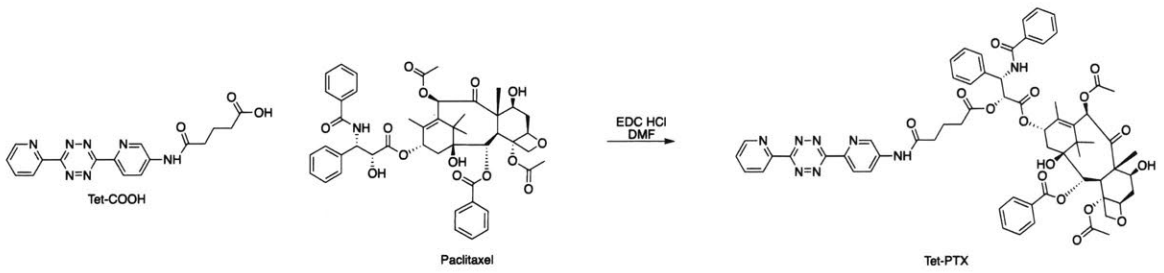


(2aR,4S,4aS,6R,9S,11S,12S,12aR,12bS)-9-(((2R,3S)-3-benzamido-2-((5-oxo-5-((6-(6-(pyridin-2-yl)-1,2,4,5-tetrazin-3-yl)pyridin-3-yl)amino)pentanoyl)oxy)-3-phenylpropanoyl)oxy)-12-(benzoyloxy)-4,11-dihydroxy-4a,8,13,13-tetramethyl-5-oxo-3,4,4a,5,6,9,10,11,12,12a-decahydro-1H-7,11-methanocyclodeca[3,4]benzo[1,2-b]oxete-6,12b(2aH)-diyl diacetate [Tet-PTX] was synthesized based on a previously reported procedure.[50]

5-oxo-5-((6-(6-(pyridin-2-yl)-1,2,4,5-tetrazin-3-yl)pyridin-3-yl)amino)pentanoic acid (287.4 mg, 0.79 mmol), 1-Ethyl-3-(3- dimethylaminopropyl)carbodiimide (200 mg, 1.06 mmol), and paclitaxel (939 mg, 1.1 mmol) were combined in a vial which was then evacuated and backfilled with nitrogen three times. 3 mL of anhydrous N,N-dimethylformamide was added and the mixture was stirred at room temperature under nitrogen overnight. The reaction solution was loaded directly onto silica gel and purified with an eluent of 0-5% methanol in dichloromethane. The product was dried under vacuum, yielding a purple solid (710 mg, 74%).

$^1$H NMR (400 MHz, DMSO) $\delta$ 9.23 (d, J = 8.6 Hz, 1H), 9.04 (d, J = 2.5 Hz, 1H), 8.94 (d, J = 4.8 Hz, 1H), 8.67 -8.56 (m, 2H), 8.41 (dd, J = 8.8, 2.5 Hz, 1H), 8.20 -8.12 (m, 1H), 7.99 (d, J = 7.3 Hz, 3H), 7.87 (dd, J = 14.2, 7.0 Hz, 3H), 7.77 - 7.60 (m, 5H), 7.57 -7.38 (m, 8H), 7.19 (s, 2H), 6.30 (s, 1H), 5.76 (s, 7H), 5.55 (t, J = 8.7 Hz, 1H), 5.39 (dd, J = 19.3, 8.1 Hz, 3H), 4.91 (d, J = 7.2 Hz, 2H), 4.63 (s, 1H), 4.11 (s, 2H), 4.02 (s, 2H), 3.59 (d, J = 7.6 Hz, 1H), 2.81 (t, J = 6.4 Hz, 1H), 2.55 (d, J = 7.5 Hz, 2H), 2.24 (d, J = 11.2 Hz, 4H), 2.11 (d, J = 2.2 Hz, 4H), 1.95 - 1.87 (m, 2H), 1.80 (d, J = 8.2 Hz, 4H), 1.62 (d, J = 12.4 Hz, 1H), 1.50 (s, 3H), 1.24 (s, 2H), 1.13 -0.98 (m, 8H), 0.85 (s, 1H).

### Standard Tetrazine Norbornene Reaction Conditions

All experiments were performed at ambient temperature in air, using standard grade solvents.

3,6-Di-2-pyridyl-1,2,4,5-tetrazine (BPTZ) (0.0017g, 0.0071 mmol) was added to a vial then dissolved in 0.36mL of water containing TEL-1 (0.030g, 0.0071 mmol) to give a 1:1 ratio of norbornene and tetrazine at a final concentration of 20 mM. The reaction was allowed to proceed for 12 hours, at which time the sample was analyzed by NMR to confirm the absence of norbornene peaks.

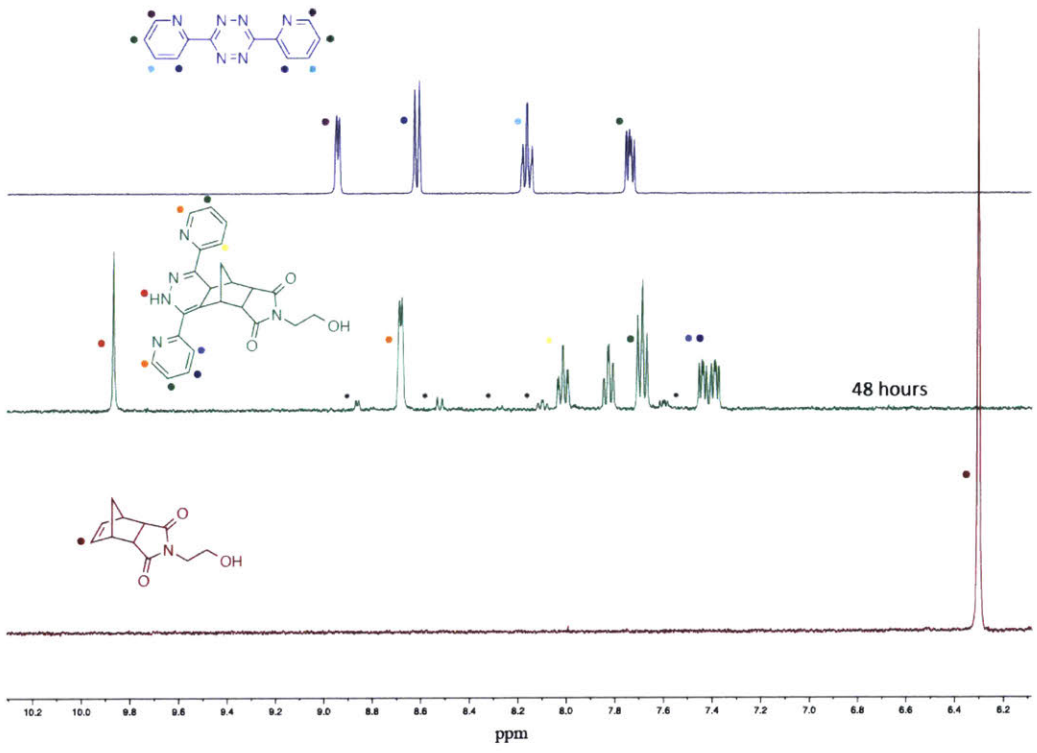


**Figure 2-7:** 1H NMR (300 MHz) spectra are shown here of BPTZ, (3aR,7aS)-2-(2-hydroxyethyl)-3a,- 4,7,7a-tetrahydro-1H-4,7-methanoisoindole-1,3(2H)-dione, and their product. This small molecule, drug free norbornene substitute was used to determine whether or not oxidation occurs in a similar time scale as the tetrazine coupling. This substitute was chosen due to its rapid kinetics of reaction, and lack of overlapping peaks at the region of interest. Of note is the complete loss of signal from protons of the double bond of norbornene at ~6.3 ppm upon reaction. *Only minor oxidation was observed after 48 hours.

### Tetrazine Norbornene Kinetics

All experiments were performed at ambient temperature in air, using standard grade solvents.

Kinetics of the reaction between macromonomer and model tetrazines were studied under pseudo first-order conditions. As the coupling reaction proceeds, the decrease of tetrazine concentration [T] is directly proportional to the decrease of absorbance at 540 nm which can be monitored via UV-Vis spectroscopy.

Standard Conditions: 47.2$\mu$L of a stock solution of BPTZ (0.1 mg/mL in dichloromethane) was added to a vial and the solvent removed under reduced pressure. 1.0 mL of water was added to dissolve the BPTZ. TEL-1 (0.026g, 0.006 mmol) was dissolved in 1.0 mL of water. The two solutions were combined in a quartz cuvette to give a total volume of 2.0 mL, a molar ratio of norbornene to tetrazine equal to 30:1, and a final concentration of macromonomer equal to 3mM. Absorbance was recorded every 0.5 minutes at 540nm for 60 minutes. [BPTZ] was calculated from the absorbance using a Beer's Law plot. The linearity of this plot confirmed that BPTZ dissolved fully in water at all concentrations used in this study. Representative plots of -ln[BPTZ] versus time are shown below. The slope of these plots gives the observed pseudo first-order constants $k'$. These values were plotted against [TEL-1] to obtain the second-order rate constant, $k$.

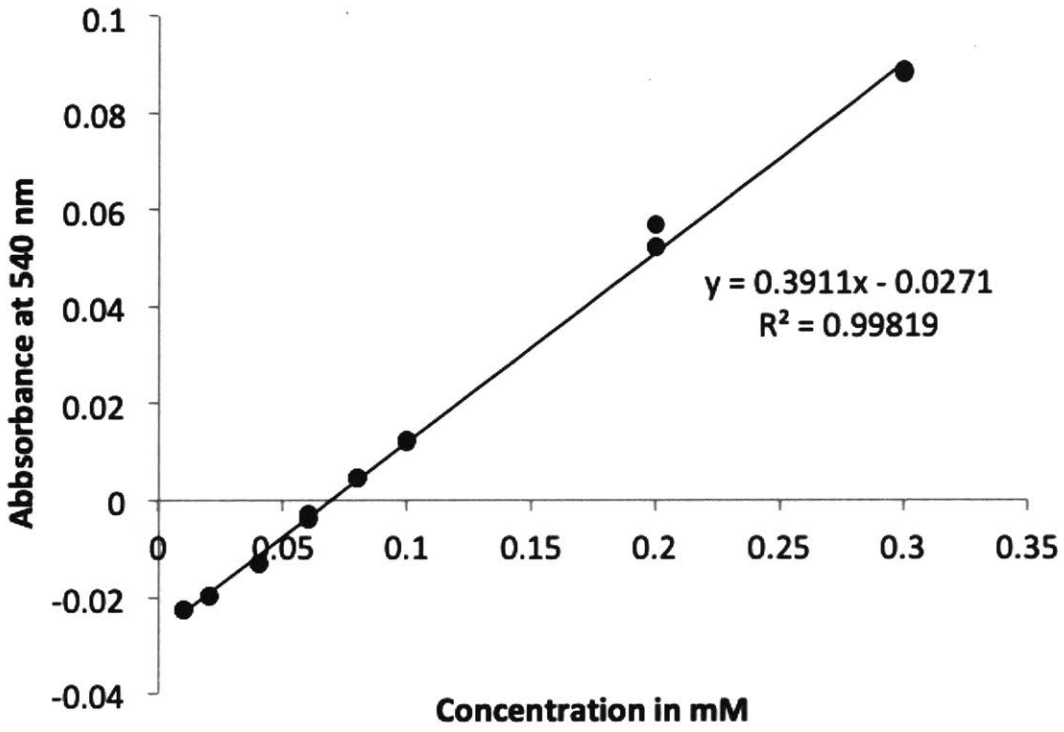


**Figure 2-8:** This Beer's Law plot of BPTZ in water was made not only to confirm that the concentrations used for the following kinetics studies were in a linear region, but also to confirm that BPTZ was soluble in water at the concentrations used.

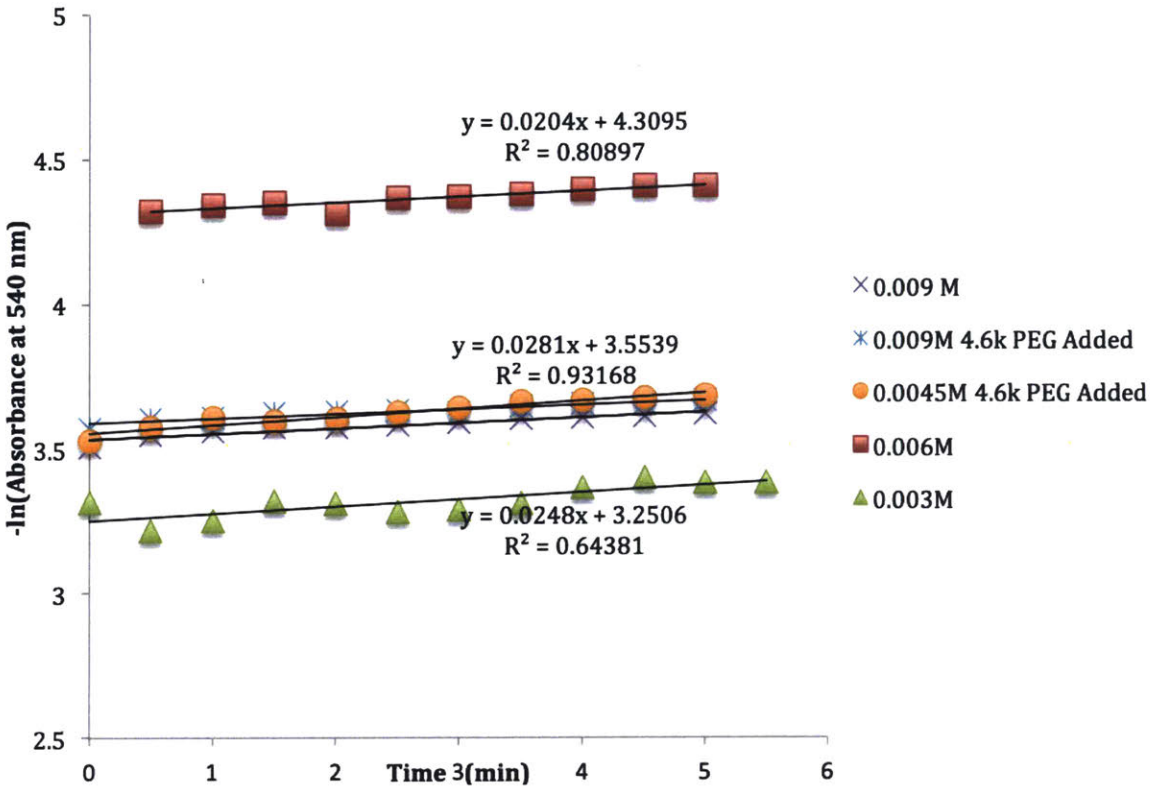


**Figure 2-9:** In order to confirm that the high viscosity of the norbornene PEG 3k telmisartan macromonomer used in the kinetics studies would not impact the rate of reaction with norbornene, BPTZ was allowed to react with a small molecule norbornene, (3aR,4R,7S,7aS)-2-(2-hydroxyethyl)-3a,4,7,7a-tetrahydro-1H-4,7-methanoisoindole-1,3(2H)-dione, with varying concentrations of 4.6K PEG. No dependence of the rate of reaction upon concentration of 4.6k PEG was seen.

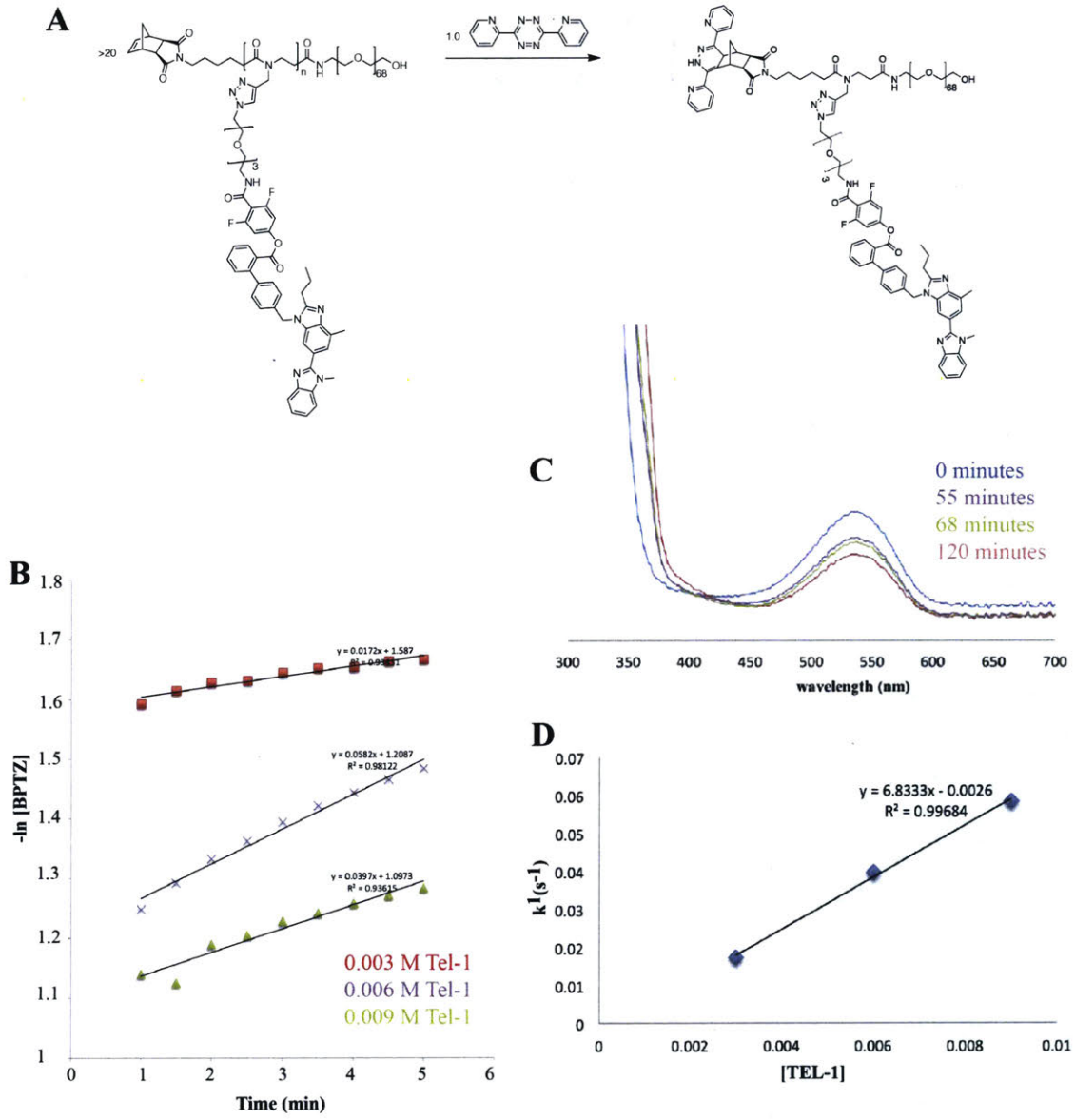


**Figure 2-10:** Structures of Tel-1, BPTZ, and the product of their reaction. B) -ln[BPTZ] plotted against time to determine $k_1$. C) UV-Vis spectra of the reaction shown in A over time. D) $k_1$ from 7B were plotted against [TEL-1] in order to determine the second-order rate constant k.

### Dynamic Light Scattering

DLS was used to study the average particle diameter as a function of amphiphile concentration. TEL-1 was used in order to determine a standard DLS concentration to use for future experiments. Samples were made at concentrations of 10 mg/mL, 1

mg/mL, 0.5 mg/mL, 0.1 mg/mL, 0.05 mg/mL, and 0.01 mg/mL through the simple dissolution of macromonomer in water. Samples were allowed to sit for 60 minutes, and DLS was taken without filtration. No change in product distribution was seen in samples re-run 1, 2, or 7 days later.

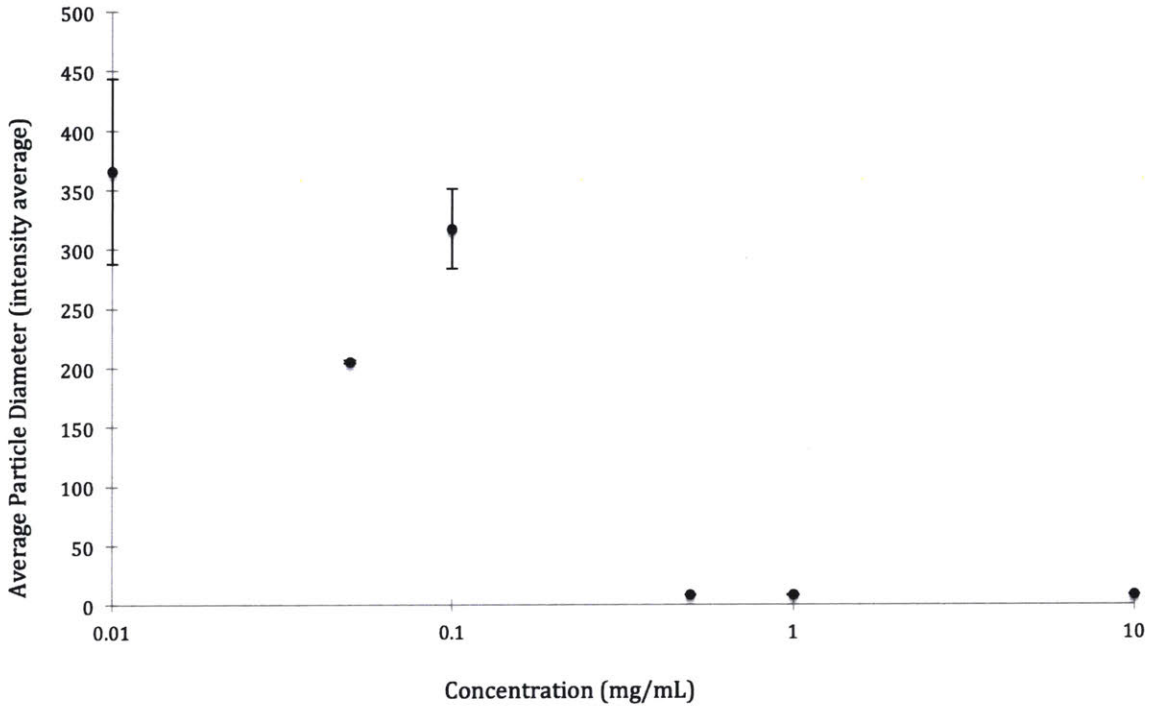


**Figure 2-11:** DLS results for TEL-1 as a function of concentration. No ~9 nm particle is detected below 0.5 mg/mL.

The intensity of the ~9 nm particle (>95% of sample by mass) was too low for detection below 0.5 mg/mL. This concentration concurs well with the CMC of these micelles. All samples at or above 0.5mg/mL showed ~9 nm particles consistently. Unsurprisingly the error in the measurements increases below 0.5mg/mL, close to the CMC of the micelles. The large particles seen at those concentrations may be minor impurities.

### Micelle Formation

There are several methods methods that are used to produce micelles. The more rapid methods may form kinetically trapped aggregates, generating multiple micellar

species or broad distributions. The best method will depend upon the amphiphile and drug loading at hand. Common methods include:

a Dissolution: The simplest method for forming self-assembled aggregates is to directly dissolve the amphiphiles in question in an aqueous solution. This method is prone to forming kinetically trapped micelles, depending on the equilibrium between monomers and aggregate.

b Dialysis: By combining the amphiphile and drug in a water miscible organic solvent such as N,N-dimethyl formamide, tetrahydrofuran, or dimethylsulfoxide and then dialyzing the solution against water, the organic solvent is slowly replaced with water, generating micelles. The dialysis membrane allows for organic solvent molecules and free drug molecules to be removed from the micelles.

c Pre-mixing: Combining the amphiphile and drug in an organic solvent which is then removed prior to the addition of an aqueous phase helps to solubilize drugs that may otherwise take a prohibitive amount of time to dissolve in a micellar solution.

d Solvent Evaporation/Emulsion: It is possible to form aggregates by combining the amphiphile and drug in an organic solvent to which water is slowly added. Regardless of whether the organic solvent is water miscible or not, stirring and evaporation will result in the formation of a drug loaded micelle. More vigorous stirring is required to emulsify a non-miscible organic solvent to help control micelle sizes.

A variety of micelle formation techniques were tested with TEL-1 to see if any would distinguish themselves. Particles were formed via straight dissolution of the macromonomer in water, dissolution in acetone followed by a slow dilution with water and evaporation of the acetone under vacuum, dissolution in DMF followed by a slow dilution with water and dialysis, and dissolution in DMF followed by a rapid addition of the solution to water. All methods produced the same size of aggregate, suggesting that the singly loaded monomers equilibrate quickly. Each macromonomer

was dissolved in dimethylformamide to create a 50.0 mg/mL stock solution. These solutions were combined in molar ratios as described below and diluted with dimethylformamide to make 10 mg/mL solutions. The mixtures were briefly sonicated and then dialyzed in 1 kDa dialysis tubing (Spectrum Labs) against nanopure water to remove dimethyl formamide for 4 hours. Water was exchanged after 1 hour and 2 hours. The removed water phases were concentrated and analyzed by LC-MS to confirm negligible drug release prior to further analysis.

### CMC Measurements

Samples were made for CMC determination by dissolving the macromonomer in MilliQ water for an initial concentration of 10 mg/mL. The macromonomer solution was then diluted serially to produce 900$\mu$L of each desired concentration, with 5 minutes of sonication between each dilution. To each solution was added 100$\mu$L of a 200$\mu$M nile red solution. The final samples were sonicated for 10 minutes, and allowed to equilibrate overnight. Fluorescence spectra were collected over a range 600-675 nm with a 1 nm step and 550 nm excitation. The intensity was averaged over three scans, and values at 636 nm recorded for each sample. The nile red solution was made through the dilution of an initial solution of 2.5mg/mL nile red in acetone with MilliQ water to make a 200$\mu$M solution. Both solutions were made fresh each day.

All fluorescent intensities at 636 nm were plotted against concentration, then two best fit lines were generated. The point at which the best fit lines overlapped was taken as the critical micelle concentration. Multiple CMC assays were run with each sample to ensure reproducibility. A shift in emission maximum was also noted at the critical micelle concentration for all samples.

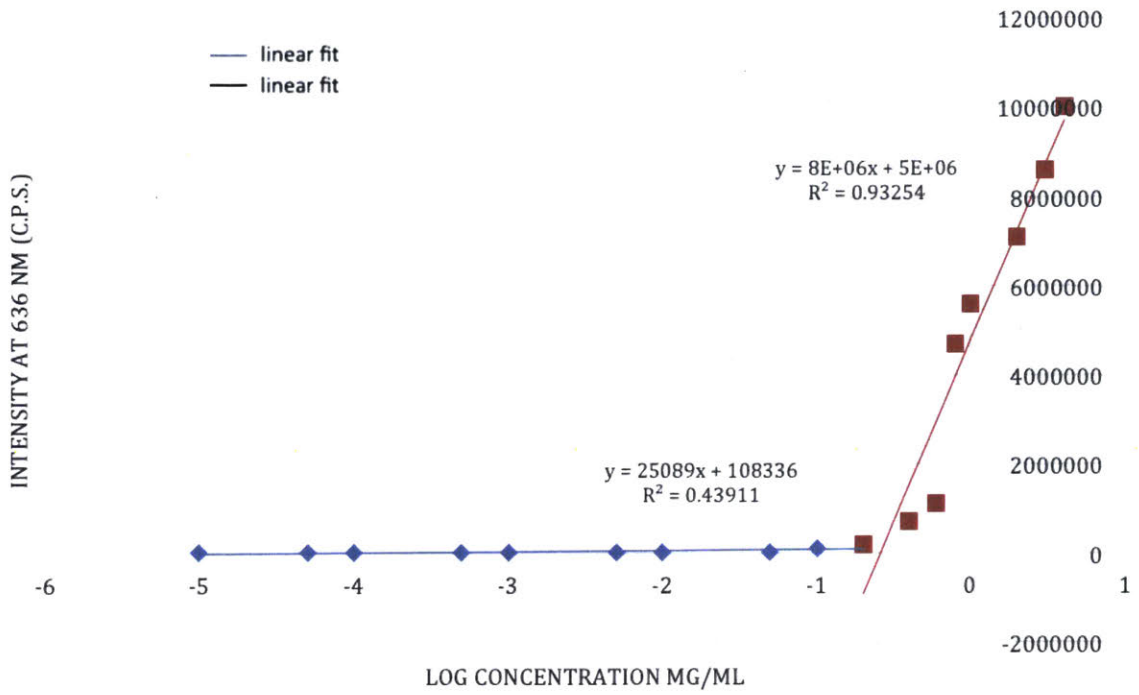


**Figure 2-12:** CMC Determination for the BPTZ Functionalized TEL-1. The CMC was found to be 0.24mg/mL, or 0.054mM.

### Standard Thiol-ene Reaction Conditions

10 mg (1.2 mmol) of TEL-1 was dissolved in 1.0 mL of dichloromethane then combined with 0.15 mg (0.6 mmol) 2,2-dimethoxy-2-phenylacetophenone, 5.8 mg (12 mmol) Pentaerythritol tetrakis(3-mercaptopropionate) from a 10 mg/mL solution in dichloromethane, and 2.8 mg (4.8 mmol) dinorbornene acetal cross linker from a 10 mg/mL solution in dichloromethane. The dichloromethane was removed under reduced pressure, and 0.1 mL of dimethyl formamide added. The sample was allowed to equilibrate overnight, then purged with nitrogen and exposed to 365 nm UV light for 30 minutes. Samples were dissolved in 5 mL of water and then dialyzed in 1 kDa dialysis tubing from Spectrum Labs against water to remove dimethyl formamide.

### Initiator Selection

Telmisartan, DMPA, and I2959 were all tested as initiators for this thiol-ene chemistry.

| Ratio of TEL-1 to Acetal to Tetrathiol | Particle Diameter by DLS |
|---|---|
| 1:0:0.25 | 193 nm (174 nm before UV) |
| 0.95:0.25:0.25 | 184 nm |
| 0.9:0.05:0.25 | 226 nm |
| 0.8:0.1:0.25 | 280 nm |
| 0.6:0.2:0.25 | 221 nm |

**Table 2.2:** Particle diameters were determined from DLS. As the ratio of TEL-1 to crosslinker decreased, the particle diameter increased.

| Initiator | Solvent | Conversion | Particle Size |
|---|---|---|---|
| Telmisartan | THF | 14% | – |
| DMPA | THF | 60% | – |
| I2959 | Water | 70% | 425 nm |

**Table 2.3:** Conversion as determined from $^1$H-NMR depended upon the initiator used. Telmisartan alone was able to initiate thiol-ene reactions, but resulted in a low conversion after 60 minutes. DMPA was eventually chosen due to it's hydrophobicity, in the hopes that it would accumulate within hydrophobic micelle cores.

0.030g (0.01 mmol, 4 eq) of a norbornene functionalized PEG 3k, 0.0052g (1 eq) of pentaerythritol tetrakis(3-mercaptopropionate), and 0.05 eq of initiator (from a 1mg/mL solution) were combined and diluted with solvent for a final concentration of 100mg/mL (0.03M) with respect to the macromonomer. Samples were purged with nitrogen for 10 minutes and then exposed to 365 nm UV. Conversion was checked by NMR after 60 minutes. DMPA was chosen for its high conversion and comparable solubility to the crosslinker chosen.

### Solvent Selection

The crosslinkers chosen in this experiment were not directly water soluble, requiring the formation of micelles to solubilize them. Initially, dimethyl formamide was chosen to solubilize the mixture, but variable amounts were necessary to dissolve the mixture. In order to standardize the crosslinking, all reagents were premixed in dichloromethane which was removed before the addition of a fixed quantity of dimethyl formamide, and standard micelle formation.

Experiments conducted in other solvents led to gelation regardless of the crosslinker

| Solvent | Concentration | Initiator | Result |
|---|---|---|---|
| Dichloromethane | 100 mg/mL | 0.05 eq | gel |
| Water | 100 mg/mL | 0.05 eq | gel |
| Dimethylformamide | 100 mg/mL | 0.05 eq | soluble |

**Table 2.4:** Dimethylformamide reliably formed soluble systems while the other systems tested often formed gels.

equivalency used.

### 2.3.3 Spectra

**Figure 2-13:** MALDI-TOF Spectrum of TET-PEG

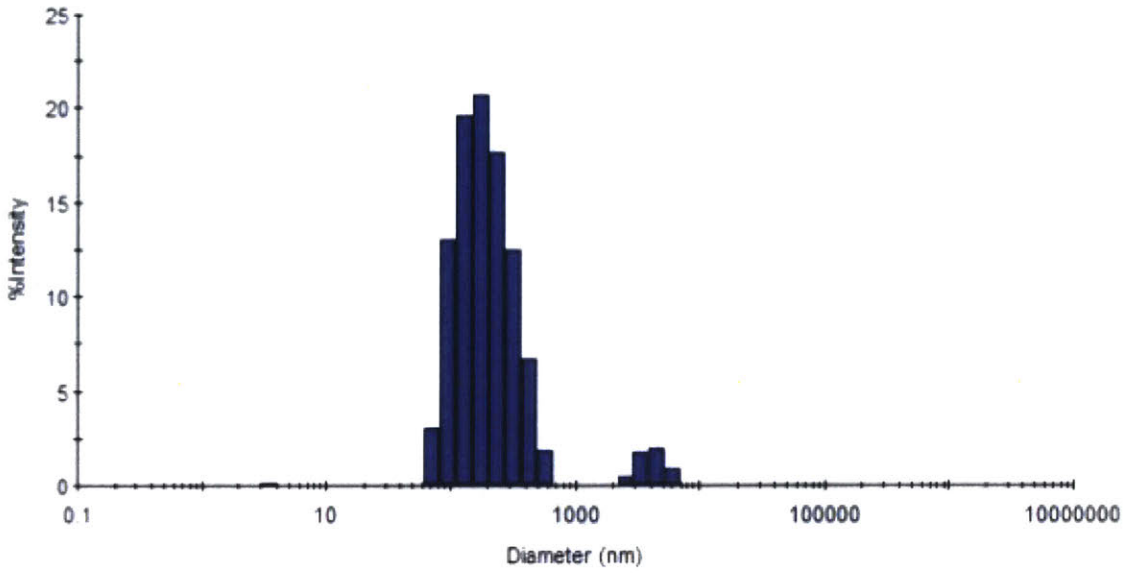


**Figure 2-14:** DLS histrogram of TEL-1 after reaction with BPTZ at 1 mg/mL in water.

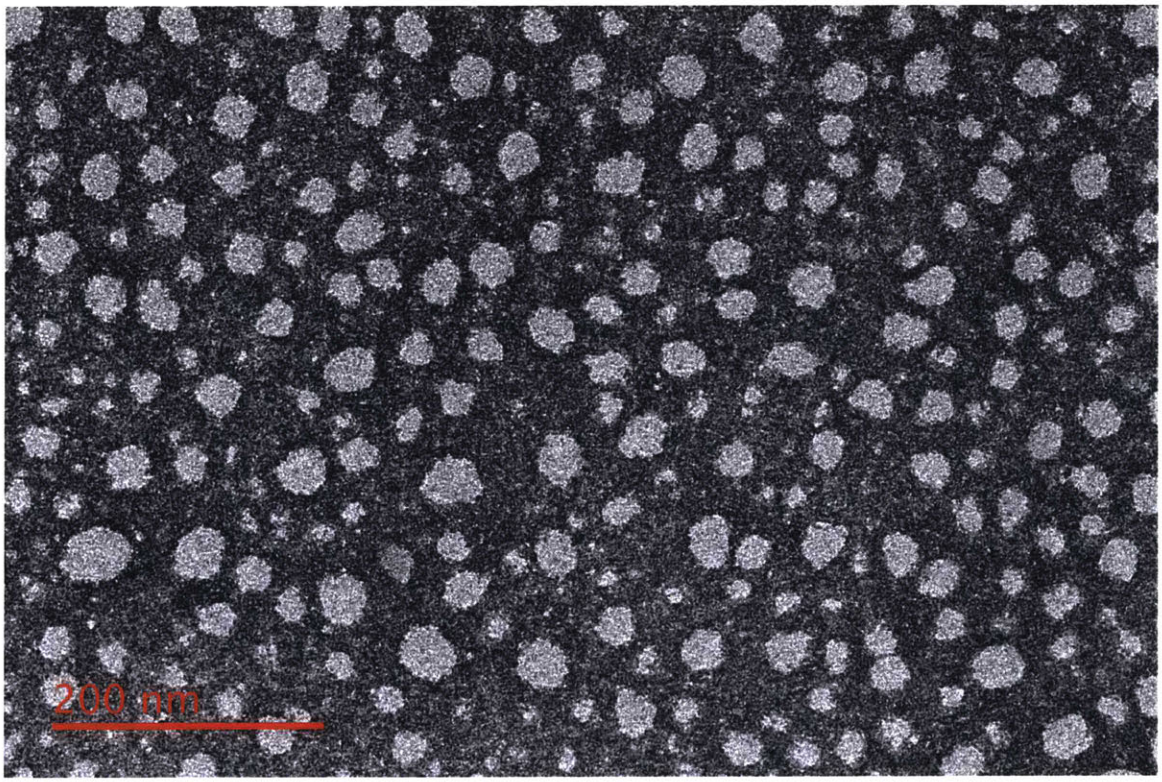


**Figure 2-15:** TEM image of BPTZ functionalized TEL-1

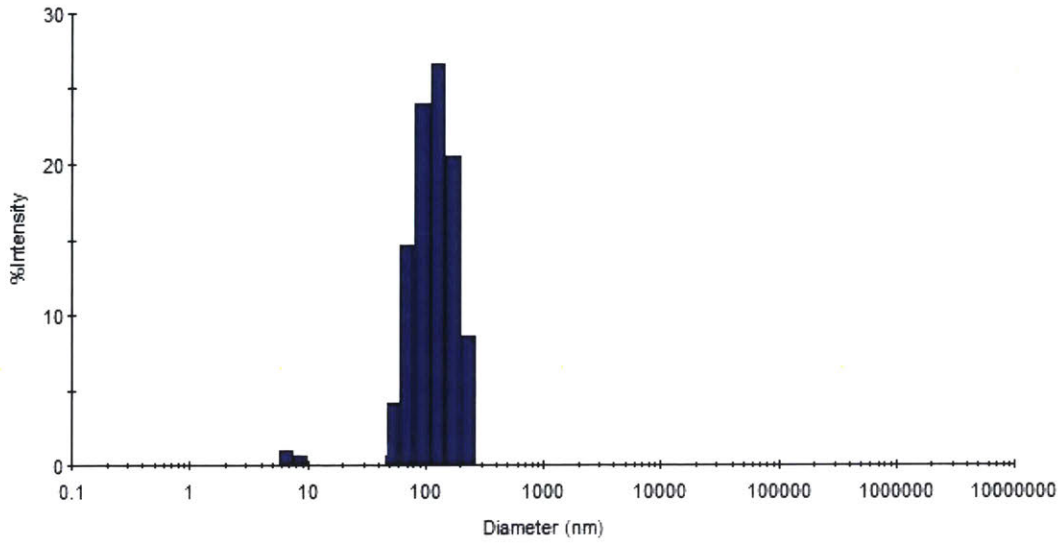


**Figure 2-16:** DLS histogram of the product of TEL-1 and TET-PEG in water.

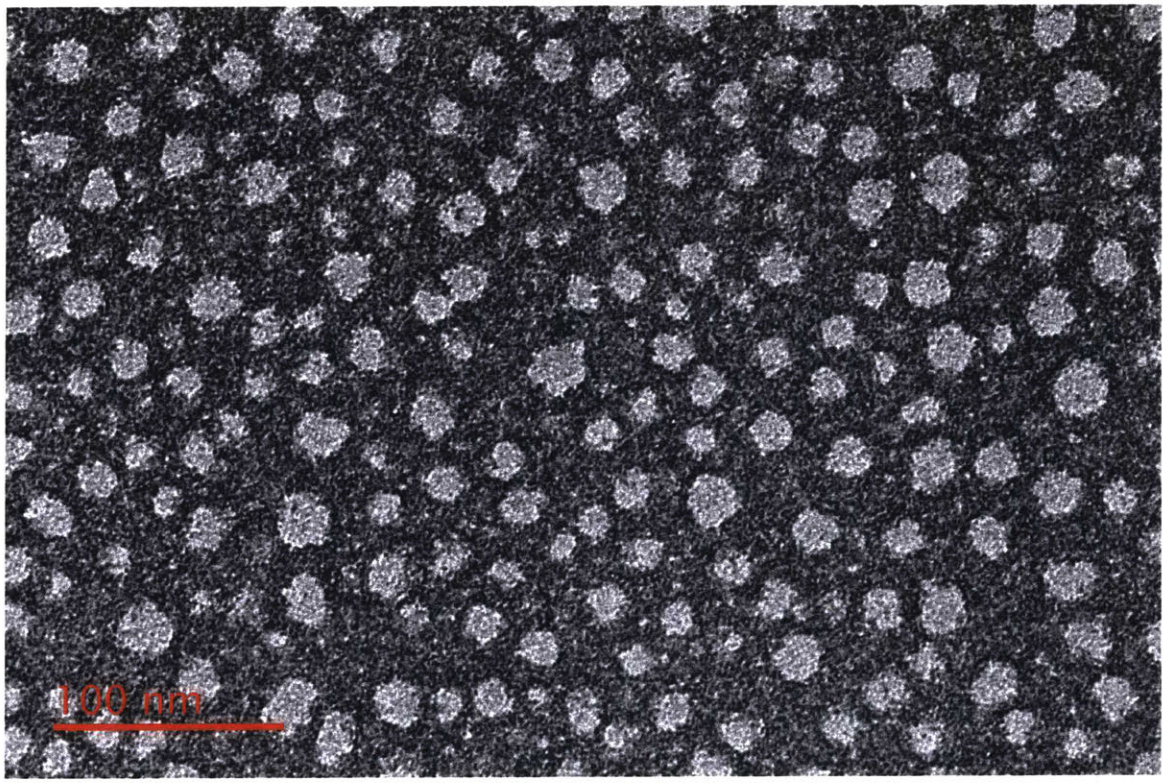


**Figure 2-17:** TEM image of TET-PEG. Particles appear uneven, with variable size.

## 2.4 References


(1) Bae, Y.; Nishiyama, N.; Fukushima, S.; Koyama, H.; Yasuhiro, M.; Kataoka, K. Preparation and biological characterization of polymeric micelle drug carriers with intracellular pH-triggered drug release property: tumor permeability, controlled subcellular drug distribution, and enhanced in vivo antitumor efficacy. *Bioconjug Chem* **2005**, *16*, 122–30.

(2) Cabral, H.; Matsumoto, Y.; Mizuno, K.; Chen, Q.; Murakami, M.; Kimura, M.; Terada, Y.; Kano, M. R.; Miyazono, K.; Uesaka, M.; Nishiyama, N.; Kataoka, K. Accumulation of sub-100 nm polymeric micelles in poorly permeable tumours depends on size. *Nat. Nanotechnol.* **2011**, *6*, 815–23.

(3) M.C., J.; Leroux, J. Polymeric micelles a new generation of colloidal drug carriers. *Eur. J. Pharm. Biopharm.* **1999**, 101–111.

(4) Maeda, H. The Tumor Blood-Vessel as an Ideal Target for Macromolecular Anticancer Agents. *J. Controlled Release* **1992**, *19*, 315–324.

(5) Maeda, H.; Seymour, L. W.; Miyamoto, Y. Conjugates of anticancer agents and polymers: advantages of macromolecular therapeutics in vivo. *Bioconjug Chem* **1992**, *3*, 351–62.

(6) Yokoyama, M. Polymeric micelles as drug carriers: their lights and shadows. *J Drug Target* **2014**, *22*, 576–83.

(7) Al-Achi, A.; Lawrence, J. Antoine Al-Achi and Jonathan Lawrence. Micelles: Chemotherapeutic Drug Delivery. Clin Pharmacol Biopharm;2(2):e114, 2013. *Clinical Pharmacology and Biopharmaceutics* **2013**, *2*, e114.

(8) Ventola, C. L. Progress in Nanomedicine: Approved and Investigational Nanodrugs. *P T* **2017**, *42*, 742–755.

(9) Blum, A. P.; Kammeyer, J. K.; Rush, A. M.; Callmann, C. E.; Hahn, M. E.; Gianneschi, N. C. Stimuli-responsive nanomaterials for biomedical applications. *J. Am. Chem. Soc.* **2015**, *137*, 2140–54.

(10) Kulthe, S. S.; Choudhari, Y. M.; Inamdar, N. N.; Mourya, V. Polymeric micelles: authoritative aspects for drug delivery. *Des. Monomers Polym.* **2012**, *15*, 465–521.

(11) Rapoport, N. Physical stimuli-responsive polymeric micelles for anti-cancer drug delivery. *Prog. Polym. Sci.* **2007**, *32*, 962–990.

(12) Israelachvili, J. N. Intermolecular and Surface Forces, 3rd Edition. *Intermolecular and Surface Forces, 3rd Edition* **2011**, 1–674.

(13) Nagarajan, R. In *Structure-Performance Relationships in Surfactants*, Esumi, K., Ueno, M., Eds., Second Edition; Marcel Dekker, Inc.: New York, NY, 2003.

(14) Israelachvili, J. N.; Mitchell, D. J.; Ninham, B. W. Theory of Self-Assembly of Hydrocarbon Amphiphiles into Micelles and Bilayers. *Journal of the Chemical Society-Faraday Transactions Ii* **1976**, *72*, 1525–1568.

(15) Kanamala, M.; Wilson, W. R.; Yang, M.; Palmer, B. D.; Wu, Z. Mechanisms and biomaterials in pH-responsive tumour targeted drug delivery: A review. *Biomaterials* **2016**, *85*, 152–67.

(16) Moghimi, S. M.; Hunter, A. C.; Murray, J. C. Long-circulating and target-specific nanoparticles: theory to practice. *Pharmacol. Rev.* **2001**, *53*, 283–318.

(17) Harnoy, A. J.; Buzhor, M.; Tirosh, E.; Shaharabani, R.; Beck, R.; Amir, R. J. Modular Synthetic Approach for Adjusting the Disassembly Rates of Enzyme-Responsive Polymeric Micelles. *Biomacromolecules* **2017**, *18*, 1218–1228.

(18) Alexandridis, P.; Holzwarth, J. F.; Hatton, T. A. Micellization of Poly(Ethylene Oxide)-Poly(Propylene Oxide)-Poly(Ethylene Oxide) Triblock Copolymers in Aqueous-Solutions - Thermodynamics of Copolymer Association. *Macromolecules* **1994**, *27*, 2414–2425.

(19) Zhang, L.; Eisenberg, A. Multiple Morphologies of "Crew-Cut" Aggregates of Polystyrene-b-poly(acrylic acid) Block Copolymers. *Science* **1995**, *268*, 1728–31.

(20) Zhang, L.; Yu, K.; Eisenberg, A. Ion-Induced Morphological Changes in "Crew-Cut" Aggregates of Amphiphilic Block Copolymers. *Science* **1996**, *272*, 1777–9.

(21) Liu, J.; Huang, Y.; Kumar, A.; Tan, A.; Jin, S.; Mozhi, A.; Liang, X. J. pH-sensitive nano-systems for drug delivery in cancer therapy. *Biotechnol. Adv.* **2014**, *32*, 693–710.

(22) Meng, F.; Zhong, Z.; Feijen, J. Stimuli-responsive polymersomes for programmed drug delivery. *Biomacromolecules* **2009**, *10*, 197–209.

(23) Rijcken, C. J.; Soga, O.; Hennink, W. E.; van Nostrum, C. F. Triggered destabilisation of polymeric micelles and vesicles by changing polymers polarity: an attractive tool for drug delivery. *J Control Release* **2007**, *120*, 131–48.

(24) Schmaljohann, D. Thermo- and pH-responsive polymers in drug delivery. *Adv Drug Deliv Rev* **2006**, *58*, 1655–70.

(25) Vaupel, P.; Kallinowski, F.; Okunieff, P. Blood flow, oxygen and nutrient supply, and metabolic microenvironment of human tumors: a review. *Cancer Res.* **1989**, *49*, 6449–65.

(26) Wike-Hooley, J. L.; Haveman, J.; Reinhold, H. S. The relevance of tumour pH to the treatment of malignant disease. *Radiother. Oncol.* **1984**, *2*, 343–66.

(27) York, A. W.; Kirkland, S. E.; McCormick, C. L. Advances in the synthesis of amphiphilic block copolymers via RAFT polymerization: stimuli-responsive drug and gene delivery. *Adv Drug Deliv Rev* **2008**, *60*, 1018–36.

(28) Jun, Y. J.; Toti, U. S.; Kim, H. Y.; Yu, J. Y.; Jeong, B.; Jun, M. J.; Sohn, Y. S. Thermoresponsive micelles from oligopeptide-grafted cyclotriphosphazenes. *Angew. Chem. Int. Ed. Engl.* **2006**, *45*, 6173–6.

(29) Chung, J. E.; Yokoyama, M.; Aoyagi, T.; Sakurai, Y.; Okano, T. Effect of molecular architecture of hydrophobically modified poly(N-isopropylacrylamide) on the formation of thermoresponsive core-shell micellar drug carriers. *J Control Release* **1998**, *53*, 119–30.

(30) Chung, J. E.; Yokoyama, M.; Okano, T. Inner core segment design for drug delivery control of thermo-responsive polymeric micelles. *J Control Release* **2000**, *65*, 93–103.

(31) Kujawa, P.; Watanabe, H.; Tanaka, F.; Winnik, F. M. Amphiphilic telechelic poly(N-isopropylacrylamide) in water: from micelles to gels. *Eur Phys J E Soft Matter* **2005**, *17*, 129–37.

(32) Nakayama, M.; Okano, T.; Miyazaki, T.; Kohori, F.; Sakai, K.; Yokoyama, M. Molecular design of biodegradable polymeric micelles for temperature-responsive drug release. *J Control Release* **2006**, *115*, 46–56.

(33) Neradovic, D.; Soga, O.; Van Nostrum, C. F.; Hennink, W. E. The effect of the processing and formulation parameters on the size of nanoparticles based on block copolymers of poly(ethylene glycol) and poly(N-isopropylacrylamide) with and without hydrolytically sensitive groups. *Biomaterials* **2004**, *25*, 2409–2418.

(34) Wei, H.; Zhang, X. Z.; Zhou, Y.; Cheng, S. X.; Zhuo, R. X. Self-assembled thermoresponsive micelles of poly(N-isopropylacrylamide-b-methyl methacrylate). *Biomaterials* **2006**, *27*, 2028–34.

(35) Amir, R. Enzyme-Responsive PEG–Dendron Hybrids as a Platform for Smart Nanocarriers. *Synlett* **2015**, *26*, 2617–2622.

(36) Ma, N.; Li, Y.; Ren, H.; Xu, H.; Li, Z.; Zhang, X. Selenium-containing block copolymers and their oxidation-responsive aggregates. *Polym. Chem.* **2010**, *1*, 1609.

(37) Napoli, A.; Valentini, M.; Tirelli, N.; Müller, M.; Hubbell, J. A. Oxidation-responsive polymeric vesicles. *Nat. Mater.* **2004**, *3*, 183–189.

(38) Li, J.; Huo, M.; Wang, J.; Zhou, J.; Mohammad, J. M.; Zhang, Y.; Zhu, Q.; Waddad, A. Y.; Zhang, Q. Redox-sensitive micelles self-assembled from amphiphilic hyaluronic acid-deoxycholic acid conjugates for targeted intracellular delivery of paclitaxel. *Biomaterials* **2012**, *33*, 2310–20.

(39) Sun, L.; Liu, W.; Dong, C. M. Bioreducible micelles and hydrogels with tunable properties from multi-armed biodegradable copolymers. *Chem Commun (Camb)* **2011**, *47*, 11282–4.

(40) Cabrini, S.; Rupp, B.; Mokari, T.; Bauer, T.; Slugovc, C. Thiol-ene reaction as tool for crosslinking of polynorbornene micelles in the nanoscale. **2009**, *7393*, 73930Y.

(41) Desai, R. M.; Koshy, S. T.; Hilderbrand, S. A.; Mooney, D. J.; Joshi, N. S. Versatile click alginate hydrogels crosslinked via tetrazine-norbornene chemistry. *Biomaterials* **2015**, *50*, 30–7.

(42) Carboni, R.; Lindsey, R. Reactions of Tetrazines with Unsaturated Compounds. **1959**.

(43) Jewett, J. C.; Bertozzi, C. R. Cu-free click cycloaddition reactions in chemical biology. *Chem. Soc. Rev.* **2010**, *39*, 1272.

(44) Blackman, M. L.; Royzen, M.; Fox, J. M. Tetrazine ligation: fast bioconjugation based on inverse-electron-demand Diels-Alder reactivity. *J. Am. Chem. Soc.* **2008**, *130*, 13518–9.

(45) Devaraj, N. K.; Weissleder, R.; Hilderbrand, S. A. Tetrazine-based cycloadditions: application to pretargeted live cell imaging. *Bioconjug Chem* **2008**, *19*, 2297–9.

(46) Liu, D. S.; Tangpeerachaikul, A.; Selvaraj, R.; Taylor, M. T.; Fox, J. M.; Ting, A. Y. Diels-Alder cycloaddition for fluorophore targeting to specific proteins inside living cells. *J. Am. Chem. Soc.* **2012**, *134*, 792–5.

(47) Alge, D. L.; Azagarsamy, M. A.; Donohue, D. F.; Anseth, K. S. Synthetically tractable click hydrogels for three-dimensional cell culture formed using tetrazine-norbornene chemistry. *Biomacromolecules* **2013**, *14*, 949–53.

(48) Zhou, H.; Woo, J.; Cok, A. M.; Wang, M.; Olsen, B. D.; Johnson, J. A. Counting primary loops in polymer gels. *Proc. Natl. Acad. Sci. U.S.A.* **2012**, *109*, 19119–24.

(49) Fairbanks, B. D.; Schwartz, M. P.; Halevi, A. E.; Nuttelman, C. R.; Bowman, C. N.; Anseth, K. S. A Versatile Synthetic Extracellular Matrix Mimic via Thiol-Norbornene Photopolymerization. *Adv. Mater.* **2009**, *21*, 5005–10.

(50) Kawamoto, K.; Grindy, S. C.; Liu, J.; Holten-Andersen, N.; Johnson, J. A. Dual Role for 1,2,4,5-Tetrazines in Polymer Networks: Combining Diels-Alder Reactions and Metal Coordination To Generate Functional Supramolecular Gels. *ACS Macro Lett.* **2015**, *4*, 458–461.

(51) Gao, A. X.; Liao, L. Y.; Johnson, J. A. Synthesis of Acid-Labile PEG and PEG-Doxorubicin-Conjugate Nanoparticles via Brush-First ROMP. *ACS Macro Lett.* **2014**, *3*, 854–857.

# Chapter 3

# Synthesis of polymers by iterative exponential growth

## 3.1 Introduction

While pursuing the same functionality as natural biopolymers such as DNA, RNA, proteins, and sugars, researchers have attempted to emulate the same sequence control seen in nature.[1] Let's take deoxyribonucleic acid, DNA, as an example. DNA contains four key monomer units known as nucleotides. Variations in the sequence of nucleotides across the length of a DNA strand define the primary sequence. This primary sequence determines how the strand folds into a secondary structure, and interacts with other molecules in a tertiary structure.[2,3] Biopolymers with absolute sequence control leading to structural control result in the genetic storage and biological machines required for life itself.[4–6]

Absolute control over polymer synthesis, although achieved for very particular subsets of polymers, remains a key challenge of polymer science.[1,7] Living polymerization methods and statistical polymerization methods have been used in conjunction to produce polymers on the kilogram scale with control over polymer dispersity and molecular weight. Atom transfer radical polymerization (ATRP),[8] reversible addition-fragmentation chain-transfer (RAFT),[9] and nitroxide-mediated polymerization (NMP)[10] offer superb control over polymer molecular weight and dispersity, without tacticity or sequence control. Ring-opening metathesis polymerization (ROMP)[11] offers a narrow distribution in molecular weight, a high tolerance for functional groups, and has been used to create polymers with structural control from the preorganization of monomers on a kilogram scale.

Methods taking advantage of kinetic phenomena[12–15] in conjunction with living polymerizations have an advantage in scalability, but suffer from a lack of absolute control, depend upon the specific structure of the monomers used, and are difficult to generalize. Methods using templation,[16–18] preorganization of monomers,[19–25] or repetitive monomer addition[26–30] have been developed for the synthesis of well-defined polymers, however these methods suffer from scalability concerns in addition to poor atom economy, complex monomer synthesis, and a lack of complete control.

Solid phase synthesis has been used to mimic the production of biopolymers with

absolute control on a limited scale.[31–33] The original resins were developed by Merrifield in the early 1960's,[34] and produces sequence defined polymers with an arbitrary sequence or structure. These methods have been used to produce sequence controlled polypeptides,[35] polynucleotides,[36] and non-natural synthetic polymers,[7] and have found use on the industrial scale to produce mail-order sequence-controlled oligonucleotides and oligopeptides. The requisite addition and unmasking steps along with any potential end-capping steps required for each monomer addition during solid phase synthesis traditionally require a large excess of reagent, resulting in poor atom economy and limiting the final product yield.[37–39]

No single method stands apart for the ability to produce polymers with absolute control over sequence, length, architecture, and stereochemistry while maintaining scalability.

In order to produce sequence-controlled polymers with a scalable, generalizable method, the Johnson group turned to iterative exponential growth (IEG). Iterative exponential growth, often called divergent convergent growth, uses orthogonal deprotections followed by a highly efficient reaction to couple $\alpha$,$\omega$-end- functionalized intermediates, doubling the chain length with each coupling cycle.[40–51] Iterative exponential growth allows for degrees of polymerization in excess of 100 to be reached in 7 cycles.[52] Whiting first explored this strategy in the context of Wittig coupling chemistry, where the orthogonal end-chain protecting groups of choice were a bromide and an aldehyde masked as an acetal group.[53] Historically, IEG polymerization has focused on making polymers with which to elucidate structure property relationships.[54–56] These materials often suffered from solubility issues that limited molecular weight.[57] Syntheses focused on improving molecular weights opposed to broadening the tool box of available monomers, showing length but not sequence control.[47,58–60] Stereochemistry was rarely considered.[52] Yields often suffered due to repetitive cycles with low yield.[61] By increasing the available monomers available for an iterative exponential growth process, it is possible to generate not only a single length defined polymer, but an unlimited series of sequence-defined polymers that cannot be prepared through statistical methods on a scale in excess of common solid phase

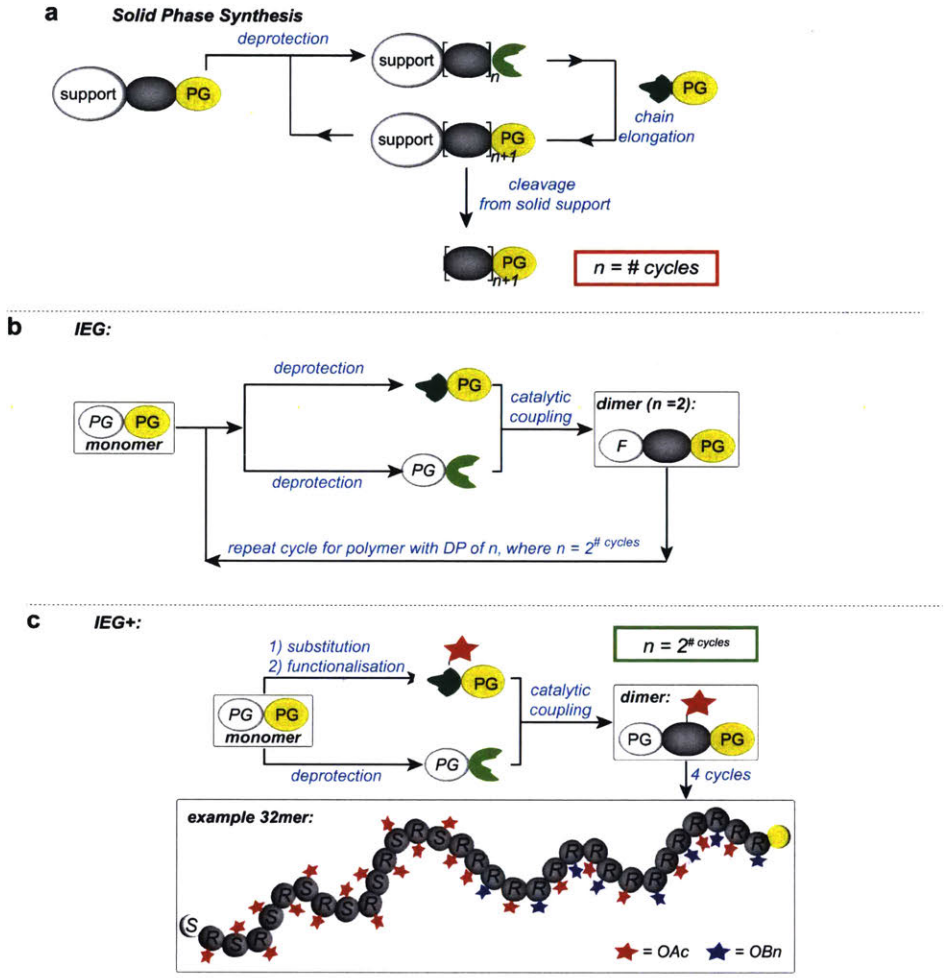


**Figure 3-1:** a) Traditional solid phase synthesis allows for the production of sequence-defined polymers, while requiring an excess of all reagents to ensure complete conversion, a full cycle for each monomer addition, and are difficult to scale. Here, PG represent orthogonal protecting groups, and $n$ the degree of polymerization. b) IEG uses orthogonally protected monomers that can go through divergent, convergent cycles of deprotection and catalytic coupling to produce sequence-defined polymers that grow in an exponential manner with the degree of polymerization doubling each cycle. Historically, these polymers have suffered from a lack of monomer diversity. Here, PG is used to indicate orthogonal protecting groups, DP and $n$ the degree of polymerization. c) IEG+ orthogonally protected monomers that can go through divergent, convergent cycles of deprotection and copper catalyzed click chemistry as coupling to produce sequence-defined polymers that grow in an exponential manner with the degree of polymerization doubling each cycle. Here, within each cycle, a side chain is produced allowing for a library of potential side chains. Each monomer has a stereocenter, allowing for stereochemical control. PG is used to represent orthogonal protecting groups, while DP and $n$ refer to the degree of polymerization. S and R refer to the chirality associated with each monomer subunit.

syntheses.

In this chapter, IEG+, an IEG polymerization unmasking a stereogenic side chain functionality within each cycle, is discussed. Polymers with molecular weights in excess of 6,000g/mol with controlled stereochemistry were made on 100 mg scales in a matter of days. A library of side chain functionalities expands the potential for these sequence defined polymers, as do alternate coupling chemistries and chain end functionalizations.

## 3.2 Results and Discussion

A schematic view of 'IEG plus side-chain functionalization' (IEG+) is shown in Figure 3-1c. The relevant chemical structures are shown in Figure 3-2. The IEG+ cycle begins with an enantiopure TBDMS-protected glycidyl propargyl ether. This monomer can be deprotected in two ways: (a) the TBDMS protected alkyne can be umasked quantitatively through reaction with tetrabutylammonium fluoride or a similar fluoride source, and (b) the epoxide can be opened through a nucleophilic attack with sodium azide revealing an alcohol. The newly revealed 2° alcohol can be further functionalized (c), serving as a handle which with to incorporate a side chain functional group in each and every IEG+ cycle. To complete the cycle, the differentially unmasked monomers can be recombined and coupled through (d) copper catalyzed alkyne-azide cycloaddition, often referred to as CuAAC, to produce the IEG+ dimer. CuAAC ćlickćhemistry has the advantage of quantitative or nearly quantitative yields, high functional group and solvent tolerance, stereospecificity, high atom economy, and minimal side reactions.[62,63] The two deprotections, side chain functionalization, and click (steps a-d) together make a single IEG+ cycle.

The monomer used to begin the IEG+ cycle, TBDMS-protected glycidyl propargyl ether, can be synthesized in two steps on a multigram scale from epichlorohydrin (99.9% enantiopure) and propargyl chloride, followed by protection of the alkyne with tert-butyldimethylsilyl chloride.

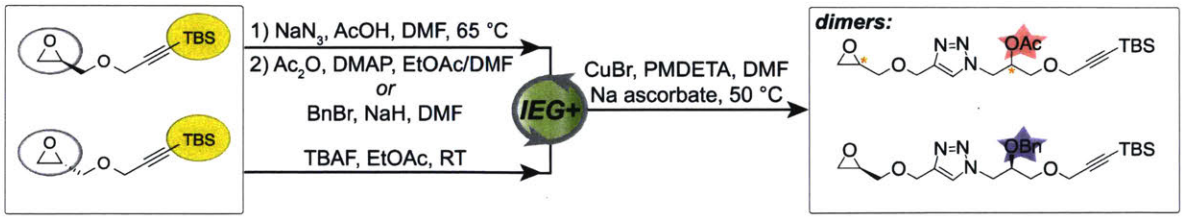


**Figure 3-2:** Shown here is one cycle of IEG+, beginning with the two enantiomeric TBDMS-protected glycidyl propargyl ether which can be differentially deprotected through azidification or desilylation, the functionalization of the unmasked alcohol after azidification, and the CuAAC click reaction to dimerize monomers. The dimer structure is dependent upon the sidechain functionalization and stereochemistry chosen, allowing for a high level of sequence control.

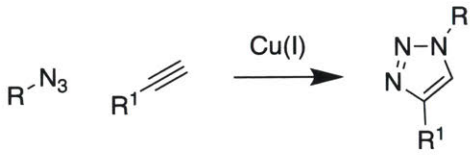


**Figure 3-3:** Shown above is a generic copper catalyzed alkyne-azide cycloaddition (CuAAC), producing a 1,4 disubstituted triazole.

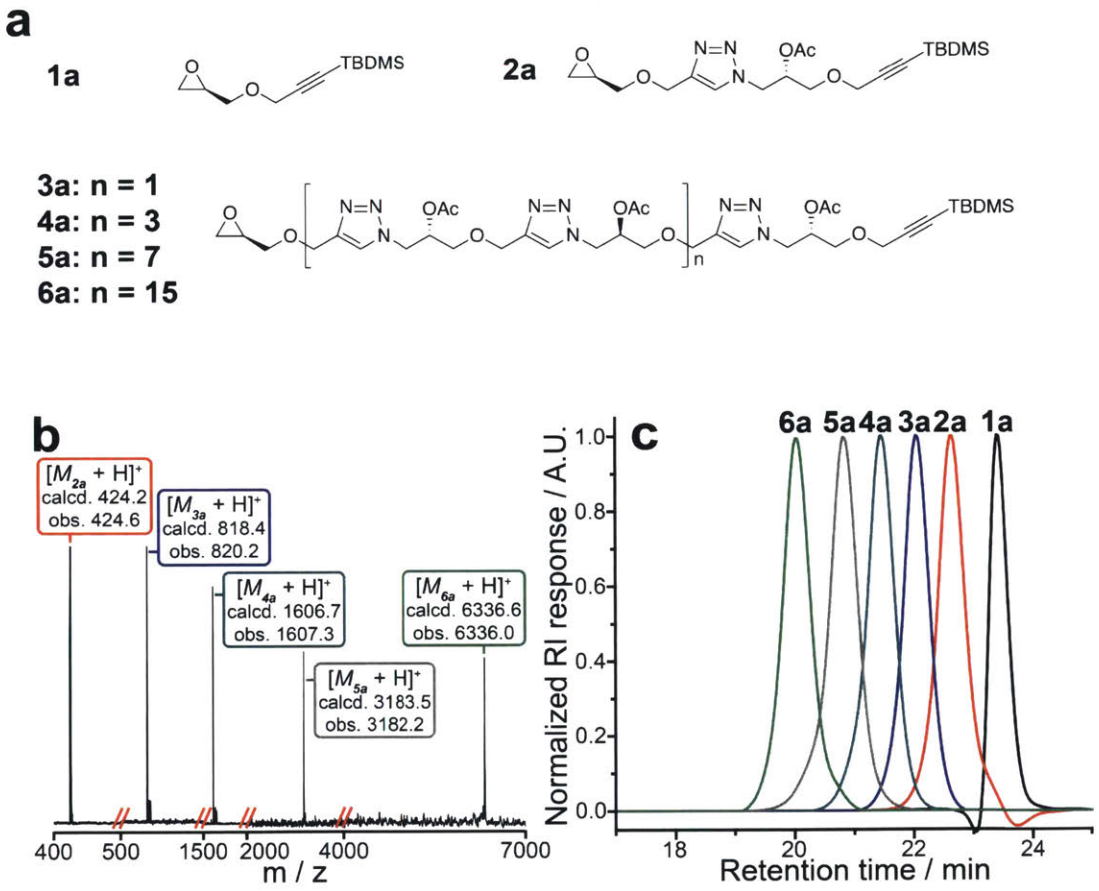


**Figure 3-4:** a) Chemical structures for the syndiotactic acetyl protected monomer up to hexadecamer are shown. b) MALDI characterization of the acetyl protected dimer up to hexadecamer show the control over molecular weight afforded by the IEG+ system. c)GPC traces of the acetyl protected dimer up to hexadecamer show the control over molecular weight afforded by the IEG+ system.

Epoxide opening was performed with excess $NaN_3$ at 65°C under acidic conditions in dimethyl formamide, to make the azido-alcohol $N_3-OH$. Excess sodium azide was removed through precipitation in ethyl acetate before further functionalizations. The newly exposed 2° alcohol was functionalized with an acetyl group for the initial series of IEG+ polymers using an excess of acetic anhydride and catalytic 4-dimethylaminopyridine for 10 minutes, forming $N_3-OAc$ in an 89% isolated yield. Alkyne deprotection was performed in EtOAc with 1.05 equiv. of a 1.0 M tetrabutylammonium fluoride (TBAF) in tetrahydrofuran to produce the alkyne in 93% isolated yield. The deprotected products were coupled in a 1 to 1 stoichiometric ratio with 5 mol% CuBr, 10 mol% N,N,N′,N″, N‴-pentamethyldiethylenetriamine (PMDETA) and 10 mol% sodium ascorbate in DMF at 50°C for 2 h to form the dimer in 86% isolated yield after silica gel chromatography.

Repetition of the IEG+ cycle produced a tetramer in a total average isolated yield of 68%, the octamer (73% IEG+ cycle yield), and the hexadecamer (63% IEG+ cycle yield). The CuAAC coupling gave a slightly decreased yield with each cycle, typical for a a CuAAC reaction on poly(triazoles).

$^1H$ NMR spectra of the IEG+ oligomers showed characteristic triazole proton signals (~7.65 ppm) and acetyl methine proton signals (~5.25 ppm) in the correct ratios to the propargylic methylene signals (~4.20 ppm), silyl protecting group signals and epoxide proton signals. Matrix-assisted laser desorption ionization (MALDI) mass spectra and gel permeation chromatography (GPC) data was used to confirm the unimolecular nature of these oligomers. Both syndiotactic and isotactic polymers were developed.

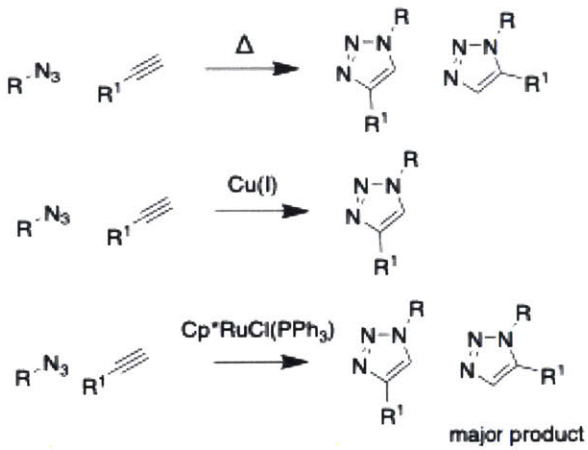


**Figure 3-5:** The original Huisgen azide-alkyne cycloadditions produced a mixture of 1,4 and 1,5 triazoles, whereas CuAAC and RuAAC can be regioselective depending upon the substrate and catalyst used.

Although the original IEG+ system relied on copper-catalyzed alkyne-azide cycloaddition (CuAAC) as the coupling reaction to polymerize IEG+ materials, selectively producing 1,4 , other high yielding azide alkyne coupling reactions are available. Huisgen azide-alkyne cycloadditions produce a mixture of 1,4 and 1,5 triazoles as seen in figure 5.[64] Ruthenium catalyzed alkyne azide cycloaddition (RuAAC) can be used to selectively produce 1,5 triazoles, as C-N bond formation occurs between the more electronegative and less sterically demanding carbon of the alkyne and the terminal azide nitrogen.[65]

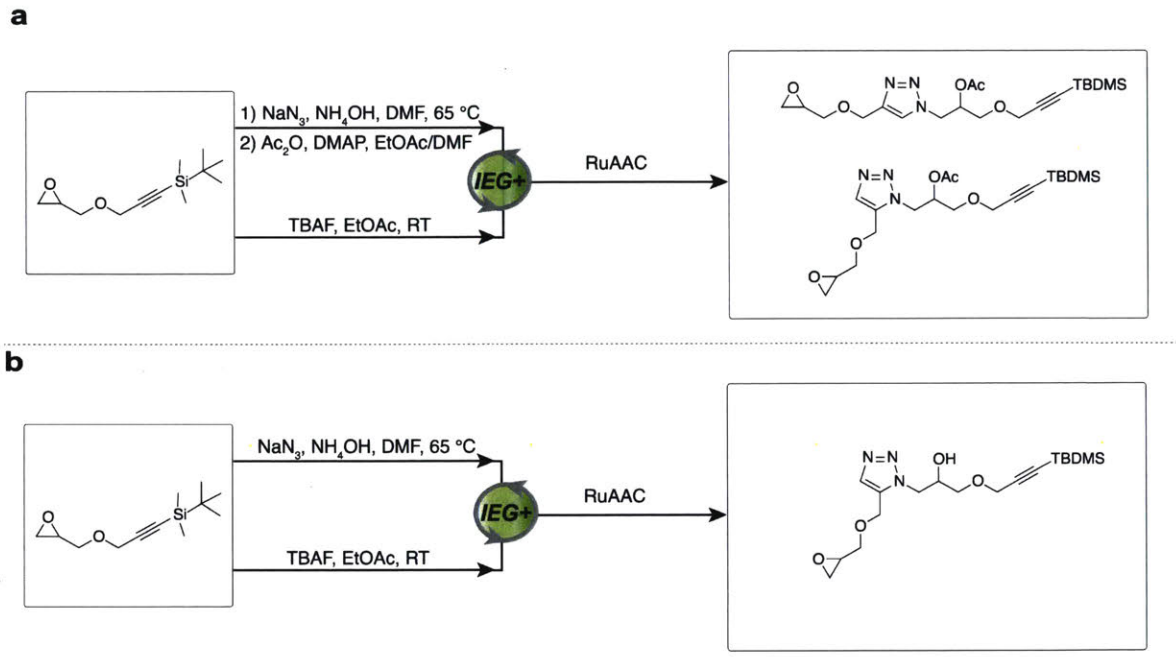


**Figure 3-6:** a) RuAAC to form the acetyl protected IEG+ dimer, 2a, and b) RuAAC to form the IEG+ dimer with alcohol side chain. Only case b was shown to be regioselective.

The incorporation of a 1,5 triazole into the backbone of an IEG+ polymer will result in a kink in the backbone, changing the conformation of the polymer, and thus its physical properties. Controlling the regioselectivity of the IEG+ polymerization will provide yet another method (in addition to sequence control, stereochemistry, and molecular weight control) to tune the structure and properties of the final material on a molecular level.

RuAAC was performed on a series of IEG+ monomers and dimers. The ratio between 1,4 and 1,5 triazoles was monitored by NMR. Most of the systems tested showed a mixture of regiochemistries, however the naked alcohol side chain was notable for forming 1,5 triazoles based dimers regioselectively. Unfortunately, this trend did not continue for the higher order structures tested.

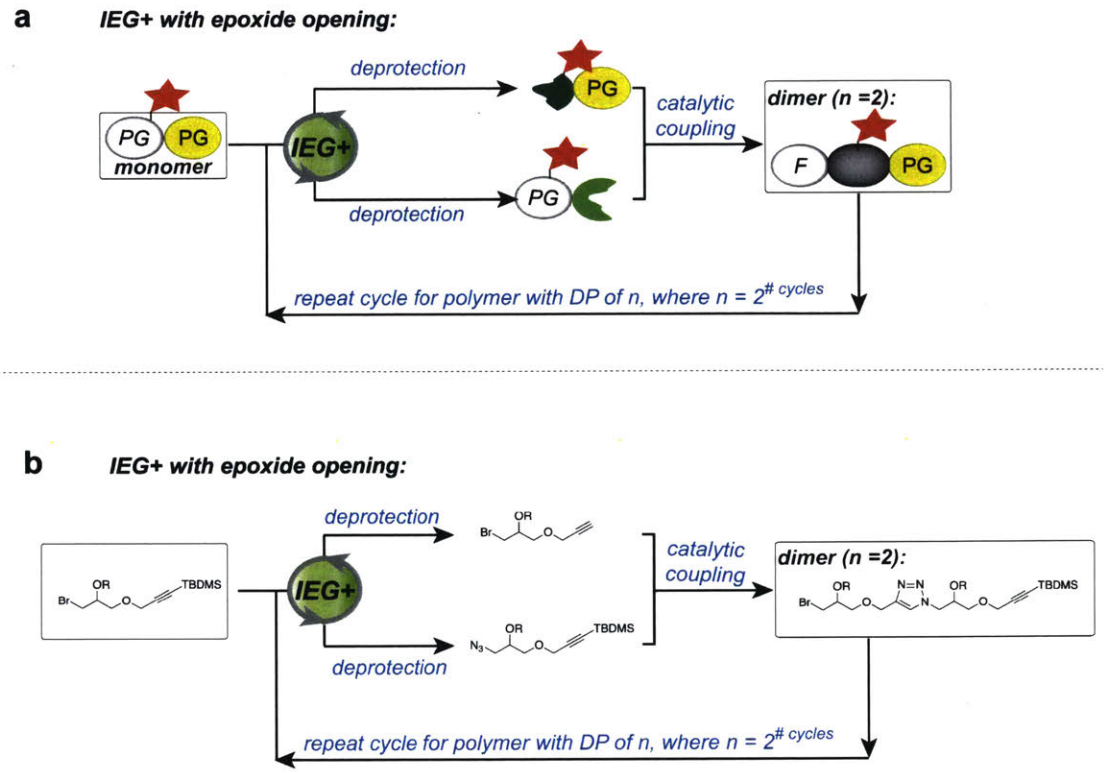


**Figure 3-7:** a) A modified version of IEG+ is shown. Previous iterations revealed a new side chain to functionalize at each and every step of the IEG+ cycle. This iteration provides the opportunity to functionalize the side chains prior to the start of the IEG+ cycle, allowing for the use of lower yielding functionalization chemistries. b) Chemical structures in the IEG+ cycle show the modifications made. Here, the possible side chains are shown as an –OR group in the starting monomer.

At each and every IEG+ cycle, a secondary alcohol is produced, allowing for functionalization. Unfortunately, the high yields required to sustainably make large IEG+ polymers severely limit the types of functionalization chemistries that can be used. Functionalization prior to the IEG+ polymerization minimizes these issues, and allows the use of lower yielding chemistries for functional group addition. In order to functionalize all monomers prior to IEG+, lithium bromide was used to facilitate epoxide opening. After side chain functionalization, azide substitution of the bromide serves as a deprotection step for the IEG+ cycle.

## 3.3 Conclusions

IEG+, a divergent convergent method for the production of precision macromolecules with controlled length, sequence, and stereochemistry was described. Polymers of over 3.000 g/mol were synthesized using these techniques. Further control was provided through the use of RuAAC to modify polymeric backbones and a modified monomer that allowed for side chain functionalization prior to polymerization.

## 3.4 Experimental Methods

### 3.4.1 Materials and General Methods

All reagents were purchased from commercial sources and used without further purification unless stated otherwise.

#### Instrumentation

Liquid chromatography-mass spectrometry (LC-MS) was performed on an Agilent 1260 instrument with an Agilent 6130 single quadrupole mass spectrometer and an Advanced Materials Technology Halo C18 (HALO) column using a binary solvent system of acetonitrile and 0.1% acetic acid in water.

Gel permeation chromatography was performed on an Agilent 1260 instrument with two Agilent PLGel mixed C columns in series, a 0.025 M lithium bromide in dimethylformamide mobile phase run at 60 celsius, a Wyatt Optilab T-rEX detector, and a Wyatt Heleos II detector.

Column chromatography was carried out on silica gel 60F (EMD Millipore, 0.040-0.063 mm).

$^{1}$H nuclear magnetic resonance ($^{1}$H-NMR) and $^{13}$C nuclear magnetic resonance ($^{13}$C-NMR) spectra were recorded on Bruker AVANCE-400 NMR spectrometers in the Department of Chemistry Instrumentation Facility at MIT. Chemical shifts are reported in ppm relative to the signals corresponding to residual non-deuterated solvents: $CDCl_3$: $\delta$H = 7.26 ppm, DMSO-d6: $\delta$H = 2.50 ppm. Spectra were analyzed on MestReNova NMR software.

Matrix-assisted laser desorption/ionization-time of flight (MALDI-TOF) mass spectra were measured on a Bruker model MicroFlex instrument using $\alpha$-cyano-4-hydroxycinnamic acid as the matrix.

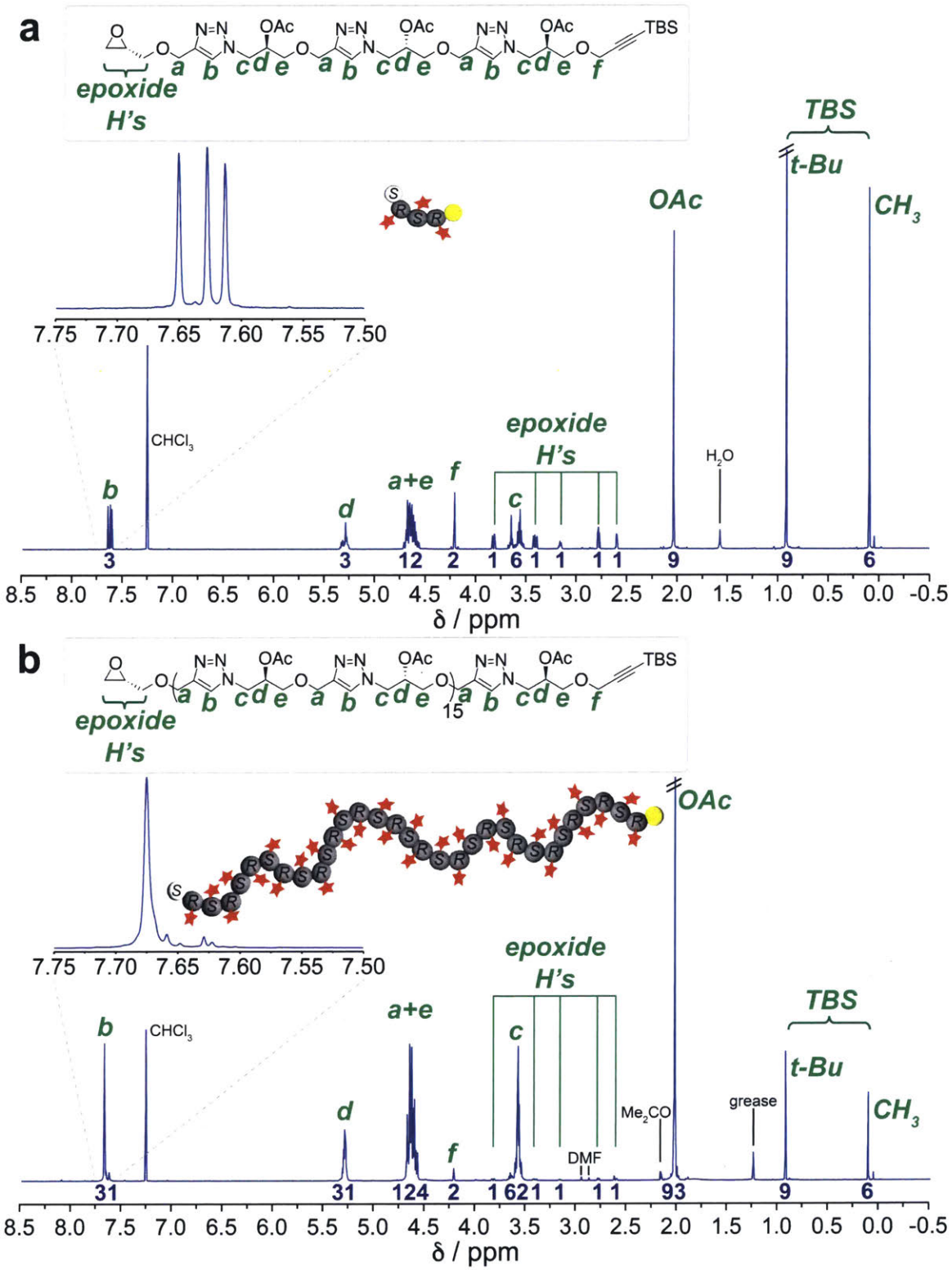


**Figure 3-8:** A) The $^{1}$H NMR spectrum of a syndiotactic tetramer after two cycles of IEG+ shows the $^{1}$H NMR spectra of the IEG+ oligomers showed characteristic triazole proton signals (~7.65 ppm) and acetyl methine proton signals (~5.25 ppm) in the correct ratios to the propargylic methylene signals (~4.20 ppm), silyl protecting group signals and epoxide proton signals. B) The $^{1}$H NMR spectrum of a syndiotactic hexadecamer

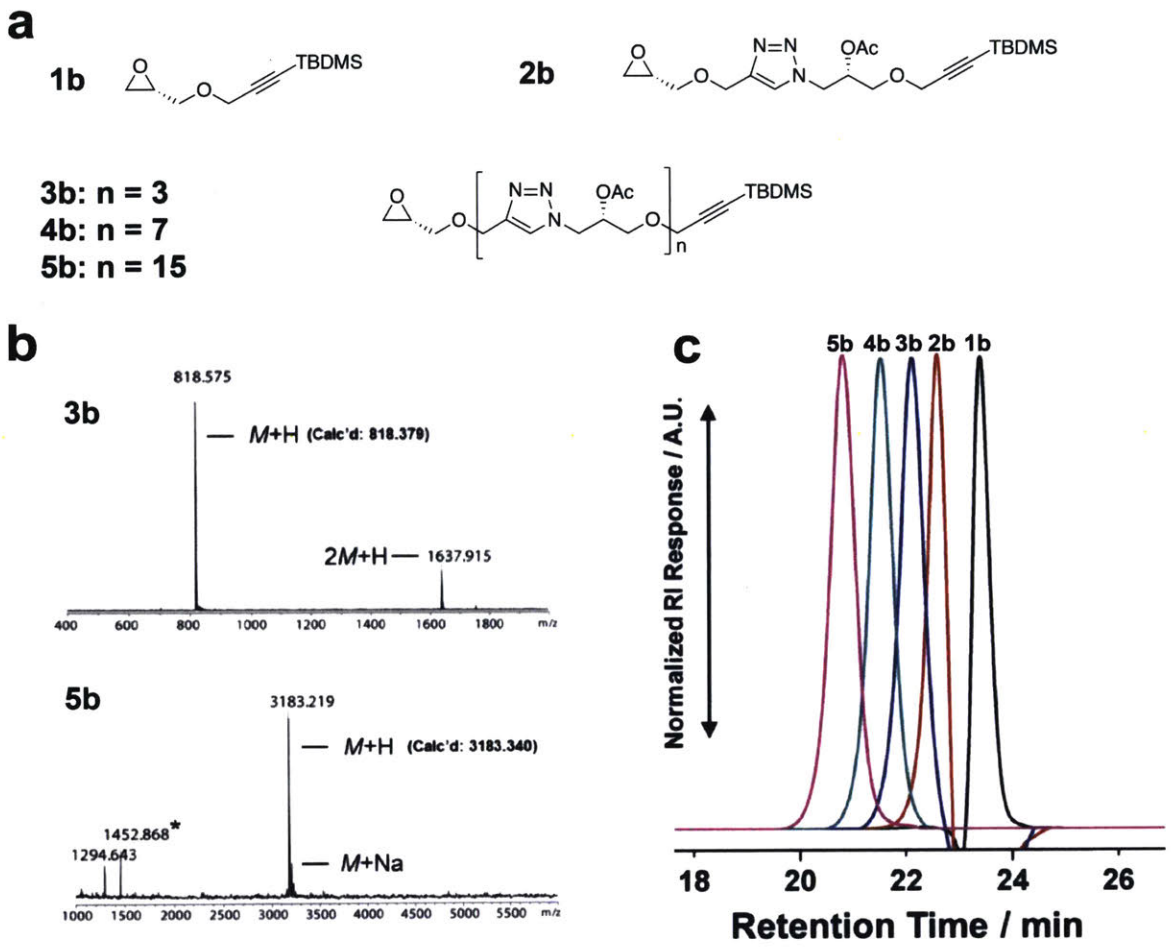


**Figure 3-9:** a) Chemical structures for the isotactic acetyl protected monomer up to hexadecamer are shown. b) MALDI characterization of the acetyl protected dimer and hexadecamer show the control over molecular weight afforded by the IEG+ system. c)GPC traces of the acetyl protected dimer up to hexadecamer show the control over molecular weight afforded by the IEG+ system.

### Synthetic Protocols

Procedures for the synthesis of IEG+ monomers and oligomers were conducted following previously reported procedures.[66] A preparation for enantiopure GPE can be found in the following references.[67,68] RuAAC was conducted using a protocol from Boren et al.[65]

**Standard Lithium Bromide Epoxide Opening Conditions**

Synthesis of 1-bromo-3-(prop-2-yn-1-yloxy)propan-2-yl acetate

Lithium bromide (3.18g, 35.5 mmol) and 20 mL of acetone were added to a scintillation vial and stirred until thoroughly dissolved. Glycidyl propargyl ether(1.0mL, 8.8mmol) and acetic acid (0.51mL, 8.8 mmol) were added dropwise. After reaction overnight, solvent was removed under vacuum, the sample was dissolved in ethyl acetate and extracted twice into water and once into brine. DMAP (0.54g, 4.42 mmol), and acetic anhydride (1.68mL, 17.7mmol) were added dropwise to the ethyl acetate solution. After two hours, the reaction was washed with 10% HCl, then water, then brine, and dried with sodium sulfate prior to concentration under vacuum. A yellow oil was isolated in 89.5% overall yield (1.85g).

NMR Data for 1-bromo-3-(prop-2-yn-1-yloxy)propan-2-ol

$^{1}$H NMR (300 MHz, $CDCl_3$) $\delta$ 4.20 (d, J = 2.4 Hz, 2H), 4.05-3.95 (m, 1H), 3.70 - 3.61 (m, 2H), 3.59-3.40 (m, 2H), 2.47 (dd, J = 2.3 Hz, 1H).

$^{13}$C NMR (75 MHz, $CDCl_3$) $\delta$ 79.31 , 75.34 , 71.36 , 70.02 , 58.90 , 35.18 .

NMR Data for 1-bromo-3-((3-(tert-butyldimethylsilyl)prop-2-yn-1-yl)oxy)propan-2-ol

$^{1}$H NMR (300 MHz, $CDCl_3$) $\delta$ 4.21 (s, 2H), 3.99 (p, J = 5.3 Hz, 1H), 3.73-3.57 (m, 2H), 3.57-3.40 (m, 2H), 2.16 (s, 1H), 1.01 - 0.81 (m, 10H), 0.20 - 0.02 (m, 6H).

$^{13}$C NMR (75 MHz, $CDCl_3$) $\delta$ 101.63 , 90.76 , 71.11 , 70.04 , 59.64 , 35.20 , 31.14 , 26.25 , 16.66 , -4.49.

NMR Data for 1-bromo-3-(prop-2-yn-1-yloxy)propan-2-yl acetate

$^{1}$H NMR (300 MHz, $CDCl_3$) $\delta$ 5.13 (tt,, J = 5.5, 4.7 Hz, 2H), 4.18 (dd, J = 2.4, 0.5 Hz, 4H), 3.84- 3.64 (m, 4H), 3.64 -3.43 (m, 4H), 2.46 (td, J = 2.4, 0.5 Hz, 2H), 2.25 - 2.07 (m, 7H), 2.02 (dd, J = 27.7, 0.5 Hz, 1H), 1.49 (s, 1H).

$^{13}C$ NMR (75 MHz, $CDCl_3$) $\delta$ 170.29 , 79.17 , 75.36 , 71.33 , 68.77 , 58.86 , 30.70 , 21.16.

NMR Data for 1-bromo-3-((3-(tert-butyldimethylsilyl)prop-2-yn-1-yl)oxy)propan-2-yl acetate

$^1H$ NMR (300 MHz, $CDCl_3$) $\delta$ 5.20 -5.07 (m, 1H), 4.19 (d, J = 0.5 Hz, 2H), 3.74 (ddd, J = 4.8, 1.8, 0.5 Hz, 2H), 3.59 (ddd, J = 10.7, 5.5, 0.5 Hz, 1H), 3.55 ? 3.44 (m, 1H), 2.26 - 1.98 (m, 7H), 1.25 (td, J = 7.2, 0.5 Hz, 1H), 1.01 - 0.82 (m, 12H), 0.17 - 0.03 (m, 7H).

$^{13}C$ NMR (75 MHz, $CDCl_3$) $\delta$ 170.29 , 166.58 , 101.48 , 90.78 , 71.44 , 68.51 , 59.56 , 30.68 , 27.55 , 26.24 , 22.38 , 21.15 , 16.64 , -4.50.

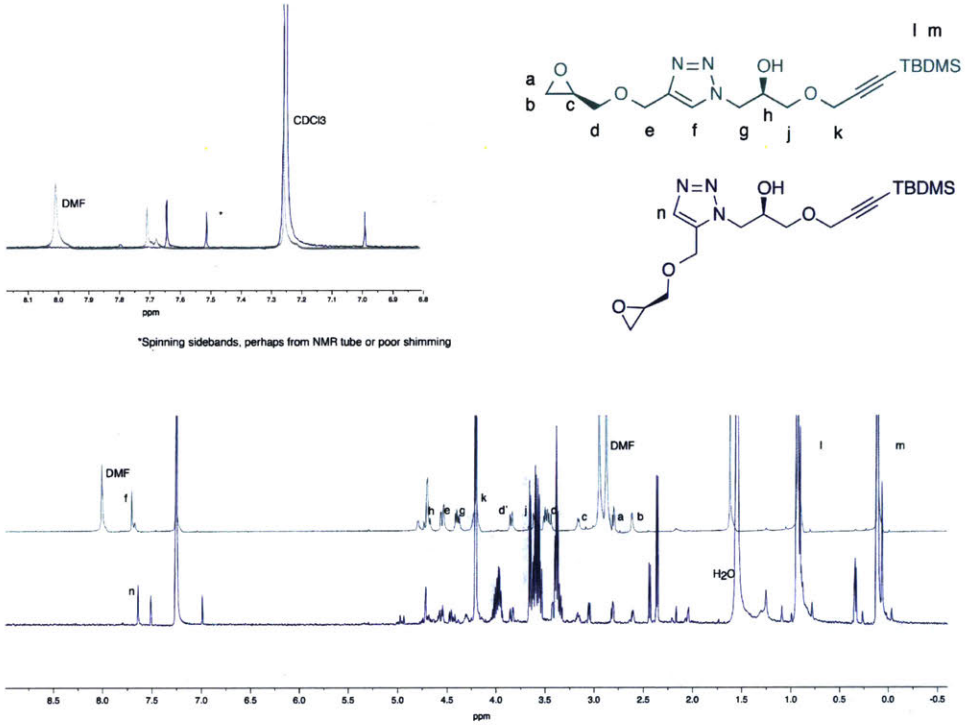


**Figure 3-10:** $^{1}$H NMR spectrum of the 1,4 triazole based dimer from CuAAC is shown in teal. A chararcteristic shift of the triazole signal is seen with RuAAC coupling chemistry, suggesting the formation of a 1,5 triazole (blue). No remaining trace of the 1,4 triazole is seen here, suggesting a regioselective reaction

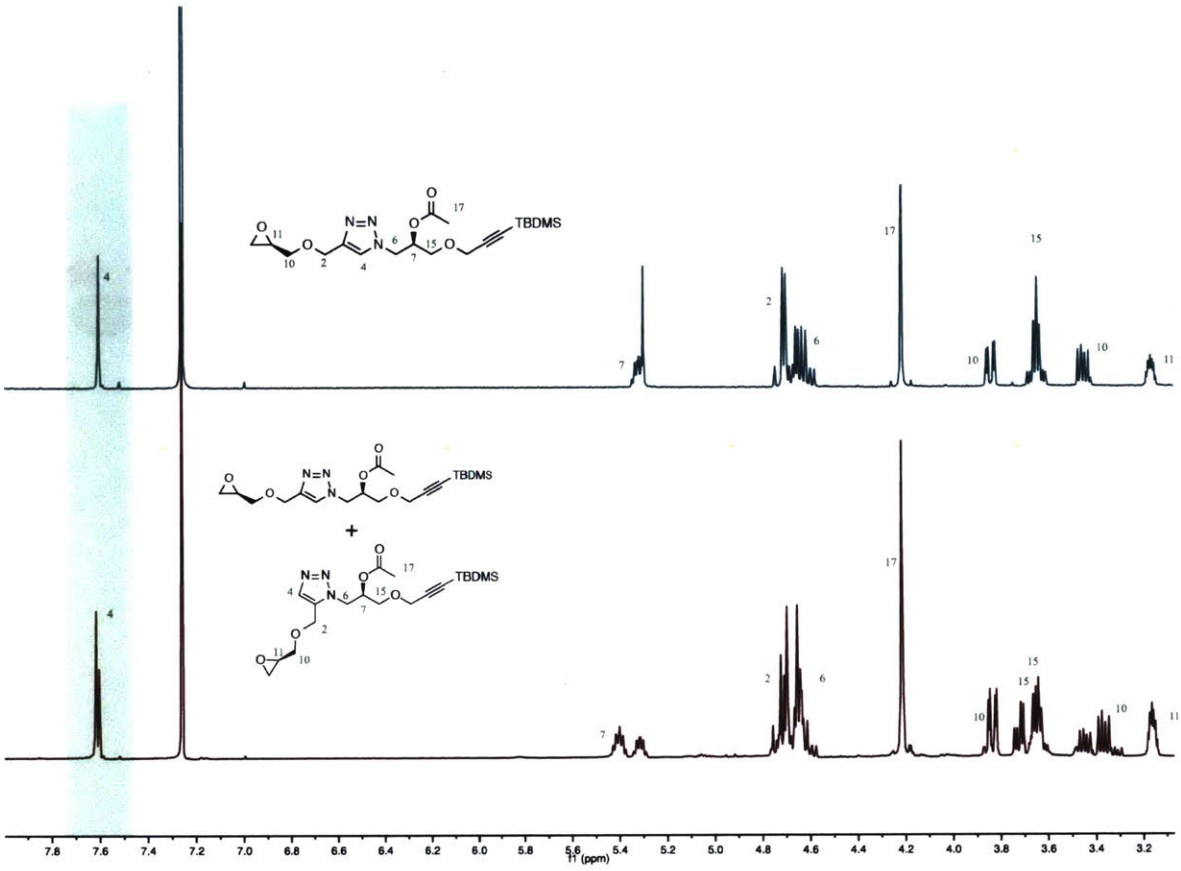


**Figure 3-11:** $^{1}$H NMR spectrum of dimers from CuAAC (teal) and RuAAC (burgundy). The highlighted triazole resonances show the lack of regioselectivity of RuAAC with this substrate.

As a control, monomers bearing both an azide and an alkyne were synthesized for CuAAc based step growth polymerization. Doubly deprotected monomers bearing both an azide and alkyne were synthesized, and polymerized. The molecular weight of the polymer produced was compared with a variety of catalysts, concentrations, and reaction times. Larger molecular weight polymers were seen when PMDETA was used as a ligand, potentially due to competitive binding of the copper with the newly formed triazoles. The molecular weight of polymer was dependent upon the concentration. Out of wide range of concentrations (0.4M-8.0M), 8.0M was chosen to produce the highest molecular weight polymer. Higher concentrations resulted in uncontrollable heat generation. All results showed high variability and a broad dispersity, showing the benefit of a controlled polymerization such as IEG+.

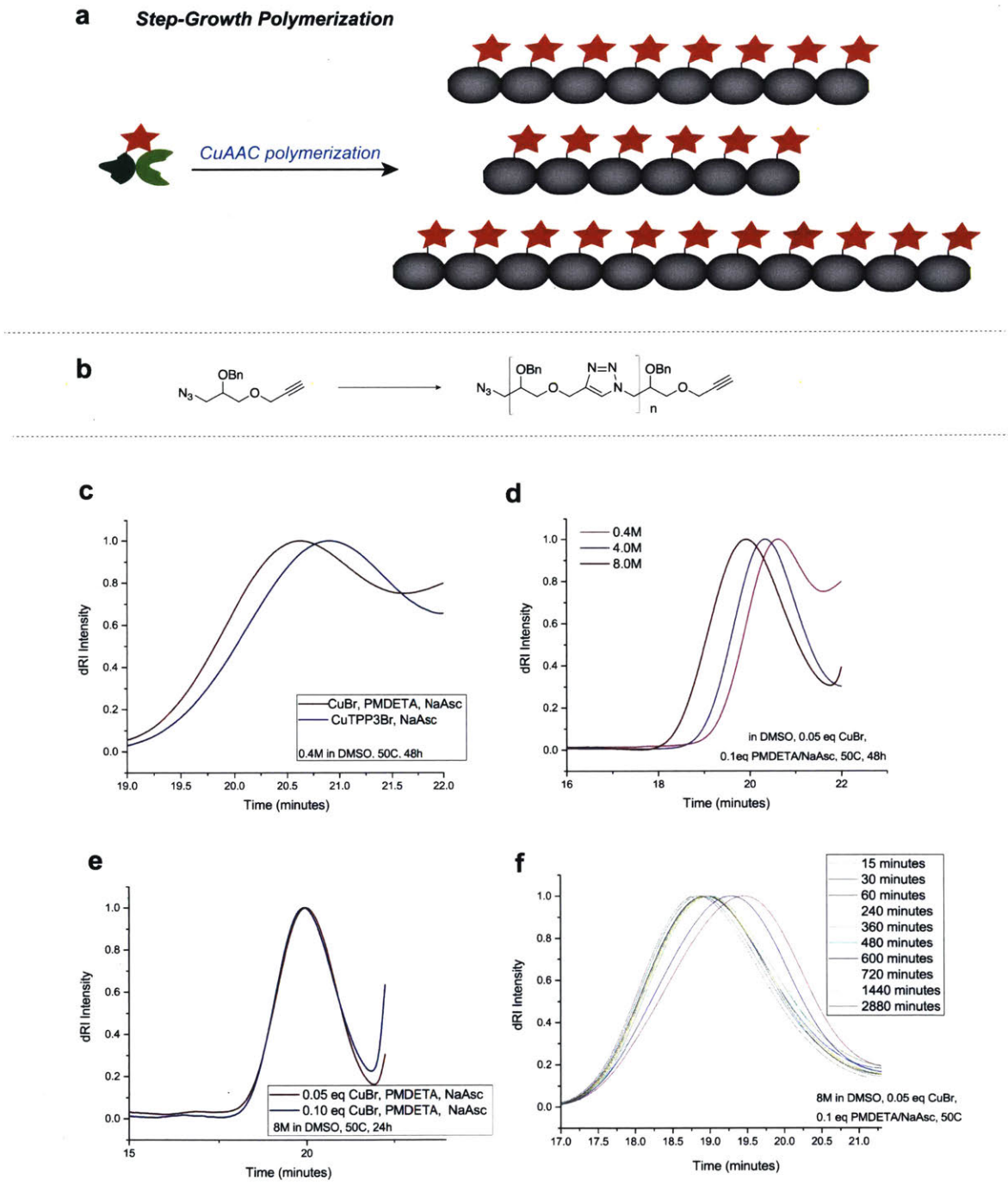


**Figure 3-12:** a) A schematic of step polymerization. showing that they are not controlled polymerizations, and result in a distribution of polymer molecular weights. b) Chemical structures of the benzylated monomers used for a step polymerization designed to produce the same polymeric backbone as IEG+. Each monomer contains an azide and alkyne. c) GPC chromatograms show how the results of step polymerization varied with the type of catalyst used. d) GPC chromatograms show how the results of step polymerization varied with the concentration of monomer. e) GPC chromatograms show that no molecular weight dependence was seen upon the concentration of catalyst. f) GPC chromatograms show how polymer molecular weight increased with reaction time. After two hours, no significant increase in molecular weight was seen.

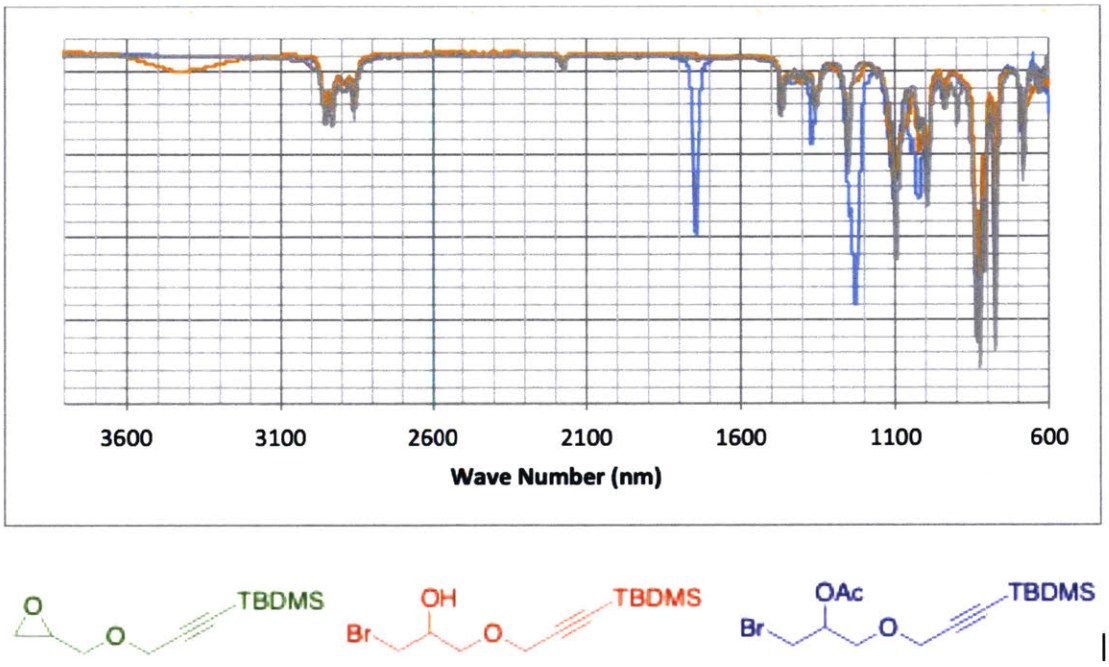


**Figure 3-13:** IR signals from the original IEG+ monomer in green, the lithium bromide opened epoxide in red, and the acetyl functionalized monomer in blue. The gain of a broad alcohol peak appears after epoxide opening in the red trace at 3300nm, and disappears after functionalization of the newly revealed alcohol. A characteristic C=O double bond signal appears at 1740nm due to acetyl functionalization.

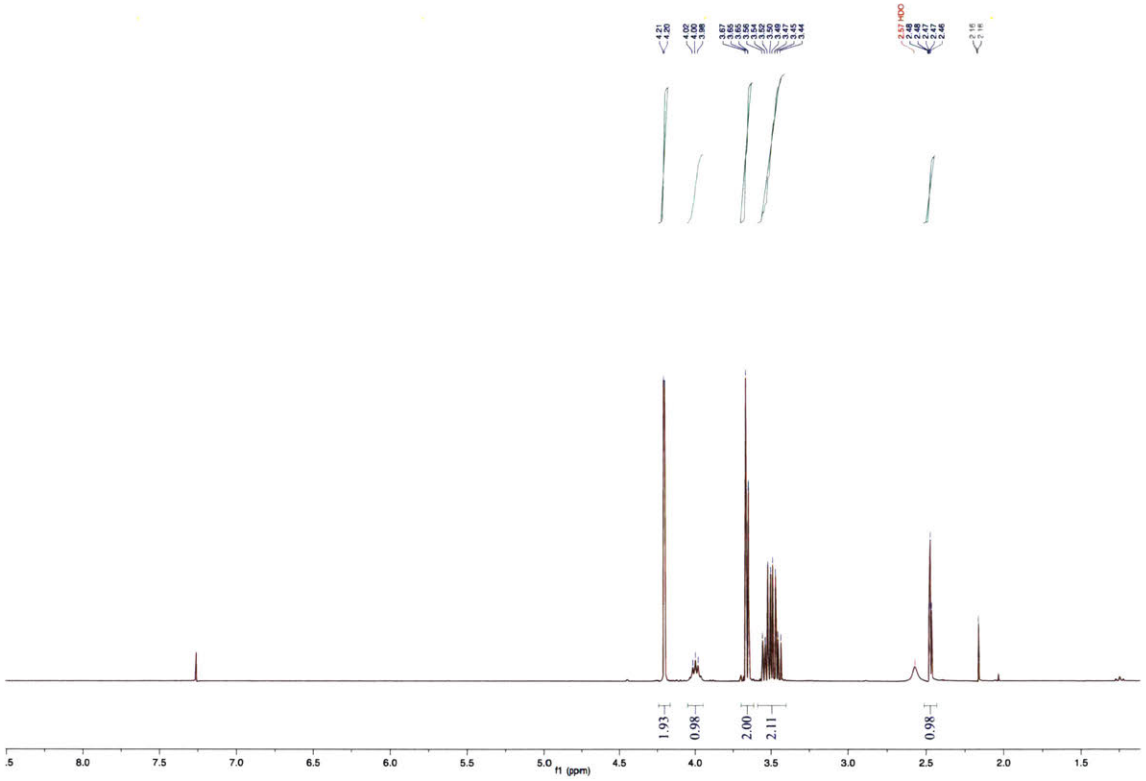


**Figure 3-14:** $^{1}$H NMR (400 MHz, $CHCl_3$) spectrum of 1-bromo-3-(prop-2-yn-1-yloxy)propan-2-yl acetate

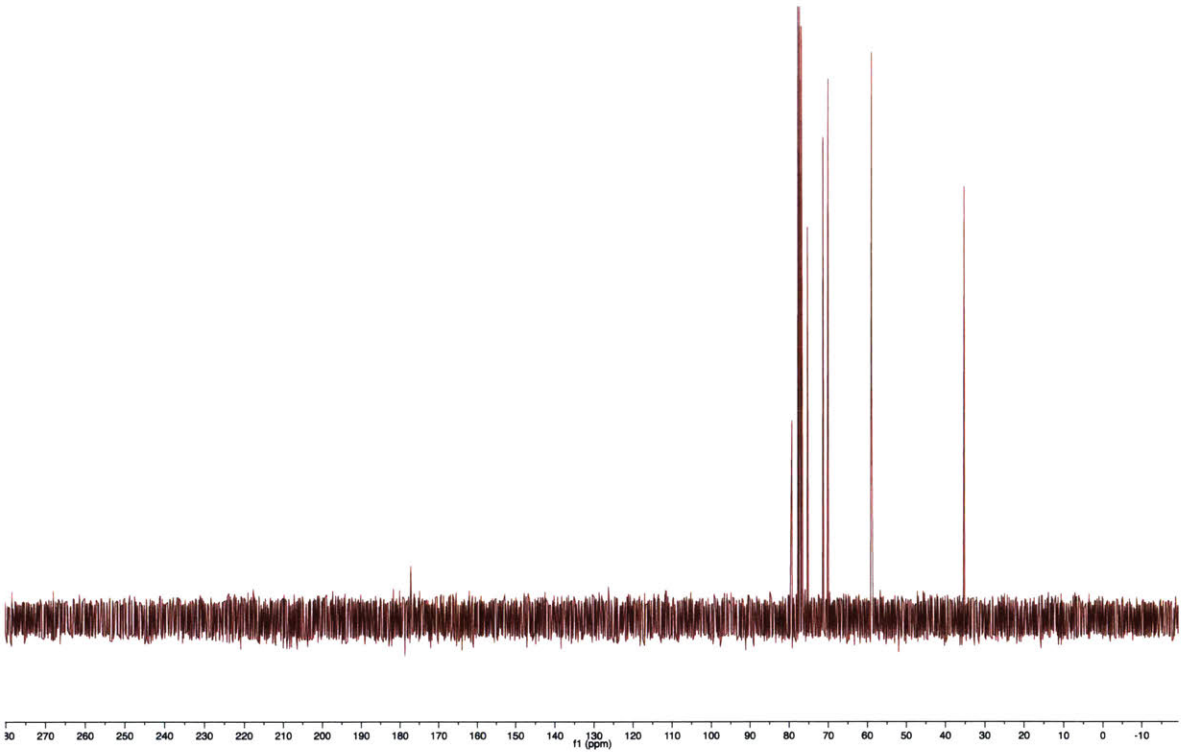


**Figure 3-15:** $^{13}C$ NMR (75 MHz, $CHCl_3$) spectrum of 1-bromo-3-(prop-2-yn-1-yloxy)propan-2-yl acetate

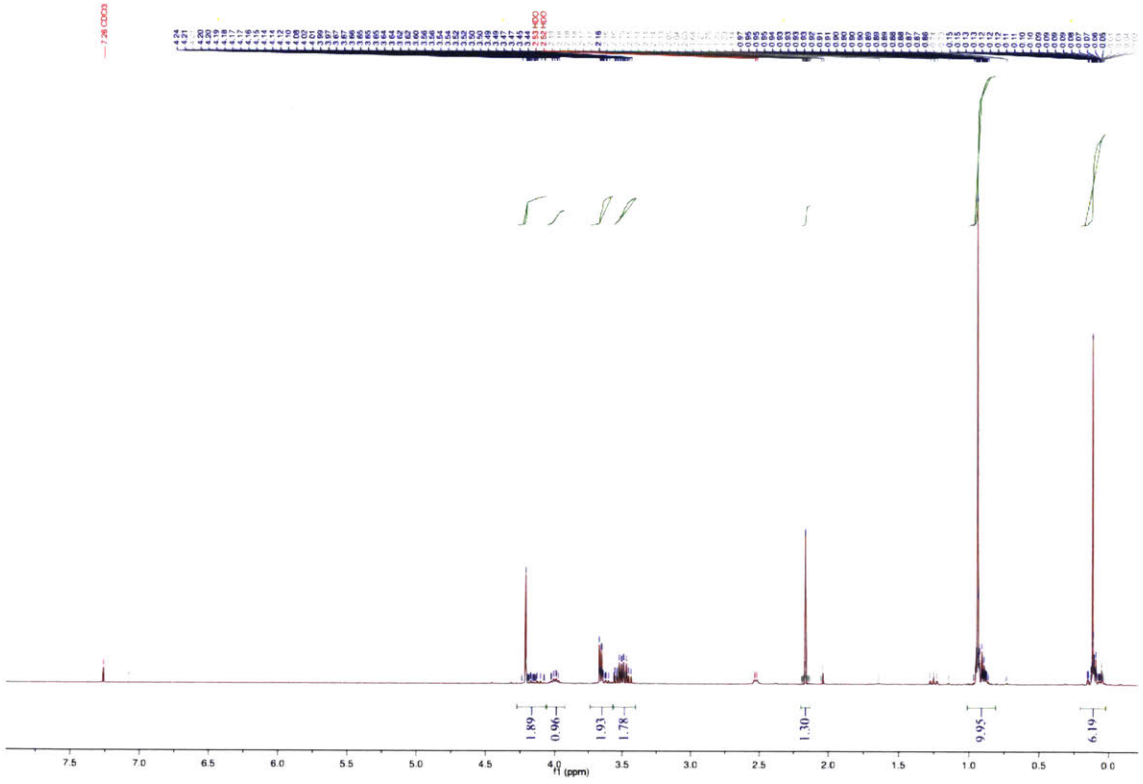


**Figure 3-16:** $^{1}$H NMR (300 MHz, $CHCl_3$) spectrum of 1-bromo-3-((3-(*tert*-butyldimethylsilyl)prop-2-yn-1-yl)oxy)propan-2-ol

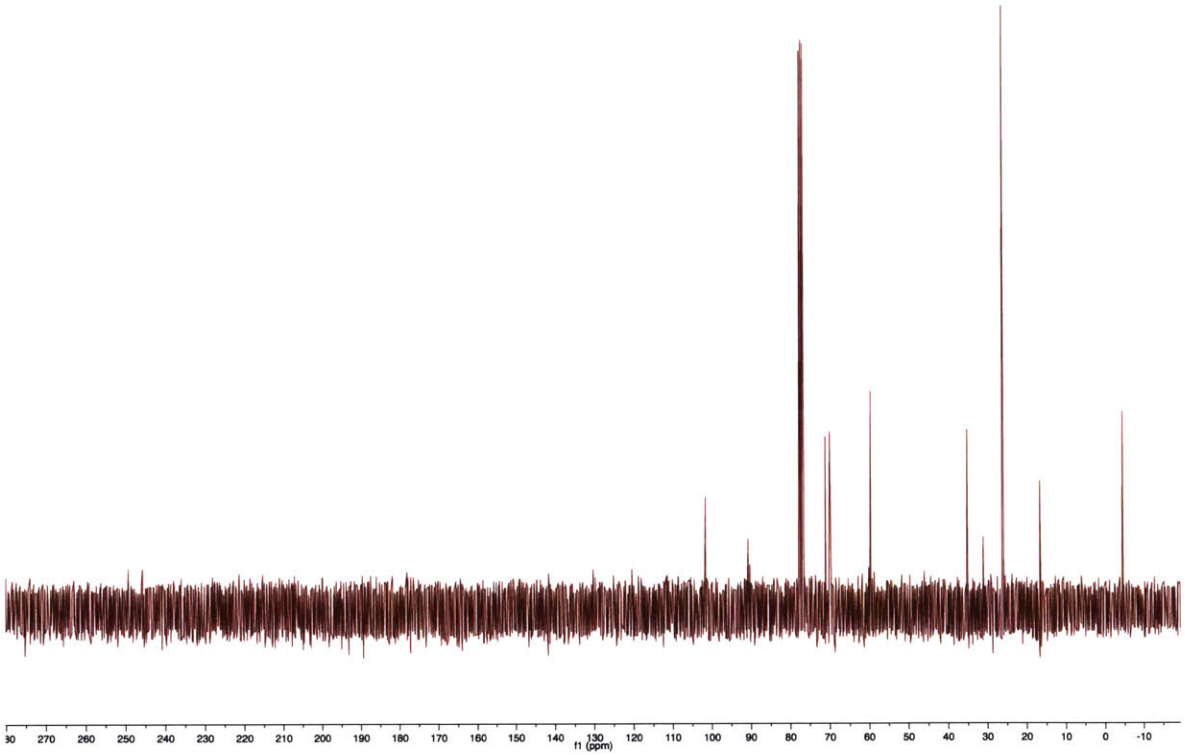


**Figure 3-17:** $^{13}C$ NMR (75 MHz, $CHCl_3$) spectrum of 1-bromo-3-((3-(*tert*-butyldimethylsilyl)prop-2-yn-1-yl)oxy)propan-2-ol

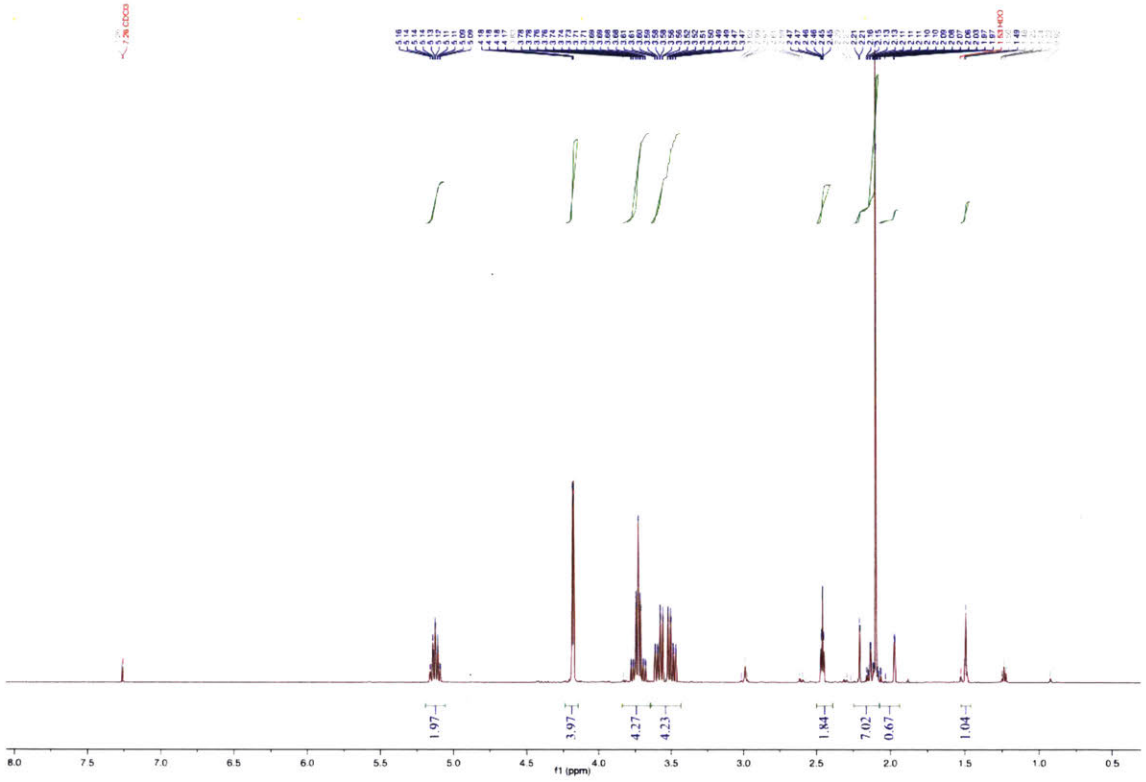


**Figure 3-18:** $^1$H NMR (300 MHz, $CHCl_3$) spectrum of 1-bromo-3-(prop-2-yn-1-yloxy)propan-2-yl acetate

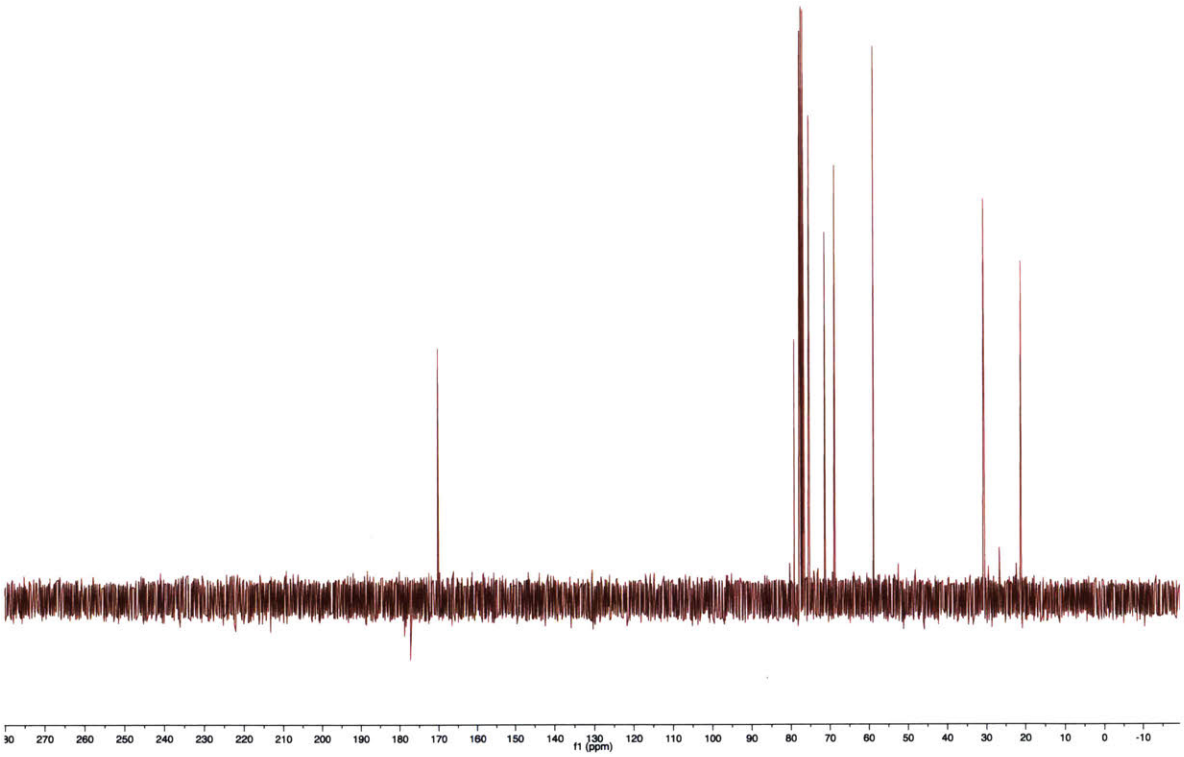


**Figure 3-19:** $^{13}C$ NMR (75 MHz, $CHCl_3$) spectrum of 1-bromo-3-(prop-2-yn-1-yloxy)propan-2-yl acetate

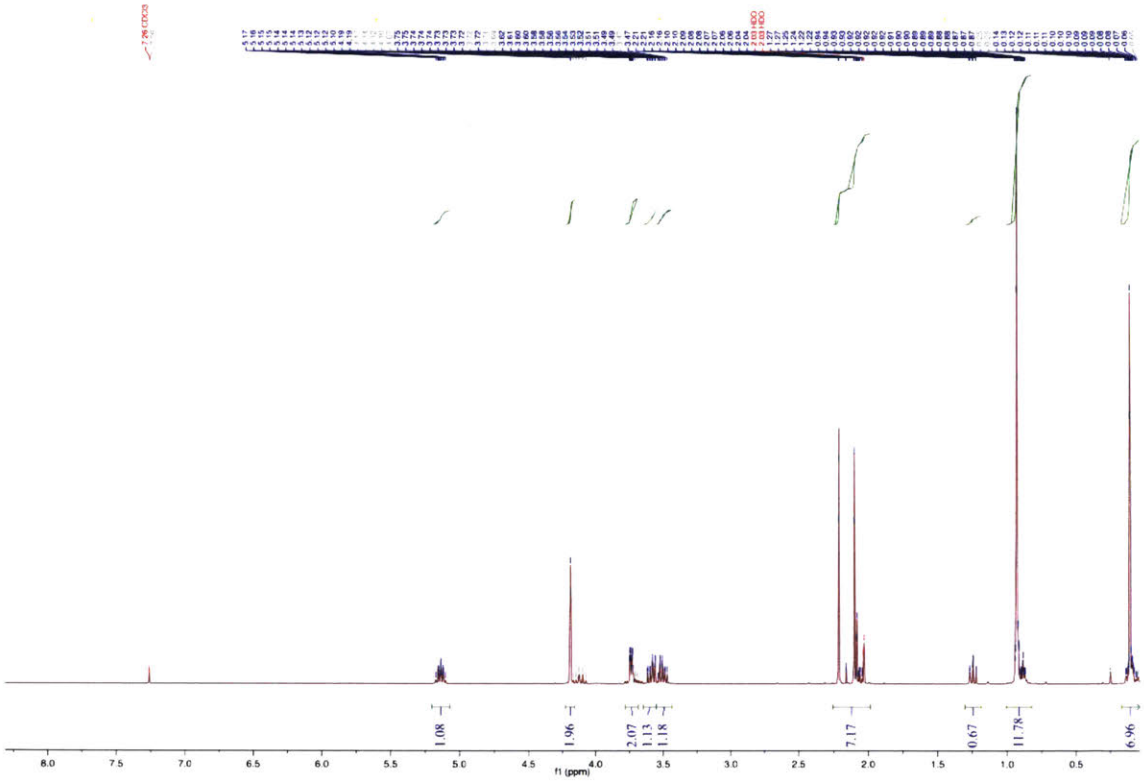


**Figure 3-20:** $^{1}$H NMR (300 MHz, $CHCl_3$) spectrum of 1-bromo-3-((3-(*tert*-butyldimethylsilyl)prop-2-yn-1-yl)oxy)propan-2-yl acetate

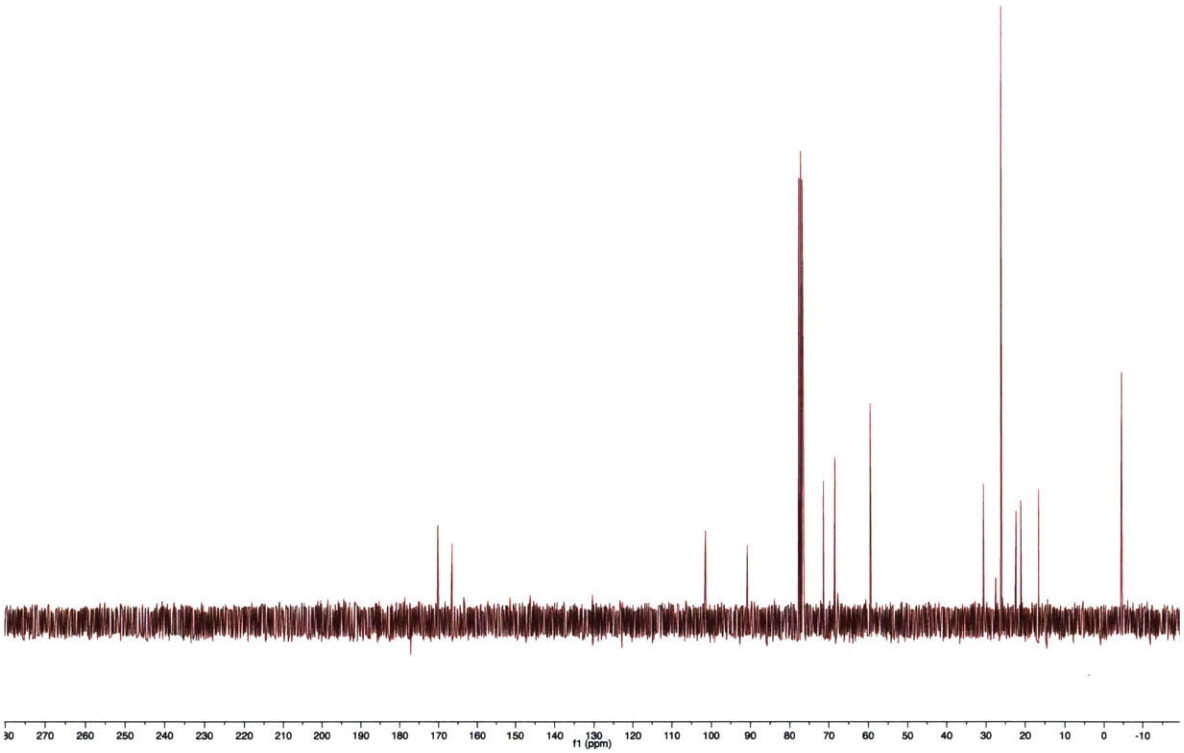


**Figure 3-21:** $^{13}C$ NMR (75 MHz, $CHCl_3$) spectrum of 1-bromo-3-((3-(*tert*-butyldimethylsilyl)prop-2-yn-1-yl)oxy)propan-2-yl acetate

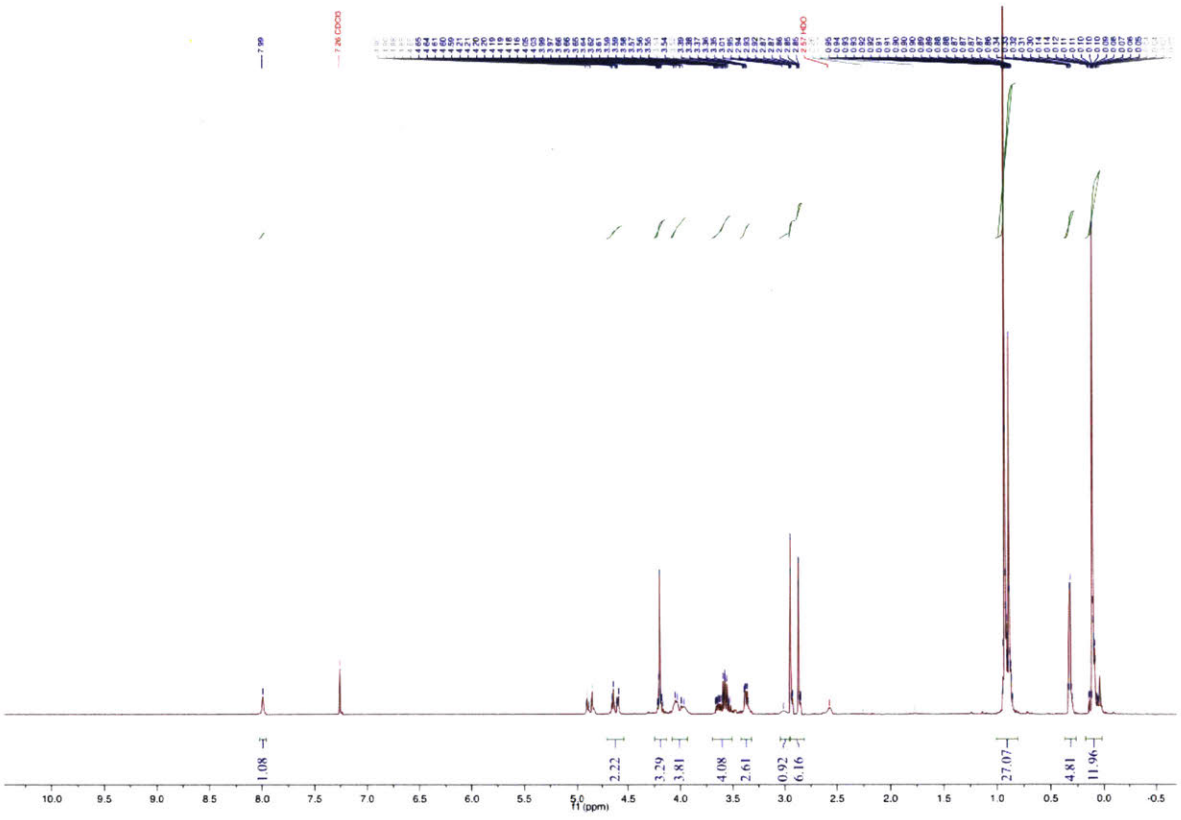


**Figure 3-22:** $^{1}$H NMR (300 MHz, $CHCl_3$) spectrum of 1-azido-3-((3-(*tert*-butyldimethylsilyl)prop-2-yn-1-yl)oxy)propan-2-ol

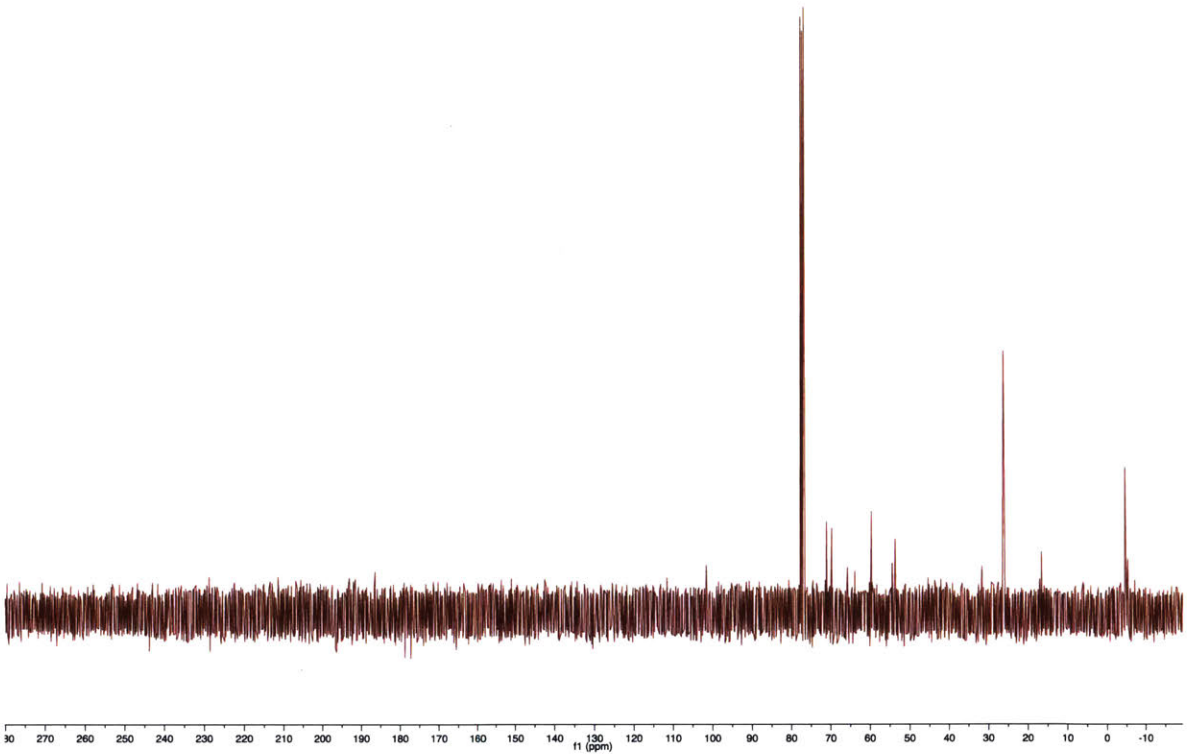


**Figure 3-23:** $^{13}C$ NMR (75 MHz, $CHCl_3$) spectrum of 1-azido-3-((3-(*tert*-butyldimethylsilyl)prop-2-yn-1-yl)oxy)propan-2-ol

## 3.5 References


(1) Van Hest, J. C. M.; Tirrell, D. A. Protein-based materials, toward a new level of structural control. *Chem. Commun.* **2001**, 1897–1904.

(2) Branden, C.; Tooze, J., *Introduction to protein structure*, 2nd; Garland Publisher, Inc.: New York, NY, 1999.

(3) Moneypenny, T. P.; Liu, H.; Yang, A.; Robertson, I. D.; Moore, J. S. Grubbs-inspired metathesis in the Moore group. *J. Polym. Sci., Part A: Polym. Chem.* **2017**, *55*, 2935–2948.

(4) De Gennes, P. Soft Matter (Nobel Lecture). *Angew. Chem. Int. Ed. Engl.* **1992**, *31*, 842–845.

(5) Franz, N.; Menin, L.; Klok, H.-A. A Post-Modification Strategy for the Synthesis of Uniform, Hydrophilic/Hydrophobic Patterned $\alpha$-Hydroxy Acid Oligomers. *Eur. J. Org. Chem.* **2009**, *2009*, 5390–5405.

(6) Rosales, A. M.; Segalman, R. A.; Zuckermann, R. N. Polypeptoids: a model system to study the effect of monomer sequence on polymer properties and self-assembly. *Soft Matter* **2013**, *9*, 8400.

(7) Lutz, J.-F. Sequence-controlled polymerizations: the next Holy Grail in polymer science? *Polym. Chem.* **2010**, *1*, 55.

(8) Matyjaszewski, K.; Gaynor, S.; Wang, J. Controlled radical polymerizations: use of alky iodides in degenerative transfer. *Macromolecules* **1995**, *28*, 2093–2095.

(9) Chiefari, J.; Chong, Y. K.; Ercole, F.; Krstina, J.; Jeffrey, J.; Le, T. P. T.; Mayadunne, R. T. A.; Meijs, G. F.; Moad, C. L.; Moad, G.; Rizzardo, E.; Thang, S. H. Living free-radical polymerization by reversible addition-fragmentation chain transfer: the RAFT process. *Macromolecules* **1998**, *31*, 5559–5562.

(10) Moad, G.; Rizzardo, E. Alkoxyamine-initiated living radical polymerization: factors affecting alkoxyamine homolysis rates. *Macromolecules* **1995**, *28*, 8722–8728.

(11) Leitgeb, A.; Wappel, J.; Slugovc, C. The ROMP toolbox upgraded. *Polymer* **2010**, *51*, 2927–2946.

(12) Alfrey, T.; Lavin, E. The Copolymerization of Styrene and Maleic Anhydride. *J. Am. Chem. Soc.* **1945**, *67*, 2044–2045.

(13) Gody, G.; Maschmeyer, T.; Zetterlund, P. B.; Perrier, S. Rapid and quantitative one-pot synthesis of sequence-controlled polymers by radical polymerization. *Nat. Commun.* **2013**, *4*, 2505.

(14) Lutz, J. F.; Pfeifer, S. A Facile Procedure for Controlling Monomer Sequence Distribution in Radical Chain Polymerizations. *J. Am. Chem. Soc.* **2007**, *129*, 9542–9543.

(15) Moatsou, D.; Hansell, C. F.; O'Reilly, R. K. Precision polymers: a kinetic approach for functional poly(norbornenes). *Chem. Sci.* **2014**, *5*, 2246–2250.

(16) Ida, S.; Ouchi, M.; Sawamoto, M. Template-assisted selective radical addition toward sequence-regulated polymerization: lariat capture of target monomer by template initiator. *J. Am. Chem. Soc.* **2010**, *132*, 14748–50.

(17) Milnes, P. J.; O'Reilly, R. K. DNA-Templated Chemistries for Sequence Controlled Oligomer Synthesis. *ACS Symp. Ser.* **2014**, *1170*, 71–84.

(18) Niu, J.; Hili, R.; Liu, D. R. Enzyme-free translation of DNA into sequence-defined synthetic polymers structurally unrelated to nucleic acids. *Nat. Chem.* **2013**, *5*, 282–92.

(19) Gutekunst, W. R.; Hawker, C. J. A General Approach to Sequence-Controlled Polymers Using Macrocyclic Ring Opening Metathesis Polymerization. *J. Am. Chem. Soc.* **2015**, *137*, 8038–41.

(20) Johnson, J. A.; Lu, Y. Y.; Burts, A. O.; Xia, Y.; Durrell, A. C.; Tirrell, D. A.; Grubbs, R. H. Drug-Loaded, Bivalent-Bottle-Brush Polymers by Graft-through ROMP. *Macromolecules* **2010**, *43*, 10326–10335.

(21) Kawamoto, K.; Zhong, M.; Gadelrab, K. R.; Cheng, L. C.; Ross, C. A.; Alexander-Katz, A.; Johnson, J. A. Graft-through Synthesis and Assembly of Janus Bottlebrush Polymers from A-Branch-B Diblock Macromonomers. *J. Am. Chem. Soc.* **2016**, *138*, 11501–4.

(22) Lewandowski, B.; De Bo, G.; Ward, J. W.; Papmeyer, M.; Kuschel, S.; Aldegunde, M. J.; Gramlich, P. M.; Heckmann, D.; Goldup, S. M.; D'Souza, D. M.; Fernandes, A. E.; Leigh, D. A. Sequence-specific peptide synthesis by an artificial small-molecule machine. *Science* **2013**, *339*, 189–93.

(23) Li, J.; Stayshich, R. M.; Meyer, T. Y. Exploiting sequence to control the hydrolysis behavior of biodegradable PLGA copolymers. *J. Am. Chem. Soc.* **2011**, *133*, 6910–3.

(24) Satoh, K.; Ozawa, S.; Mizutani, M.; Nagai, K.; Kamigaito, M. Sequence-regulated vinyl copolymers by metal-catalysed step-growth radical polymerization. *Nat. Commun.* **2010**, *1*, 6.

(25) Zhang, J.; Matta, M. E.; Hillmyer, M. A. Synthesis of Sequence-Specific Vinyl Copolymers by Regioselective ROMP of Multiply Substituted Cyclooctenes. *ACS Macro Lett.* **2012**, *1*, 1383–1387.

(26) Burns, M.; Essafi, S.; Bame, J. R.; Bull, S. P.; Webster, M. P.; Balieu, S.; Dale, J. W.; Butts, C. P.; Harvey, J. N.; Aggarwal, V. K. Assembly-line synthesis of organic molecules with tailored shapes. *Nature* **2014**, *513*, 183–8.

(27) Norris, B. N.; Zhang, S.; Campbell, C. M.; Auletta, J. T.; Calvo-Marzal, P.; Hutchison, G. R.; Meyer, T. Y. Sequence Matters: Modulating Electronic and Optical Properties of Conjugated Oligomers via Tailored Sequence. *Macromolecules* **2013**, *46*, 1384–1392.

(28) Porel, M.; Alabi, C. A. Sequence-defined polymers via orthogonal allyl acrylamide building blocks. *J. Am. Chem. Soc.* **2014**, *136*, 13162–5.

(29) Rosenbaum, I.; Avinery, R.; Harnoy, A. J.; Slor, G.; Tirosh, E.; Hananel, U.; Beck, R.; Amir, R. J. Reversible Dimerization of Polymeric Amphiphiles Acts as a Molecular Switch of Enzymatic Degradability. *Biomacromolecules* **2017**, *18*, 3457–3468.

(30) Solleder, S. C.; Meier, M. A. Sequence control in polymer chemistry through the Passerini three-component reaction. *Angew. Chem. Int. Ed. Engl.* **2014**, *53*, 711–4.

(31) Merrifield, R. Solid Phase Peptide Synthesis: The Synthesis of a Tetrapeptide. *J. Am. Chem. Soc.* **1963**, *85*, 2149–2154.

(32) Serpell, C. J.; Edwardson, T. G.; Chidchob, P.; Carneiro, K. M.; Sleiman, H. F. Precision polymers and 3D DNA nanostructures: emergent assemblies from new parameter space. *J. Am. Chem. Soc.* **2014**, *136*, 15767–74.

(33) Wojcik, F.; Ponader, D.; Mosca, S.; Hartmann, L. Recent Advances in Solid Phase Polymer Synthesis: Polyamides from Tailor-Made Building Blocks. *ACS Symp. Ser.* **2014**, *1170*, 85–101.

(34) Merrifield, R. B. Solid-phase synthesis (Nobel Lecture). *Angew. Chem., Int. Ed.* **1985**, *24*, 799–810.

(35) Gutte, B.; Merrifield, R. B. The synthesis of ribonuclease A. *J. Biol. Chem.* **1971**, *246*, 1922–1941.

(36) Miyoshi, K.; Arentzen, R.; Huang, T.; Itakura, K. Solid-phase synthesis of polynucleotides. IV. Usage of polystyrene resins for the synthesis of polydeoxyribonucleotides by the phosphotriester method. *Nucleic Acids Res.* **1980**, *8*, 5507–5517.

(37) Chan-Seng, D.; Lutz, J.-F. Solid-Phase Synthesis as a Tool for the Preparation of Sequence-Defined Oligomers Based on Natural Amino Acids and Synthetic Building Blocks. *ACS Symp. Ser.* **2014**, *1170*, 103–116.

(38) Roy, R. K.; Meszynska, A.; Laure, C.; Charles, L.; Verchin, C.; Lutz, J. F. Design and synthesis of digitally encoded polymers that can be decoded and erased. *Nat. Commun.* **2015**, *6*, 7237.

(39) Zuckermann, R. N.; Kerr, J. M.; Kent, S. B. H.; Moos, W. H. Efficient method for the preparation of peptoids [oligo(N-substituted glycines)] by Submonomer Solid-Phase Synthesis. *J. Am. Chem. Soc.* **1992**, *114*, 10646–10647.

(40) Binauld, S.; Damiron, D.; Connal, L. A.; Hawker, C. J.; Drockenmuller, E. Precise synthesis of molecularly defined oligomers and polymers by orthogonal iterative divergent/convergent approaches. *Macromol. Rapid Commun.* **2011**, *32*, 147–68.

(41) Binauld, S.; Hawker, C. J.; Fleury, E.; Drockenmuller, E. A modular approach to functionalized and expanded crown ether based macrocycles using click chemistry. *Angew. Chem. Int. Ed. Engl.* **2009**, *48*, 6654–8.

(42) Wang, H.; Raghupathi, K. R.; Zhuang, J.; Thayumanavan, S. Activatable Dendritic 19F Probes for Enzyme Detection. *ACS Macro Lett.* **2015**, *4*, 422–425.

(43) Cai, C.; Vasella, A. Oligosaccharide Analogues of Polysaccharides. *Helv. Chim. Acta* **1996**, *79*, 255–268.

(44) Huang, B.; Hermes, M. Homogeneous polyesters of predetermined length, Composition, and Sequence: Model Synthesis of Alternating Glycolic-Acid-co-(1)-Lactic-Acid Oligomers. *J. Polym. Sci., Part A: Polym. Chem.* **1995**, *33*, 1419–1429.

(45) Koch, F. P.; Smith, P.; Heeney, M. "Fibonacci's route" to regioregular oligo(3-hexylthiophene)s. *J. Am. Chem. Soc.* **2013**, *135*, 13695–8.

(46) Liess, P.; Hensel, V.; Schluter, A. D. Oligophenylene Rods: A Repetitive Approach. *Liebigs Annalen* **1996**, 1037–1040.

(47) Louie, J.; Hartwig, J. The Largest Discrete Oligo(m-aniline). An Exponential Growth Strategy Using Palladium-Catalyzed Amination of Aryl Sulfonates. *Macromolecules* **1998**, *31*, 6737–6739.

(48) Paynter, O. I.; Simmonds, D. J.; Whiting, M. C. The Synthesis of Long-chain Unbranched Aliphatic Compounds by Molecular Doubling. *J. Chem. Soc. Chem. Commun.* **1982**, 1165–1166.

(49) Percec, V.; Asandei, A. Monodisperse Linear Liquid Crystalline Polyethers. *Macromolecules* **1997**, *30*, 7701–7720.

(50) Sadighi, J. P.; Singer, R. A.; Buchwald, S. L. Palladium-Catalyzed Synthesis of Monodisperse, Controlled-Length, and Functionalized Oligoanilines. *J. Am. Chem. Soc.* **1998**, *120*, 4960–4976.

(51) Williams, J. B.; Chapman, T. M.; Hercules, D. M. Synthesis of Discrete Mass Poly(butylene glutarate) Oligomers. *Macromolecules* **2003**, *36*, 3898–3908.

(52) Schumm, J. S.; Pearson, D. L.; Tour, J. M. Iterative Divergent/Convergent Approach to Linear Conjugated Oligomers by Successive Doubling of the Molecular Length: A Rapid Route to a 128A-Long Potential Molecular Wire. *Angew. Chem. Int. Ed. Engl.* **1994**, *33*, 1360–1363.

(53) Paynter, O. I.; Simmonds, D. J.; Whiting, M. C. The synthesis of long-chain unbranched aliphatic-compounds by molecular doubling. *J. Chem. Soc., Chem. Commun.* **1982**, 1165–1166.

(54) Pearson, D. L.; Schumm, J. S.; Tour, J. M. Iterative Divergent/Convergent Approach to Conjugated Oligomers by a Doubling of Molecular Length at Each Iteration. A Rapid Route to Potential Molecular Wires. *Macromolecules* **1994**, *27*, 2348–2350.

(55) Takizawa, K.; Tang, C.; Hawker, C. J. Molecularly defined caprolactone oligomers and polymers: synthesis and characterization. *J. Am. Chem. Soc.* **2008**, *130*, 1718–26.

(56) Takizawa, K.; Nulwala, H.; Hu, J.; Yoshinaga, K.; Hawker, C. J. Molecularly defined (L)-lactic acid oligomers and polymers: Synthesis and characterization. *J. Polym. Sci., Part A: Polym. Chem.* **2008**, *46*, 5977–5990.

(57) Zhang, J. S.; Moore, J. S.; Xu, Z. F.; Aguirre, R. A. Controlled Synthesis of Phenylacetylene Sequences. *J. Am. Chem. Soc.* **1992**, *114*, 2273–2274.

(58) Li, G.; Wang, X.; Li, J.; Zhao, X.; Wang, F. Synthesis of Monodisperse Oligo[(1,4-Phenyleneethynylene)-Alt-(2,5-Thiopheneethynylene)]s. *Synth. Commun.* **2005**, *35*, 115–119.

(59) Li, G.; Wang, X.; Wang, F. A novel in situ deprotection/coupling and iterative divergent/convergent strategy for the synthesis of oligo(1,4-phenyleneethynylene)s. *Tetrahedron Lett.* **2005**, *46*, 8971–8973.

(60) Martin, R. E.; Diederich, F. Linear Monodisperse pi-Conjugated Oligomers: Model Compounds for Polymers and More. *Angew. Chem. Int. Ed. Engl.* **1999**, *38*, 1350–1377.

(61) Lengweiler, U. D.; Fritz, M. G.; Seebach, D. Synthese monodisperser h e a r e r und cyclischer Oligomere der (R)-3-Hydroxybuttersaure mit bis zu 128 Einheiten. *Helv. Chim. Acta* **1996**, *79*, 670–701.

(62) Kolb, H. C.; Finn, M. G.; Sharpless, K. B. Click Chemistry: Diverse Chemical Function from a Few Good Reactions. *Angew. Chem. Int. Ed. Engl.* **2001**, *40*, 2004–2021.

(63) Rostovtsev, V. V.; Green, L. G.; Fokin, V. V.; Sharpless, K. B. A stepwise huisgen cycloaddition process: copper(I)-catalyzed regioselective "ligation" of azides and terminal alkynes. *Angew. Chem. Int. Ed. Engl.* **2002**, *41*, 2596–9.

(64) Huisgen, R. 1,3-Dipolar Cycloadditions. *Proc. Chem. Soc.* **1961**, *0*, 357–396.

(65) Boren, B.; S., N.; Rasmussen, L.; Zhang, L.; Zhao, H.; Lin, A.; Jia, G.; Fokin, V. Ruthenium-Catalyzed Azide-Alkyne Cycloaddition: Scope and Mechanism. *J. Am. Chem. Soc.* **2008**, *130*, 8923–8930.

(66) Barnes, J. C.; Ehrlich, D. J.; Gao, A. X.; Leibfarth, F. A.; Jiang, Y.; Zhou, E.; Jamison, T. F.; Johnson, J. A. Iterative exponential growth of stereo- and sequence-controlled polymers. *Nat. Chem.* **2015**, *7*, 810–5.

(67) Golder, M. R.; Jiang, Y.; Teichen, P. E.; Nguyen, H. V.; Wang, W.; Milos, N.; Freedman, S. A.; Willard, A. P.; Johnson, J. A. Stereochemical Sequence Dictates Unimolecular Diblock Copolymer Assembly. *J. Am. Chem. Soc.* **2018**, *140*, 1596–1599.

(68) Jiang, Y.; Golder, M. R.; Nguyen, H. V.; Wang, Y.; Zhong, M.; Barnes, J. C.; Ehrlich, D. J.; Johnson, J. A. Iterative Exponential Growth Synthesis and Assembly of Uniform Diblock Copolymers. *J. Am. Chem. Soc.* **2016**, *138*, 9369–72.

# Chapter 4

# Introduction to PDMS elastomer toughening strategies

## 4.1 Overview

In this summary, we will discuss silicone elastomers in terms of network structure, the impact of network structure upon physical properties, and modifications to elastomers.

Silicones are ubiquitous. They can be found in applications ranging from waterproofing agents, sealants, rubber seals, and electrical insulation in the contstruction domain to consumer products such as detergent antifoaming agents, high temperature resistant utensils, and moisturizers.[1] If we take the example of a car, we'd find that silicones are used in over 25 separate components,[1] ranging from insulation for the electronics, to hosing, to various rubber seals, to coatings on the air bags. 30,000 people are involved in the $11 billion dollar industry of silicones, roughly 2.6 times the enrollment at MIT as of 2018.[2]

On the academic side, silicone elastomers have been used to make microfluidic devices,[3,4] flexible electronics,[5] drug delivery vehicles,[6–8] and biomedical implants.[9] These materials are valued for their high thermal stability, chemical resistance, electrical resistance, hydrophobicity, and biocompatibility.

## 4.2 Understanding Elastomer Structure

As a group, polymers with alternating silicon oxygen backbones are known as siloxanes, a name derived from the words silicon, oxygen, and alkane. Siloxanes are interchangeably named as silicones, a nomenclature originating from the now refuted theory that these polymers have a double bonded structure analogous to a poly(ketone).[10] Instead, the structure of siloxanes has a repeat unit –[$R_2Si-O$]-, where the R group is generally an organic substituent at the silicon atom. The most common substituents are two methyl groups, forming poly(dimethylsiloxane), also known as dimethicone. Potential R substituents also include ethyl, propyl, phenyl, hydrogen, vinyl, or a mixed systems.

Siloxane elastomers are networks made of polymers with an alternating silicon and oxygen atom backbone. The Si-O bond length (1.63 Å) is significantly greater than the C-C bond length (1.53 Å), as is the Si-O-Si bond angle (143°) in comparison to the C-C-C bond angle (109°).[11] The backbone structure leads to greater flexibility than an analogous carbon system, a low $T_g$ that leads to amorphous materials at room temperature, and a large operational temperature range.

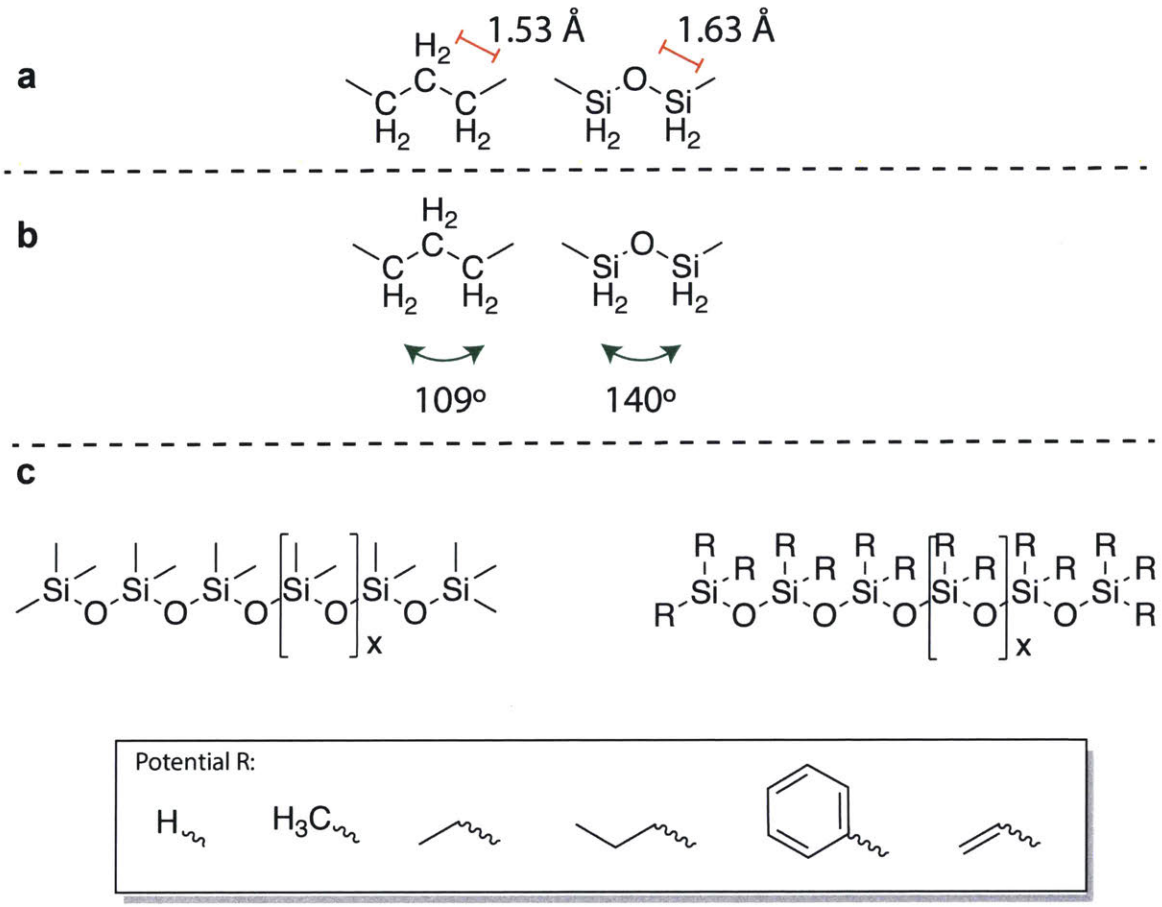


**Figure 4-1:** Siloxane elastomers are made of an alternating silicon and oxygen atom backbone. a) The Si-O bond length (1.63 Å) is significantly greater than the C-C bond length (1.53 Å), as is b) the Si-O-Si bond angle (143°) in comparison to the C-C-C bond angle (109°), leading to great flexibility in the polymer. c) The general structure of siloxanes has a repeat unit $-[R_2Si-O]-$, where the R group is generally an organic substituent.

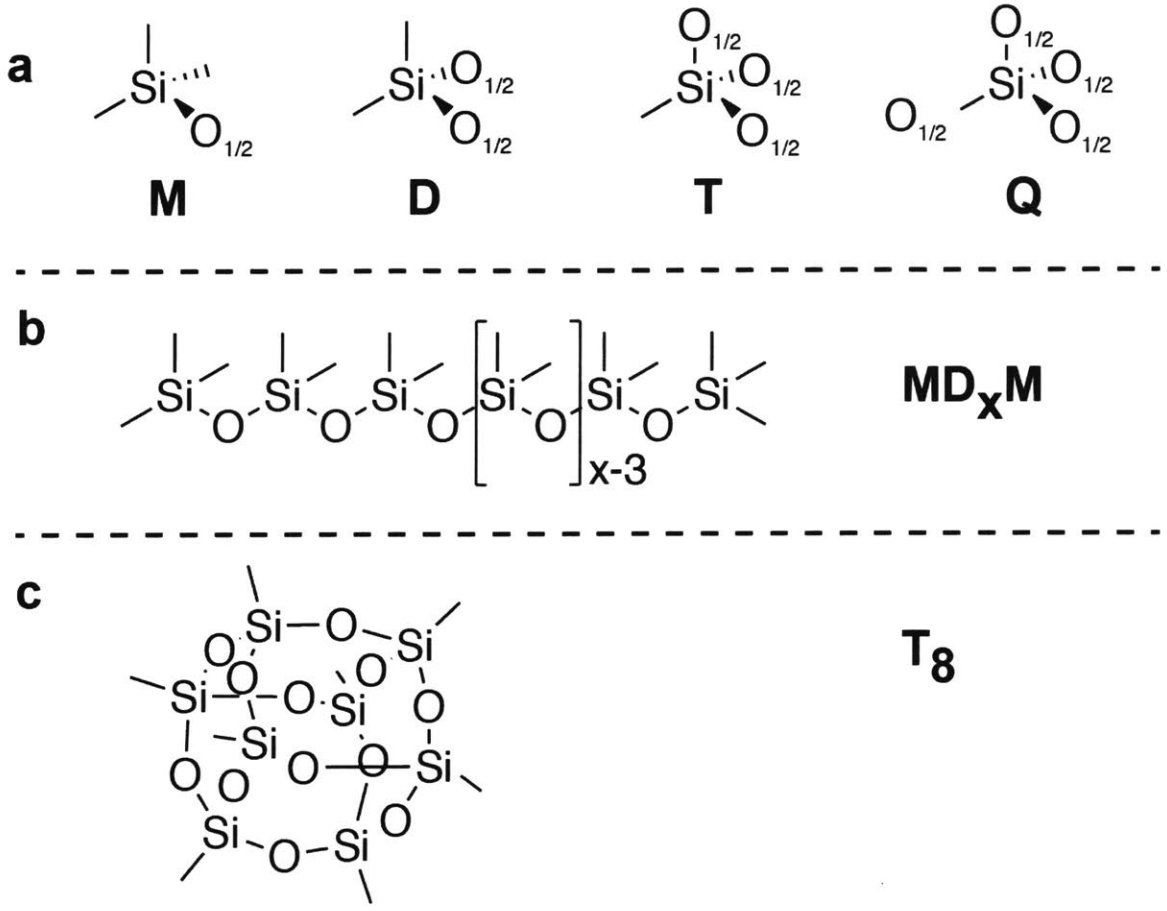


**Figure 4-2:** a) Silicone resins are composed of multifunctional monomers, MDTQ, shown here with example methyl functionality. These basic units can be used to form a wide array of systems. A linear polymer, composed of MDM units is shown in b), as is c) the polyoctahedral silsesquioxane known as 'POSS' composed of $T_8$.

Although this discussion primarily revolves around elastomers, a thorough background on siloxanes should describe silicone resins. These resins are composed of multifunctional monomers, MDTQ, categorized by the degree of functionality. Monofunctional monomers used to terminate a network, $R_3SiO_{1/2}$, are labeled 'M'. Difunctional monomers, which can extend the distance between crosslinks, $R_2SiO_{2/2}$, are labeled 'D'. Crosslinking monomers include 'T', the trifunctional $R_3SiO_{3/2}$, and tetrafunctional $R_3SiO_{4/2}$, or 'Q'. Combination of these monomers forms branched and crosslinked systems ranging from resins to rubbers. Of particular note are MDxM, a description of a linear siloxane containing 72 repeat units and two end groups, and T8, the polyoctahedral silsesquioxane known as 'POSS'.

The ideal network is an infinite system, which can be thought of as any DTQ network, without terminating M units. Ideal networks are generally thought as a combination of long polymer chains with two reactive groups per chain, and a multifunctional crosslinker. The relative functional group ratio, or reactivity ratio, determines the final crosslink density of the network, and thus the mechanical properties. The modulus of an elastomer can be taken as a function of crosslink density from the theory of rubber elasticity, where if $M_e$ is the molecular weight between crosslinks, $\rho$ is the polymer density, and $G_{N0}$ is the modulus at the rubbery plateau, $M_e = \rho \frac{RT}{G_{NO}}$.[12]

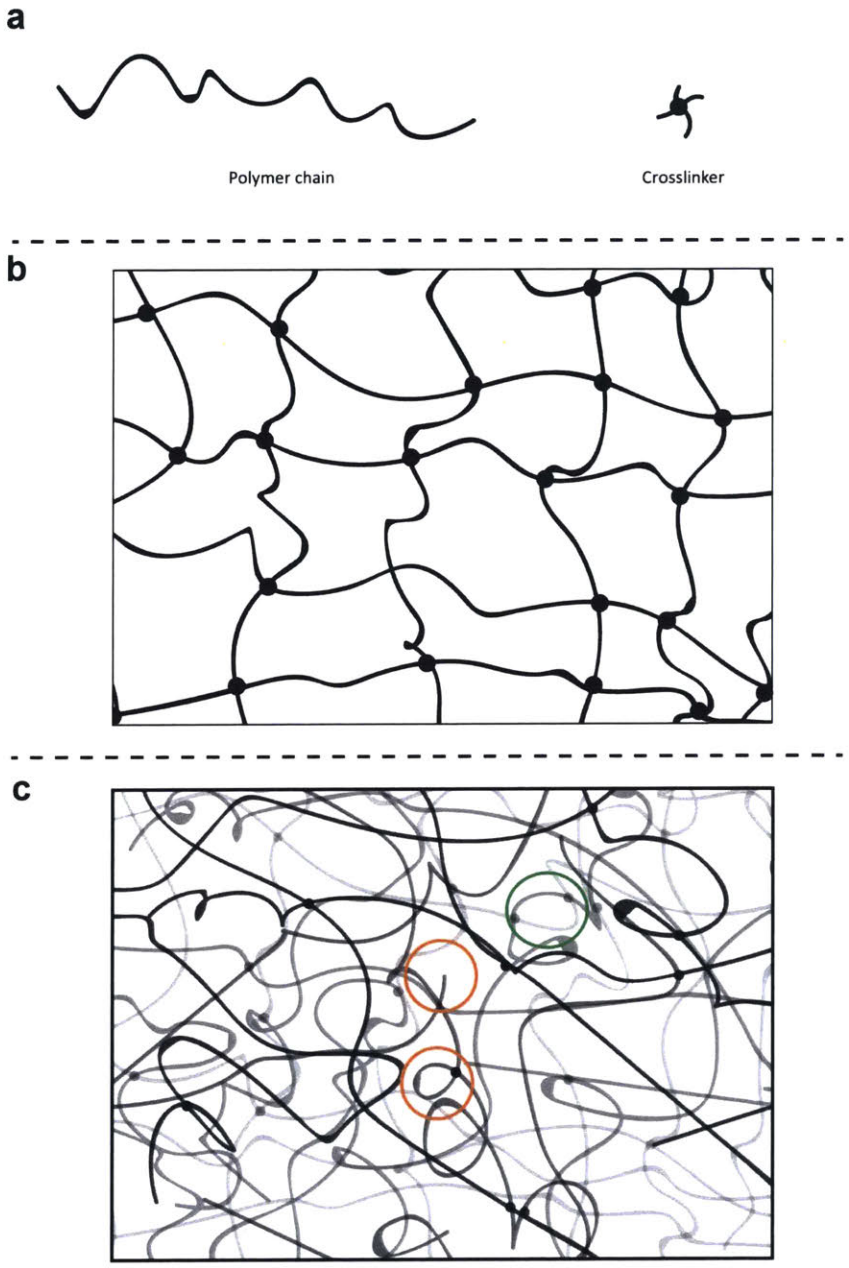


**Figure 4-3:** a) The polymer network shown in this figure was made from a long polymer chain with terminal functionality shown on the left and a tetrafunctional crosslinker shown on the right. b) An ideal two dimensional network is shown, without defects, loops, or entanglements. c) A more realistic polymer network is shown here. Non-elastically active defects such as dangling ends and primary loops are circled in red. An elastically active defect, a secondary loop, is circled in green.

Crosslinkers vary in chemical structure and functionality, as can potential additives and the final stoichiometric composition. In the ideal case, only the functionality of monomers determines the gel point. At the gel point $p_c = \frac{1}{f-1}$, where $f$ is the monomer functionality and $p$ is the extent of reaction, the system transitions between finite branched polymers and an infinite network.[13] In a real system, defects must be taken into account in addition to practical concerns such as shelf life, pot life, and cure temperature. Often, the specific composition of a commercially available silicone elastomer is a trade secret.

Common crosslinking chemistries include hydrosilylation and condensation. Condensation cured materials are tin or titanium catalyzed with atmospheric moisture triggering the cure process at room temperature. Hydrosilylations are most often cured with a platinum catalyst, although radical, copper, and ruthenium cured systems are known.[14] In these reactions, a alkene substrate and hydride react in an anti-maokovnikov manner to form an alkane. Karstedt's catalyst, $Pt_2[(Me_2SiCH{=}CH_2)_2O]_3$, is the standard. This catalyst exists as a dimer containing two platinum atoms and three divinyltetramethyldisiloxyl ligands that increase solubility in a siloxane matrix. Despite it's utility, Karstedt's catalyst can be easily inhibited by amines, thiols, and other common lab contaminants. The small quantities of contaminants required to inhibit the reaction consequently require strict laboratory cleanliness protocols, and are not trivially achieved in a shared space.[15]

Earlier in the discussion of elastomeric networks, it was implied that the networks structure is dependent solely upon the functionality of components and length of the polymeric chain, which determines crosslinker density. In an ideal network, this would be the case. Real networks on the other hand have loops, dangling ends, and higher order defects that impact mechanical properties. Neither first order loops nor dangling ends contribute elastically to the network, and lower the crosslinking density in comparison to an ideal network. Higher order loops may be elastically active. Zhou et al[16,17] showed how to quantify the loop density independently from bulk mechanical properties, and were quickly followed by others applying related methods to a wide range of networks.[18] Gu et al showed that network topology, or the density of defects

such as loops, could be controlled through the feed ratio and semi-batch monomer addition.[19]

## 4.3 Entanglements as a structural feature

Entanglements, or topological restrictions due to the close proximity of long polymeric chains, are a key factor in the mechanical properties of a bulk polymer or polymer network. Entanglements come into play above a molecular weight characteristic to each polymer – in the case of polydimethylsiloxane at around 12,000g/mol.[20] The entanglement molecular weight can be determined from the critical molecular weight where the relationship between polymeric viscosity and molecular weight sharply changes. The exact relationship depends upon the chemical structure, stiffness, and architecture of the polymer chain.[20] One way to modify entanglement molecular weight is through modification of the polymer architecture. Brush polymers for example have an increased entanglement molecular weight due to the extension of side chains and backbones resulting from steric repulsions.[21,22] Cyclic polymers experience a increase in entanglement molecular weight as a result of the lack of chain ends, and small hydrodynamic volume.[23]

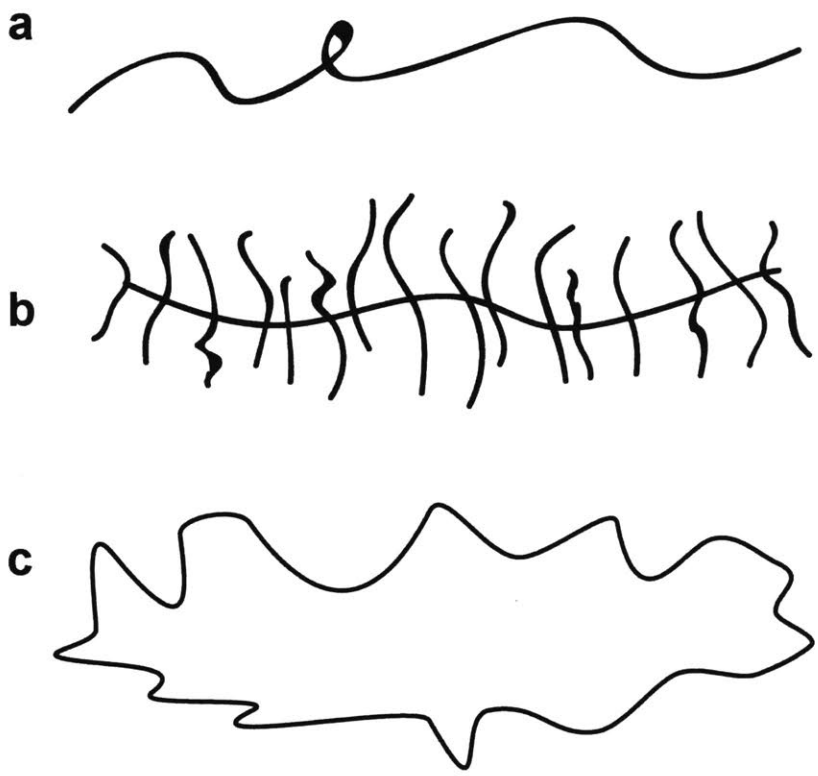


**Figure 4-4:** Variations from the common linear polymer (a) to brush polymers (b) or cyclic polymers (c) increase the entanglement molecular weight of a given polymer.

Entanglements restrict the motion of the polymers to reptation, a snake like thermal motion. Reptation theory[13] can be described as conceptually confining a polymer chain to a theoretical tube in a dense network of the other polymer chains in the bulk. As a result of the other polymer chains, the polymer chain in question cannot move in all dimensions, only along the tube. As this tube is already filled with polymer, motion begins at the chain ends. This phenomenon suggests the increase in entanglement molecular weight described for cyclic polymers above, but does not provide an explanation of cyclic polymer motion.[13] When the network is put under stress, entanglements prevent chain movement, similar to a crosslink.[24] The characteristic entanglement molecular weight for a polymer can be seen as a constant entanglement density for bulk polymer. Given that the mechanical properties of a bulk polymer depend strongly crosslink density,[12] and that entanglements act as crosslinks in the bulk, it is possible to gain understanding of material properties from the entanglement molecular weight of the bulk polymer.

**Figure 4-5:** As a graphical aid to understand entanglements and reputation, a polymer chain is shown confined to a theoretical tube, shown in green, in a dense network of other entangled polymer chains in the bulk.

## 4.4 Modifying Elastomer Properties

There is a wealth of past precedent aimed towards understanding and improving silicone elastomers. Common strategies add fillers, create sacrificial structures, or modify entanglement densities to control mechanical properties. Details such as cure temperature can have significant impact.[19,25] These strategies have been used successfully in a wide range of polymeric elastomers,[26,27] but the focus below will rest on siloxanes when possible.

### 4.4.1 Fillers

The relationship between filler concentration, size, and functionality with mechanical properties has been thoroughly investigated. Aranguren et al[28] performed rheological and tensile studies on silicone rubbers filled with silica loadings ranging from 0 to 40 phr (parts per hundred) and found that the moduli of the elastomers not only increased with higher silica filler concentration but also increased with the concentration of silanol functionality on the silica. Hawley et al[29] performed a similar study and observed a correlation between filler content and increased modulus and ultimate tensile strength by comparing the stress strain curves for PDMS samples with 0 to 35 phr (parts per hundred) content of amorphous silicon dioxide. A Mullins effect, or reduction in stress during repeated tensile experiments,[30] was observed by Hanson et al to occur only normal to the initial stress, leading them to suggest that entanglement removal is a possible origin for this effect.[29,31]

The mechanism for toughening seen in filler loaded networks varies as a function of filler size. Huang et al studied the rubber toughening of a polyamide and determined that the impact resistance of rubber toughened polymers depends on concentration, size, and size distribution of particles, where small particles (below 0.2-0.4$\mu$m) work well to dissipate stress when shear yielding dominates and large particles work well to absorb energy during crazing.[27] Donald and Kramer[32] studied films of acrylonitrile butadiene styrene resins under tension by TEM. They observed that films with 0.1$\mu$m solid rubber particles deformed through cavitation and shear deformation (leading to

voids) opposed to shear yielding. When a mixture of particle sizes was used within a film, crazes nucleated solely at the larger particles. Bucknall et al[33,34] modeled the impact of filler particle size and volume fraction on impact behavior. By mapping particle cavitation, crazing, and shear yielding at a defect, they were able to determine that the maximally effective particle size varies with particle concentration. With that in mind, the maximum toughness is achieved at an equilibrium between particles that are large enough to cavitate but not large enough to induce unstable crazing behavior. Although fillers can be used to control mechanical properties successfully, with siloxanes, the final materials often suffer from a loss of optical transparency due to a refractive index mismatch.[15]

### 4.4.2 Modifying mechanical properties through entanglements

Entanglements have been primarily studied in terms of polymer blends and their impact on the failure mechanism of filled elastomers although conclusions can be drawn for unfilled polymer networks.

The changes in entanglement density due to deformation, and how entanglement density impacts deformation have been studied both theoretically and experimentally. Kramer studied the formation and breakdown of craze fibrils.[35] They related the scale of fibrulation to the entanglement mesh size and density, and theorized that chain scission or disentanglement must accompany crazing in entangled polymers in order to form high surface area fibrils. This both lowers the entanglement density of the polymer after deformation, and implies that as the entanglement density increases the energy required to break network strands and form high surface area fibrils increases. Deformation through shear yielding occurs through the polymer elongating homogeneously, and does not depend as strongly upon the original entanglement density, explaining why the mechanism of deformation transitions from crazing to shear yielding as the entanglement density increases.[36] Henkee and Kramer showed experimentally that the formation of fibrils during crazing requires a loss of entangled strand density.[37] They put crosslinked networks under tension to induce crazing and entanglement density loss, then crosslinked them further prior to heating them

to speed relaxation. The networks retracted to try to maintain the original entanglement density but could not retract fully due to the second set of crosslinks. The equilibrium seen was used to determine that 25-50% of networks strands were lost during fibrillation, with minimal loss in shear deformation zones.[37]

Souheng Wu determined a similar relationship between entanglement density, the characteristic ratio, and whether a sample deforms via crazing or yielding behavior.[38] The numerous publications by Souheng Wu include thorough analysis of entanglements between dissimilar chains,[39] a fascinating study of entanglement reduction in compatible polymer blends due to segmental alignment,[40] and a predictive model for determining the entanglement molecular weight for dozens of polymers including PDMS.[41]

Modifications of entanglement density through blending polymers, and studies on how modifications to the entanglement impact deformation have been studied experimentally. Prest Jr. et al found that blending poly(2,6-dimethylphenylene oxide) with polystyrene led to changes in the entanglement molecular weights as determined through the modulus of the rubbery plateau for each blend.[42] Kim et al[43] investigated how ductility relates to the fracture toughness of elastomers toughened with a styrene-acrylonitrile rubber by blending styrene copolymers with acrylonitrile, maleic anhydride, acrylic acid, and poly (methyl methacrylate). They determined that the toughness of the final blend correlated with the inherent ductility of the blended matrix, a function of entanglement density.[44] Song et al[45] studied the deformation mechanism in blended systems of PVC (poly(vinyl chloride)), $\alpha$-MSAN ($\alpha$-methylstyrene-acrylonitrile), toughened with a constant PB-g-SAN (poly butadiene-g-poly(styrene-co-acrylonitrile filler content. $\alpha$-MSAN has a low entanglement density, while PVC has a high entanglement density. PVC and $\alpha$-MSAN were miscible over the entire range studied (0/100 to 100/0 PVC/MSAN), as seen by a single $T_g$ value. Thus, it was possible to achieve intermediate entanglement densities and control over the entanglement density through the ratio of PVC and $\alpha$-MSAN used. As the PVC content increased, or as the entanglement density increased, the tensile strength increased and elongation at break increased suggesting that the toughness of the blends

was improved. The mechanism of this change was studied by SEM and TEM. At low entanglement density, a clear cut fracture surface implying brittle fracture was seen by SEM but as the entanglement density increased, fibrils, cavities, and stress whitening increased, also a sign of toughening. Internal morphology studied by TEM showed crazes without elongation at low entanglement densities, suggesting the deformation mechanism was crazing. At higher entanglement densities, voids seen by vacitation or debonding and particle elongation were seen, indicating shear deformation. Thus, as entanglement density increased, the mechanism changed from mainly crazing to mainly shear yielding. At intermediate entanglement densities, both effects were seen.

Throughout these studies, entanglement density was seen to increase the energy cost for fibril formation, thus increasing the energy required for deformation through crazing, and increasing the toughness of the material. As the entanglement density increased, the mechanism of deformation transitioned to shear yielding.

## 4.5 Topological Networks

In topological networks, stress dissipation occurs without a permanent change to the network structure. Topological networks are formed through topological crosslinks – distinct from both chemical and physical crosslinks due to a lack of bond formation. In a chemical crosslink, a permanent chemical bond is formed between two network structures – often a long polymeric chain and smaller multifunctional crosslinks. In a physical crosslink, an impermanent ionic bond is formed between two network structures – often a mixture of multifunctional polymers. Physical networks can be strong enough to act analogously to chemically crosslinked networks or have weak bonds that constantly break and reform forming reversible networks. Dynamic covalent bonds, metal ligand coordination bonds, and hydrogen bonds will not be included in the discussion here, despite having been used to make networks with intriguing properties.[46–48] A topological crosslink is unique because the constituent network fragments are not connected through atomic bonding. Instead, they are linked topologically through rings like structures. These crosslinks can pass freely along a polymer chain with minimal energy required for movement.

Topological networks,[49–57] formed from topological crosslinks, have been described as models with which to better understand rubber elasticity[58–60] and as models with which to understand other dynamic crosslinks.[61,62] De Gennes' pursued a theoretical understanding of topological gels to better understand the properties of a physical network shown by Cliffel and Murray. In theory, the chains in this physical gel could slide freely, giving the bulk material an anomalous softness which not seen in practice. In topological gel, chains could slide freely through cyclical crosslinks, requiring only a weak force to extend the material. For both cases, De Gennes found that the osmotic pressure within a gel was sufficient to extend the material, resulting in a swollen gel without additional extensibility.

Okumura and Ito synthesized a topological gel by crosslinking cyclodextrins on two different poly(rotaxane) chains.[63] Here, the poly(rotaxanes) were formed from diamino PEG (MW 20000) with on average 64 alpha-cyclodextrin units on each poly-

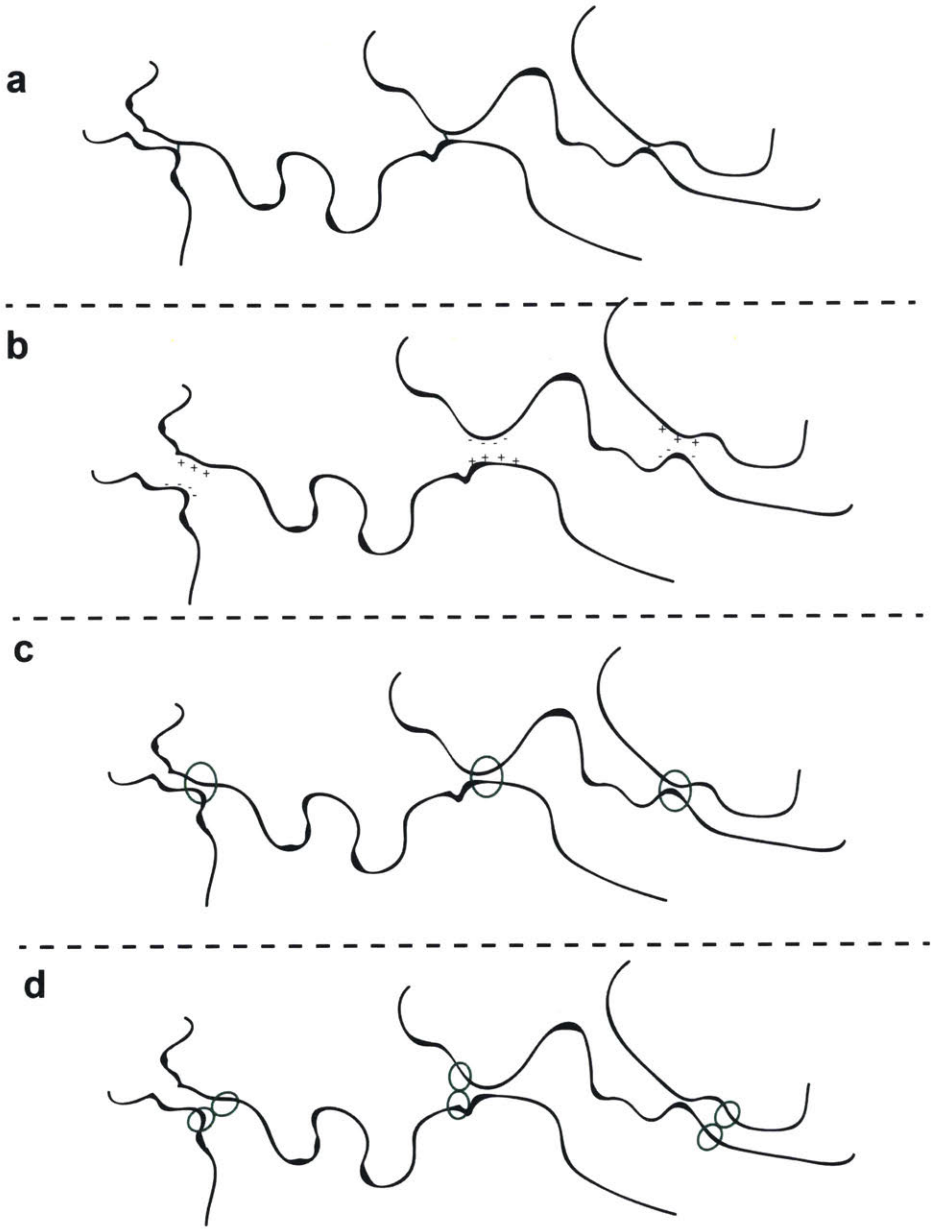


**Figure 4-6:** a) A chemical crosslink is shown with a permanent covalent bond (green) between polymer chains to form a network structure. b) A physical cross linking system is shown with ionic bonding between polymer chains that form a network structure. c) A type of topological bond with multiple chains threaded through a crosslink (shown in green). Due to the lack of chemical bonds between the chain and crosslink, the crosslinks can move freely. d) A figure eight topological crosslink is depicted, of the type used by the Ito group to make topological gels.

mer. A bulky endcap was used to prevent loss of the alpha-cyclodextrin, which were then crosslinked to form figure 8 topological crosslinkers. These crosslinks moved freely on the threaded PEG chains, resulting in unusual mechanical properties.[64] These topological gels have been studied in depth by the Ito group[63–68] and many others.[69]

Although crosslinking the cyclodextrins formed a clear gel, the same mixture made without inclusion complexes did not form a gel. Without the bulky end group used to maintain the inclusion complex, the gel quickly liquified, showing the free movement expected from topological crosslinks.[66] As a result of the crosslinks moving freely on a threading chain, they are able to dissipate tension much like a pulley.[63] This movement results in the intriguing mechanical properties exhibited by slide ring materials: low modulus, high extensibility and swellability.[65]

The free movement of chains threading through crosslinks leads to an additional type of entropy in the system. Uncrosslinked cyclodextrin units distribute in order to maximize distributional entropy, independent of any polymer conformational entropy. After crosslinking, upon anisotropic deformation, the polymer chains move through the topological figure eight crosslinks to relax the deformation to an isotropic form, a phenomenon named the 'pulley effect'. However, residual uncrosslinked cyclodextrin units are trapped between the topological crosslinks resulting in reduced distributional entropy upon chain rearrangement.[64] In order to confirm the pulley effect, Karino et al used SANS in order to observe inhomogeneities in the gel.[66] They expected to see inhomogeneities relaxed by the sliding motion of the crosslinks. Generally, anisotropic stretching of a gel amplifies spatial inhomogeneities however slide ring materials showed normal butterfly patterns when stretched, suggesting that the pulley effect allows the crosslinks to slide with the polymer chains when stretched opposed to the typical displacement of crosslinkers in a network under stress.

Fleury et al[69] systematically studied the bulk properties of poly(rotaxanes) as a function of network structure. By controlling the complexation degree of cyclodextrin with PEG and thus the crosslinking density, it was possible to control the bulk properties. As cross linker fraction increased, so did the modulus and scattering intensity

implying a smaller mesh size. Topological networks are a unique class of materials due to their movable crosslinks with mechanical properties explained by the equilibrium the pulley effect and the distributional entropy of unfunctionalized rings, allowing for stress dissipation without permanent changes to the network structure.

## 4.6 Conclusions

Siloxane elastomers have unique properties due to the alternating silicon oxygen atoms in the polymer backbone. Networks formed from these elastomers are valued for their high thermal stability, chemical resistance, electrical resistance, hydrophobicity, and biocompatibility. The relationship between fillers and enhanced mechanical properties has been studied in depth, as has the relationship between entanglement density and mechanical properties. The means and effect of modifying entanglements have been studied for polymer blends, but not within systems of constant composition.

## 4.7 References


(1) Sun Care Protection Solutions & Sunscreen Formulation Solutions., `https://consumer.dow.com/en-us/industry/ind-beauty-personal-care/mkt-beauty-sun-care.html`, Online; accessed 23-January-2019, 2019.

(2) Ahuja, K.; Singh, S. *Silicone Elastomers Market Size By Product (High Temperature Vulcanized, Room Temperature Vulcanized, Liquid Silicone Rubber), By Application (Electrical & Electronics, Automotive & Transportation, Industrial Machinery, Consumer Goods, Construction, Others), Industry Analysis Report, Regional Outlook (U.S., Germany, UK, France, Italy, China, India, Japan, South Korea, Brazil), Application Potential, Price Trends, Competitive Market Share & Forecast, 2016 - 2023*; Report; 2016.

(3) De Jong, J.; Lammertink, R. G.; Wessling, M. Membranes and microfluidics: a review. *Lab. Chip* **2006**, *6*, 1125–39.

(4) Thorsen, T.; Maerkl, S.; Quake, S. Microfluidic Large-Scale Integration. *Science* **2002**, *298*, 580–584.

(5) Adly, N.; Weidlich, S.; Seyock, S.; Brings, F.; Yakushenko, A.; Offenhäusser, A.; Wolfrum, B. Printed microelectrode arrays on soft materials: from PDMS to hydrogels. *npj Flexible Electronics* **2018**, *2*, DOI: `10.1038/s41528-018-0027-z`.

(6) Fu, Y.; Kao, W. J. Drug release kinetics and transport mechanisms of non-degradable and degradable polymeric delivery systems. *Expert Opin. Drug Deliv.* **2010**, *7*, 429–44.

(7) Gadad, N.; Shivayyanavar, N.; Viannie, L. R.; Jayachandra, S. Y.; Banapurmath, N. R.; Shettar, A. S.; Shellikeri, A.; Kaulgud, V. Fabrication and development of magnetically actuated PDMS micropump for drug delivery. *IOP Conference Series: Materials Science and Engineering* **2018**, *376*, 012128.

(8) Mishra, G.; Bhattacharyya, S.; Bhatia, V.; Ateeq, B.; Sharma, A.; Sivakumar, S. Direct Intranuclear Anticancer Drug Delivery via Polydimethylsiloxane Nanoparticles: in Vitro and in Vivo Xenograft Studies. *ACS Appl. Mater. Interfaces* **2017**, *9*, 34625–34633.

(9) Dunn, K. W.; Hall, P. N.; Khoo, C. T. Breast implant materials: sense and safety. *Br. J. Plast. Surg.* **1992**, *45*, 315–21.

(10) Mojsiewicz-Pienkowska, K.; Jamrogiewicz, M.; Szymkowska, K.; Krenczkowska, D. Direct Human Contact with Siloxanes (Silicones) - Safety or Risk Part 1. Characteristics of Siloxanes (Silicones). *Front. Pharmacol.* **2016**, *7*, 132.

(11) Zheng, P.; McCarthy, T. J. Rediscovering silicones: molecularly smooth, low surface energy, unfilled, UV/vis-transparent, extremely cross-linked, thermally stable, hard, elastic PDMS. *Langmuir* **2010**, *26*, 18585–90.

(12) Flory, P. J. Network structure and the elastic properties of vulcanized rubber. *Chem. Rev.* **1944**, *35*, 51–75.

(13) Rubinstein, M.; Colby, R., *Poymer Physics*; Oxford University Press: New York, 2003.

(14) Marciniec, B., *Hydrosilylation, a comprehensive review on recent advances*; Advances in SIlicon Science; Springer Netherlands: 2009.

(15) Mazurek, P.; Vudayagiri, S.; Skov, A. L. How to tailor flexible silicone elastomers with mechanical integrity: a tutorial review. *Chem. Soc. Rev.* **2019**, *48*, 1448–1464.

(16) Zhou, H.; Schon, E. M.; Wang, M.; Glassman, M. J.; Liu, J.; Zhong, M.; Diaz Diaz, D.; Olsen, B. D.; Johnson, J. A. Crossover experiments applied to network formation reactions: improved strategies for counting elastically inactive molecular defects in PEG gels and hyperbranched polymers. *J. Am. Chem. Soc.* **2014**, *136*, 9464–70.

(17) Zhou, H.; Woo, J.; Cok, A. M.; Wang, M.; Olsen, B. D.; Johnson, J. A. Counting primary loops in polymer gels. *Proc. Natl. Acad. Sci. U.S.A.* **2012**, *109*, 19119–24.

(18) Kawamoto, K.; Zhong, M.; Wang, R.; Olsen, B. D.; Johnson, J. A. Loops versus Branch Functionality in Model Click Hydrogels. *Macromolecules* **2015**, *48*, 8980–8988.

(19) Gu, Y.; Kawamoto, K.; Zhong, M.; Chen, M.; Hore, M. J. A.; Jordan, A. M.; Korley, L. T. J.; Olsen, B. D.; Johnson, J. A. Semibatch monomer addition as a general method to tune and enhance the mechanics of polymer networks via loop-defect control. *Proc. Natl. Acad. Sci. U.S.A.* **2017**, *114*, 4875–4880.

(20) Fetters, L.; Lohse, D.; Milner, S.; Graessley, W. Packing Length Influence in Linear Polymer Melts on the Entanglement, Critical, and Reptation Molecular Weights. *Macromolecules* **1999**, *32*, 6847–6851.

(21) Cai, L. H.; Kodger, T. E.; Guerra, R. E.; Pegoraro, A. F.; Rubinstein, M.; Weitz, D. A. Soft Poly(dimethylsiloxane) Elastomers from Architecture-Driven Entanglement Free Design. *Adv. Mater.* **2015**, *27*, 5132–40.

(22) Paturej, J.; Sheiko, S. S.; Panyukov, S.; Rubinstein, M. Molecular structure of bottlebrush polymers in melts. *Sci. Adv.* **2016**, *2*, e1601478.

(23) Williams, R. J.; Dove, A. P.; O'Reilly, R. K. Self-assembly of cyclic polymers. *Polym. Chem.* **2015**, *6*, 2998–3008.

(24) Abadi, M.; Serag, M. F.; Habuchi, S. Entangled polymer dynamics beyond reptation. *Nat. Commun.* **2018**, *9*, 5098.

(25) Johnston, I. D.; McCluskey, D. K.; Tan, C. K. L.; Tracey, M. C. Mechanical characterization of bulk Sylgard 184 for microfluidics and microengineering. *J. Micromech. Microeng.* **2014**, *24*, 035017.

(26) Dompas, D.; Groeninckx, G.; Isogawa, M.; Hasegawa, T.; Kadokura, M. Cavitation versus debonding during deformation of rubber-modified poly(vinyl chloride). *Polymer* **1995**, *36*, 437–441.

(27) Huang, J. J.; Keskkula, H.; Paul, D. R. Rubber toughening of an amorphous polyamide by functionalized SEBS copolymers: morphology and Izod impact behavior. *Polymer* **2004**, *45*, 4203–4215.

(28) Aranguren, M.; Mora, E.; Macosko, C.; Saam, J. Rheological and mechanical properties of filler rubber: Silica-Silicone. *Rubber Chem. Technol.* **1994**, *67*, 820–833.

(29) Hawley, M. E.; Wrobleski, D. A.; Orler, E. B.; Houlton, R.; Chitanvis, K. E.; Brown, G. W.; Hanson, D. E. Mechanical Properties and Filler Distribution as a Function of Filler Content in Silica Filled PDMS Samples. *MRS Proceedings* **2011**, *791*, DOI: 10.1557/proc-791-q4.4.

(30) Mullins, L.; Tobin, N. Theoretical Model for the Elastic Behavior of Filler-Reinforced Vulcanized Rubbers. *Rubber Chem. Technol.* **1957**, *30*, 555–571.

(31) Hanson, D. E.; Hawley, M.; Houlton, R.; Chitanvis, K.; Rae, P.; Orler, E. B.; Wrobleski, D. A. Stress softening experiments in silica-filled polydimethylsiloxane provide insight into a mechanism for the Mullins effect. *Polymer* **2005**, *46*, 10989–10995.

(32) Donald, A. M.; Kramer, E. J. Plastic deformation mechanisms in poly(acrylonitrile-butadiene styrene) [ABS]. *Journal of Materials Science* **1982**, *17*, 1765–1772.

(33) Bucknall, C. B.; Paul, D. R. Notched impact behavior of polymer blends: Part 1: New model for particle size dependence. *Polymer* **2009**, *50*, 5539–5548.

(34) Bucknall, C. B.; Paul, D. R. Notched impact behaviour of polymer blends: Part 2: Dependence of critical particle size on rubber particle volume fraction. *Polymer* **2013**, *54*, 320–329.

(35) Kramer, E. J. Craze Fibril Formation and Breakdown. *Polym. Eng. Sci.* **1984**, *24*, 761–769.

(36) Henkee, C. S.; Kramer, E. J. Crazing and shear deformation in crosslinked polystyrene. *Journal of Polymer Science Part B: Polymer Physics* **1996**, *34*, 2825–2841.

(37) Henkee, C. S.; Kramer, E. J. Loss of entanglement density during crazing. *Journal of Materials Science* **1986**, *21*, 1398–1404.

(38) Wu, S. Chain structure, phase morphology, and toughness relationships in polymers and blends. *Polym. Eng. Sci.* **1990**, *30*, 753–761.

(39) Wu, S. Entanglement between dissimilar chains in compatible polymer blends: poly(methyl methacrylate) and poly(vinylidene fluoride). *Journal of Polymer Science Part B: Polymer Physics* **1987**, *25*, 557–566.

(40) Wu, S. Entanglement, friction, and free volume between dissimilar chains in compatible polymer blends. *Journal of Polymer Science Part B: Polymer Physics* **1987**, *25*, 2511–2529.

(41) Wu, S. Predicting Chain Conformation and Entanglement of Polymers From Chemical Structure. *Polym. Eng. Sci.* **1992**, *32*, 823–830.

(42) Prest Jr., W. M.; Porter, R. S. Rheological properties of poly(2,6-dimethylphenylene oxide)—polystyrene blends. *Journal of Polymer Science Part A-2: Polymer Physics* **1972**, *10*, 1639–1655.

(43) Kim, H.; Keskkula, H.; Paul, D. The role of inherent ductility in rubber toughening of brittle polymers. *Polymer* **1991**, *32*, 2372–2376.

(44) Bartczak, Z. Effect of Chain Entanglements on Plastic Deformation Behavior of Linear Polyethylene. *Macromolecules* **2005**, *38*, 7702–7713.

(45) Song, L.; Ren, L.; Zhang, M.; Sun, S.; Gao, G.; Gui, Y.; Zhang, L.; Zhang, H. Effect of Entanglement Density on Mechanical Properties and Deformation Behavior of Rubber-Modified PVC/$\alpha$-MSAN Blends. *Ind. Eng. Chem. Res.* **2013**, *52*, 12567–12573.

(46) Feng, Z.; Yu, B.; Hu, J.; Zuo, H.; Li, J.; Sun, H.; Ning, N.; Tian, M.; Zhang, L. Multifunctional Vitrimer-Like Polydimethylsiloxane (PDMS): Recyclable, Self-Healable, and Water-Driven Malleable Covalent Networks Based on Dynamic Imine Bond. *Ind. Eng. Chem. Res.* **2019**, *58*, 1212–1221.

(47) Schmolke, W.; Perner, N.; Seiffert, S. Dynamically Cross-Linked Polydimethylsiloxane Networks with Ambient-Temperature Self-Healing. *Macromolecules* **2015**, *48*, 8781–8788.

(48) Zhang, H.; Cai, C.; Liu, W.; Li, D.; Zhang, J.; Zhao, N.; Xu, J. Recyclable Polydimethylsiloxane Network Crosslinked by Dynamic Transesterification Reaction. *Sci. Rep.* **2017**, *7*, 11833.

(49) Delaviz, Y.; Gibson, H. Macrocyclic Polymers. 2.f Synthesis of Poly(amide crown ether)s Based on Bis(5-carboxy-l,3-phenylene)-32-crown-10. Network Formation through Threading. *Macromolecues* **1992**, *25*, 4859–4862.

(50) Gibson, H.; Nagvekar, D.; Powell, J.; Gong, C.; Bryant, W. Polyrotaxanes by In Situ Self Threading During Polymerization of Functional Macrocycles. Part 2*: Poly(ester crown ether)s. *Tetrahedron* **1997**, *53*, 15197–15207.

(51) Gong, C.; Gibson, H. Supramolecular chemistry with macromolecules: Macromolecular knitting, reversible formation of branched polyrotaxanes by self-assembly. *Macromol. Chem. Phys.* **1998**, *199*, 1801–1806.

(52) Kubo, M.; Hibino, T.; Uno, T.; Itoh, T. Synthesis and Copolymerization of Cyclic Macromonomer Based on Cyclic Polystyrene: Gel Formation via Chain Threading. *Macromolecules* **2002**, *35*, 5816–5820.

(53) Kubo, M.; Kato, N.; Uno, T.; Itoh, T. Preparation of Mechanically Cross-Linked Polystyrenes. *Macromolecules* **2004**, *37*, 2762–2765.

(54) Oike, H.; Mouri, T.; Tezuka, Y. A Cyclic Macromonomer Designed for a Novel Polymer Network Architecture Having Both Covalent and Physical Linkages. *Macromolecules* **2001**, *34*, 6229–6234.

(55) Watanabe, J.; Ooya, T.; Nitta, K. H.; Park, K. D.; Kim, Y. H.; Yui, N. Fibroblast adhesion and proliferation on poly(ethylene glycol) hydrogels crosslinked by hydrolyzable polyrotaxane. *Biomaterials* **2002**, *23*, 4041–8.

(56) Zada, A.; Avny, Y.; Zilkha, A. Monomers for non-bond crosslinking of vinyl polymers. *Eur. Polym. J.* **1999**, *35*, 1159–1164.

(57) Zada, A.; Avny, Y.; Zilkha, A. Monomers for non-bond crosslinking of vinyl polymers II. Cyclic octaethylene glycol 5-methacrylamido- isophthalate. *Eur. Polym. J.* **2000**, *36*, 351–357.

(58) Ball, R. C.; Doi, M.; Edwards, S. F.; Warner, M. Elasticity of Entangled Networks. *Polymer* **1981**, *22*, 1010–1018.

(59) Edwards, S. F.; Vilgis, T. The Effect of Entanglements in Rubber Elasticity. *Polymer* **1986**, *27*, 483–492.

(60) Rubinstein, M.; Panyukov, S. Elasticity of polymer networks. *Macromolecules* **2002**, *35*, 6670–6686.

(61) De Gennes, P. G. Sliding gels. *Physica A* **1999**, *271*, 231–237.

(62) Koyama, Y. Synthesis of topologically crosslinked polymers with rotaxane-crosslinking points. *Polym. J.* **2014**, *46*, 315–322.

(63) Okumura, Y.; Ito, K. The polyrotaxane gel: A topological gel by figure-of-eight cross-links. *Adv. Mater.* **2001**, *13*, 485.

(64) Ito, K. Topological Gels. **2013**, 1–8.

(65) Ito, K. Novel entropic elasticity of polymeric materials: why is slide-ring gel so soft? *Polym. J.* **2011**, *44*, 38–41.

(66) Karino, T.; Shibayama, M.; Ito, K. Slide-ring gel: Topological gel with freely movable cross-links. *Physica B* **2006**, *385-386*, 692–696.

(67) Noda, Y.; Hayashi, Y.; Ito, K. From topological gels to slide-ring materials. *J. Appl. Polym. Sci.* **2014**, *131*, 40509.

(68) Shinohara, Y.; Kayashima, K.; Okumura, Y.; Zhao, C. M.; Ito, K.; Amemiya, Y. Small-angle X-ray scattering study of the pulley effect of slide-ring gels. *Macromolecules* **2006**, *39*, 7386–7391.

(69) Fleury, G.; Schlatter, G.; Brochon, C.; Travelet, C.; Lapp, A.; Lindner, P.; Hadziioannou, G. *Macromolecules* **2007**, *40*, 535–543.

# Chapter 5

# Topology modification of polydimethylsiloxane elastomers through loop formation

## 5.1 Introduction

The methods for polymer toughening discussed in the previous chapter revolve around stress dissipation mechanisms. Kramer related the formation of fibrils to the entanglement density, theorizing that chain scission or disentanglement must accompany crazing in entangled polymers.[1] As the entanglement density increases, the energy required to induce deformation does as well, resulting in a toughened material. Song et al saw the same improvement in mechanical properties when blending two polymers to control the entanglement density of the final material.[2] Huang et al studied the relationship between fillers and stress dissipation mechanisms. They determined that small particles (below 0.2-0.4um) as elastomeric fillers work well to dissipate stress when shear yielding dominates as the deformation mechanism and large particles work well to absorb energy during crazing.[3] Topological networks were used by Ito and others to create highly extensible networks with stress dissipation due to the free movement of crosslinks, called the 'pulley effect'.[4–17]

### 5.1.1 Loop-rich Brushes

Although there has been significant research involving brush polymers,[18–20] and brush polymer networks,[21] loop-rich brush polymers are less prevalent. Baum et al[22] were able to make a side loop polymer through the hydrosilylation of poly(butadiene) with poly(dimethylsiloxane) dihydride.[22] Dilute conditions were used to ensure a high loop concentration. These side loop polymers could be crosslinked with a long polymer chain threading through the side loops to form a hybrid chemical and topological network, incorporating aspects from each system.

We were inspired to make materials with a high loop concentration in order to see if the pulley effect would be observed on materials with only partial topological crosslinking. This would allow for stress dissipation in a system with a higher modulus than that achievable through topological crosslinks alone.

By making a loop-rich brush, abbreviated here as a loopy brush, then crosslinking the loop rich system with a long linear polymer chain, it would be possible to

make crosslinks that threaded through the side-loops in a statistical manner. Energy dissipation through the pulley effect would result in a high extensibility. Chemical crosslinking would produce a high modulus system, resulting in an increased overall toughness when compared to a system with solely topological or chemical crosslinking.

## 5.2 Results and Discussion

### 5.2.1 Polybutadiene/PDMS Networks

To form loopy brushes, we began by using a 1,400g/mol polybutadiene with 70% 1,2 addition, representing an average of 18 vinyl groups per chain to react with 1,000 g/mol hydride terminated polydimethylsiloxane (PDMS) under the dilutions used by Baum, Baum, and Ho.[22] At these dilutions, we expected intramolecular reactions to be favored over intermolecular reactions, forming loop rich systems. In our hands, these samples formed gels even under dilute conditions. Additional dilution to 22 mg/mL in toluene, dichloromethane, or chloroform formed materials that did not gel prior to concentration as seen through a vial inversion test.

As a brief check into whether these systems formed elastically inactive loops or hyperbranched networks, the polymers were hydrosilylated overnight, concentrated beyond the point shown previously to gel, and left under hydrosilyation conditions overnight. No gels were seen through vial inversion, suggesting that the vinyl and hydride groups were no longer available after the initial reaction, indicating the formation of loops opposed to network segments that could be crosslinked further to form gels.

A series of elastomers were made from these loopy brushes. Here, 1,000g/mol hydride terminated polydimethylsiloxane (PDMS) was reacted with the 1,400g/mol polybutadiene mentioned above under dilute hydrosilylation conditions overnight to favor intramolecular reactions. After the formation of loop-rich brushes, the solutions were concentrated to isolate the brushes. The concentrated brushes were allowed to equilibrate with more hydride terminated PDMS, and hydrosilylated with a second aliquot of catalyst under neat conditions to form an elastomer.

In order to study the relationship between loop density and mechanical properties, a series of elastomers was made with varying quantities of PDMS added under dilute conditions. This series will be referred to PBD1.4kPDMS1k. In all cases, the final stoichiometric functional group ratio between vinyl and hydride functional groups was kept at 1. The total sum of PDMS added under dilute and concentrated conditions

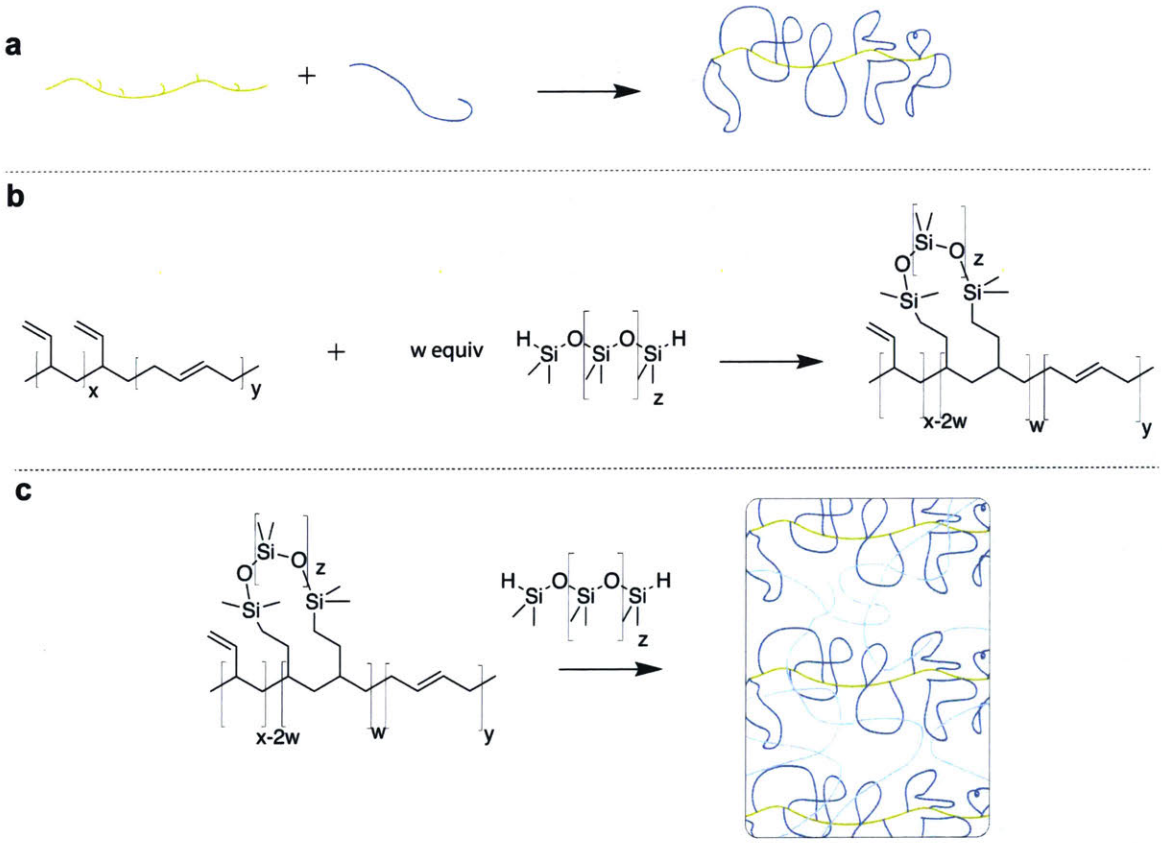


**Figure 5-1:** a) A graphic of the formation of loopy brushes is shown here. Polybutadiene with a high 1,2 functionality (shown in yellow), is combined under dilute conditions with a PDMS dihydride (shown in blue) and a platinum hydrosilylation catalyst to form 'loopy' brushes where loops are favored due to high dilution. b) Chemical structures for the formation of loopy brushes are shown here. Polybutadiene with a high 1,2 functionality was combined under dilute conditions with a PDMS dihydride and a platinum hydrosilylation catalyst to form 'loopy' brushes where loops are favored due to high dilution. Here, brushes were made with both a 1.4k polybutadiene (x=17, y=7), a 5k polybutadiene with (x=13, y=79), a 1k PDMS (z=12), and a 5k PDMS (z=59). c) Brushes were crosslinked under concentrated conditions to form elastomers. Both a 1k PDMS (z=12), and a 5k PDMS (z=59) were used for elastomer formation, forming series PBD1kPDMS1k and PBD5kPDMS4.5k respectively.

was kept constant. The amount of PDMS added under dilute conditions ranged from 0% of the total molar quantity of PDMS to 100% of the total molar quantity of PDMS.

Elastomers were made on a milligram scale to confirm conversion and then a multi-gram scale for characterization. Series PBD1.4kPDMS1k proved to be too difficult to handle for tensile testing. Changes in the sample size and aspect ratio did not produce samples robust enough for tensile testing. No tensile data could be collected with the PBD1.4kPDMS1k series, however rheological and gel swelling data are shown in the experimental section. The gel swelling data corresponded well to the PDMS molecular weight until greater than 80% of the total PDMS was added under dilute conditions.

In order to obtain samples that could be handled for tensile testing, the stoichiometric functional group ratio was decreased to 0.5 hydride/vinyl groups, the hydride terminated PDMS molecular weight was increased to 4,500 g/mol, and the polybutadiene was increased in molecular weight to a 5,000g/mol, 13.8% vinyl functionality polybutadiene. All changes served to decrease the final crosslinker density.

A series of elastomers (PBD5kPDMS4.5k) was made with the aforementioned changes to simplify elastomer handling. 5,000g/mol hydride terminated (PDMS) was hydrosilylated with the 5,000g/mol polybutadiene mentioned above under dilute conditions overnight to form loop-rich brushes. The hydrosilylation under dilute conditions was tracked by $^{1}$H-NMR. After 18 hours, the conversions observed by NMR tracked well with the anticipated conversion for a stoichiometric functional group ratio of 0.5 hydride/vinyl, suggesting that the hydrosilylation went to complete conversion. Peak broadening was seen when 100% of the PDMS was added under dilute conditions.

After brush formation, the solutions were concentrated to isolate the brushes. The concentrated brushes were allowed to equilibrate with a second portion of hydride terminated PDMS, and hydrosilylated with a second aliquot of catalyst under neat conditions to form an elastomer.

In order to study the relationship between loop density and mechanical properties,

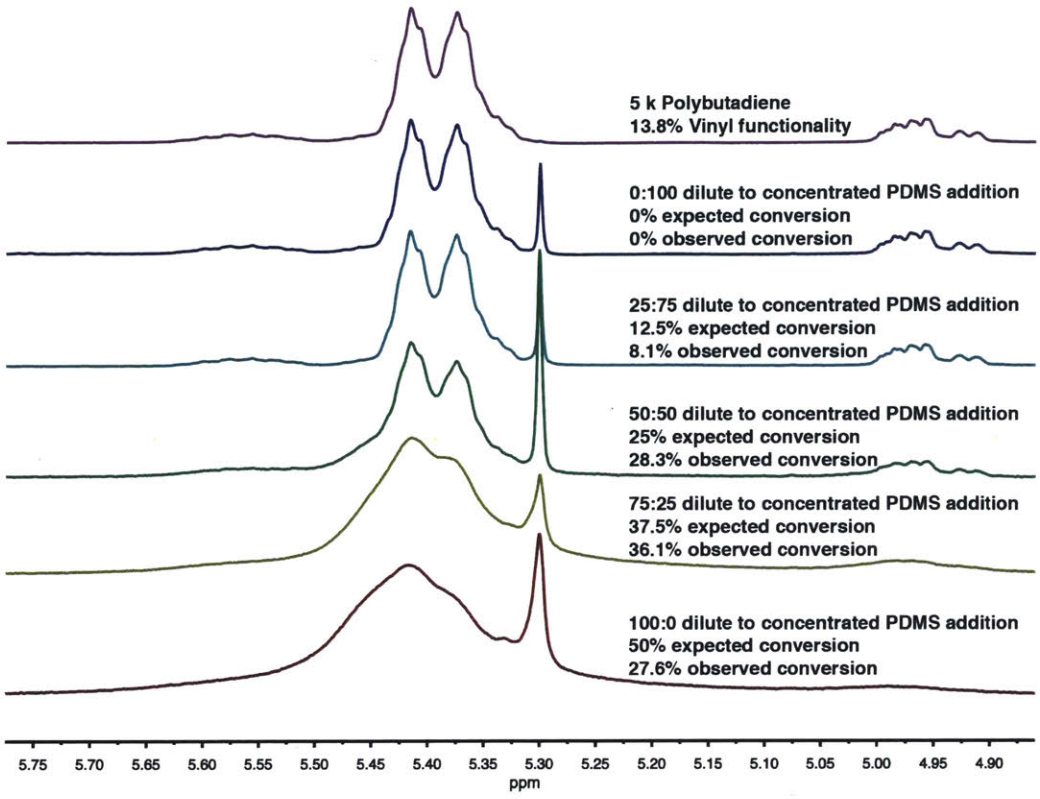


**Figure 5-2:** $^{1}$H-NMR spectra of loopy brushes from series PBD5kPDMS4.5k are shown. Polybutadiene(5,000g/mol, 13.8% vinyl functionality) was hydrosilylated with polydimethyl silioxane (4,500g/mol) under dilute conditions to form loop-rich brushes. Here, $^{1}$H-NMR was used to track conversion of the vinyl groups after reaction with percentages of the total molar quantity of PDMS used for elastomer formation ranging from 0% to 100%.

a series of elastomers was made with varying quantities of PDMS added under dilute conditions. This series will be referred to PBD5kPDMS4.5k. In all cases, the final stoichiometric functional group ratio between vinyl and hydride functional groups was kept at 0.5. The total sum of PDMS added under dilute and concentrated conditions was kept constant. The amount of PDMS added under dilute conditions ranged from 0% of the total molar quantity of PDMS to 100% of the total molar quantity of PDMS, with the amount of PDMS added under concentrated conditions to form the elastomer adjusted accordingly.

A series of different tensile testing methods were used in an attempt to improve data collection while using less material than required by the ASTM D-412 standard.

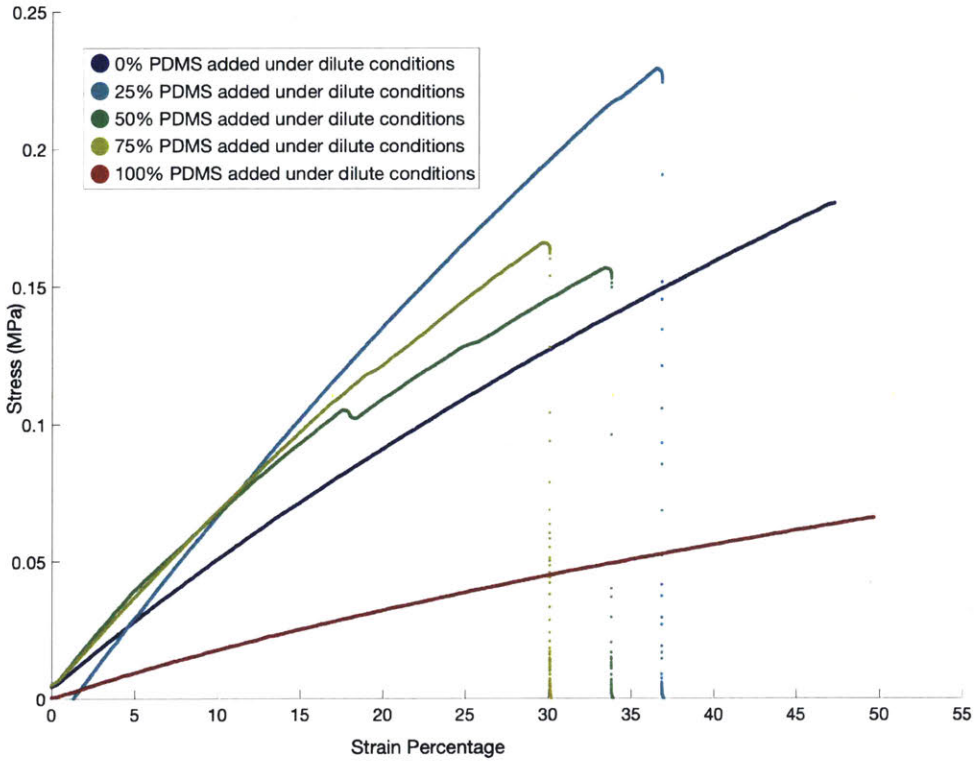


**Figure 5-3:** Tensile data is shown for a series of samples, PBD5kPDMS5k, with differing quantities of PDMS added under dilute conditions. Although there is not a clear trend between loop concentration and toughness, the modulus decreased for samples with 100% of PDMS added under dilute conditions.

Initially, rectangular samples were cut from thick films and clamped directly into the instrument. These samples would often slip from the grips midway during testing, or crush under the pressure of the sample grips. Modifications to the sample aspect ratio or molecular weight of network components improved the percentage of successful tensile tests, but were not completely successful. Rectangular samples were glued to a cardstock frame, which was then gripped for tensile testing. When these cardboard frames were used, no deformation was seen in the glued part of the sample, and each run of multiple trials broke at a different location.

Tensile data is shown for a series of samples, PBD5kPDMS5k, with differing quantities of PDMS added under dilute conditions. When elastomers were made with 100% of PDMS added under dilute conditions, the final material formed a network,

indicative of a small fraction of unreacted functional groups that crosslinked under concnetrated conditions. These materials had a lower modulus and higher extensibility then elastomers in the same series with less PDMS added under dilute conditions. Materials with less PDMS added under dilute conditions and thus a lower loop density showed a higher modulus, and lower extensibility. These changes in the mechanical property could be due to stress dissipation through the pulley effect, or a lower crosslinker density. A combination of these properties would be ideal.

### 5.2.2 PDMS networks with loop rich brushes

In order to produce optically clear materials, the next series of elastomers were made with PDMS used for both the vinyl and hydride bearing polymers. A 28,000g/mol vinylmethylsiloxane dimethylsiloxane copolymer with 7-8% vinyl functionality (28k vinyl PDMS), representing an average of 29 vinyl groups per chain was used as the vinyl-bearing constituent in each elastomer reported in this section.

A series of loop-rich brushes was made through the hydrosilylation of a 28k vinyl PDMS with 5,000 g/mol hydride terminated PDMS under dilute conditions. After the reaction completed, as monitored by NMR, the brushes were concentrated and combined with a second portion of hydride terminated PDMS and a second aliquot of catalyst under neat conditions to form elastomers. In order to study the relationship between loop density and mechanical properties, a series of elastomers (PDMS27kPDMS5k) was made with varying quantities of PDMS added under dilute conditions. In all cases, the final stoichiometric functional group ratio between vinyl and hydride functional groups was kept at 0.5. The total sum of PDMS added under dilute and concentrated conditions was kept constant. The amount of PDMS added under dilute conditions ranged from 0% of the total molar quantity of PDMS to 50% of the total molar quantity of PDMS, with the amount of PDMS added under concentrated conditions to form the elastomer adjusted accordingly. Elastomers made with larger fractions of PDMS added under dilute conditions failed to cure reliably.

In order to determine whether the decrease in modulus seen in the PBD5kPDMS5k series of elastomers as the percentage of PDMS added under dilute conditions in-

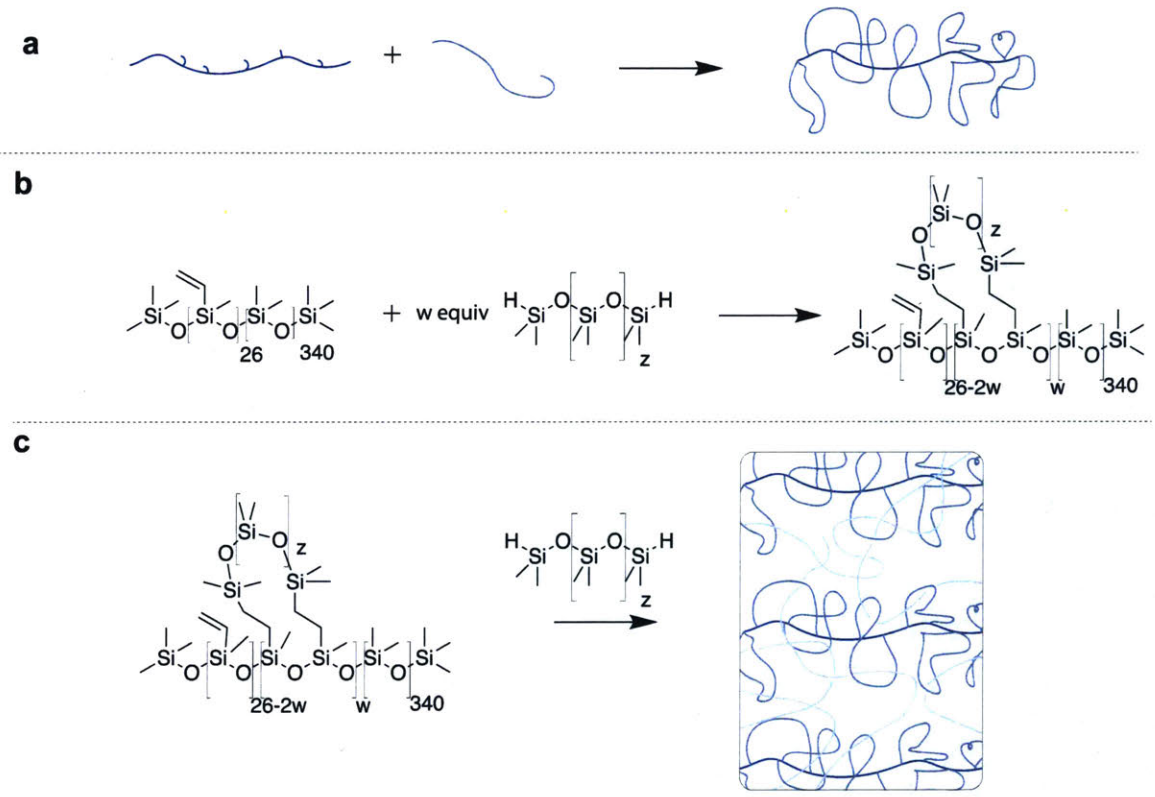


**Figure 5-4:** a) A graphic of the formation of loopy brushes is shown here. 28k vinylmethylsiloxane dimethylsiloxane with 7-8% vinyl functionality (shown in dark blue), was combined under dilute conditions with a PDMS dihydride (shown in blue) and a platinum hydrosilylation catalyst to form 'loopy' brushes where loops are favored due to high dilution. b) Chemical structures for the formation of loopy brushes are shown here. Brushes were formed with the 28k vinyl methyl siloxane dimethyl siloxane and either a 5k PDMS (z=59) or 17k PDMS (z=230). c) Both a 5k PDMS (z=59) and 17k PDMS (z=230) were used for elastomer formation, forming series PDMS28kPDMS5k and PDMS28kPDMS17k respectively. The quantity of PDMS added under dilute conditions, 'w', varied with each elastomer within the series.

creased was caused by a difference in the crosslink density or an effect due to the presence of loop-rich brushes, a control series of elastomers was made. This series (PDMS28kPDMSm5k) was made similarly to the series above with one crucial distinction. Instead of the 5,000 g/mol hydride terminated PDMS with a hydride functionality at each side of the chain, a 5,000 g/mol monohydride terminated PDMS (PDMS monohydride) with a single hydride terminus was used.

To make series PDMS28kPDMSm5k, a series of traditional brush polymers was made through the hydrosilylation of a 28k vinyl PDMS with 5,000 g/mol monohydride terminated PDMS under dilute conditions. After concentration of the brushes, a combination of PDMS monohydride and PDMS dihydride were used to form the elastomer. All final elastomers contained a 1:1 molar ratio of PDMS monohydride and PDMS dihydride. Elastomers were made with 0%, 20%, 40%, and 50% of the total molar quantity of PDMS added under dilute conditions.

Tensile testing was conducted on both elastomer series PDMS28kPDMS5k and elastomer series PDMS28kPDMSm5k. The elastomers made with monohydride terminated PDMS showed a lower modulus and ultimate tensile strength across the board when compared to elastomers made with solely dihydride terminated PDMS, suggesting that the PDMS added under dilute conditions is elastically active within the final elastomer. No clear dependence upon the amount of PDMS added under dilute conditions was observed in the tensile properties.

A similar result was seen for a series of elastomers (PDMS28kPDMS17k17k) made with 17,000 g/mol PDMS dihydride, as described in the experimental section. No clear dependence upon the amount of PDMS added under dilute conditions was observed in the tensile properties.

### 5.2.3 PDMS Networks with variable size loop rich brushes

In order to determine whether the relative lengths of PDMS added under dilute conditions and concentrated conditions impact mechanical properties, two series of elastomers (PDMS28kPDMS5k17k and PDMS28kPDMS17k5k) were made with varying percentages of the total PDMS added under dilute conditions. Here, the final

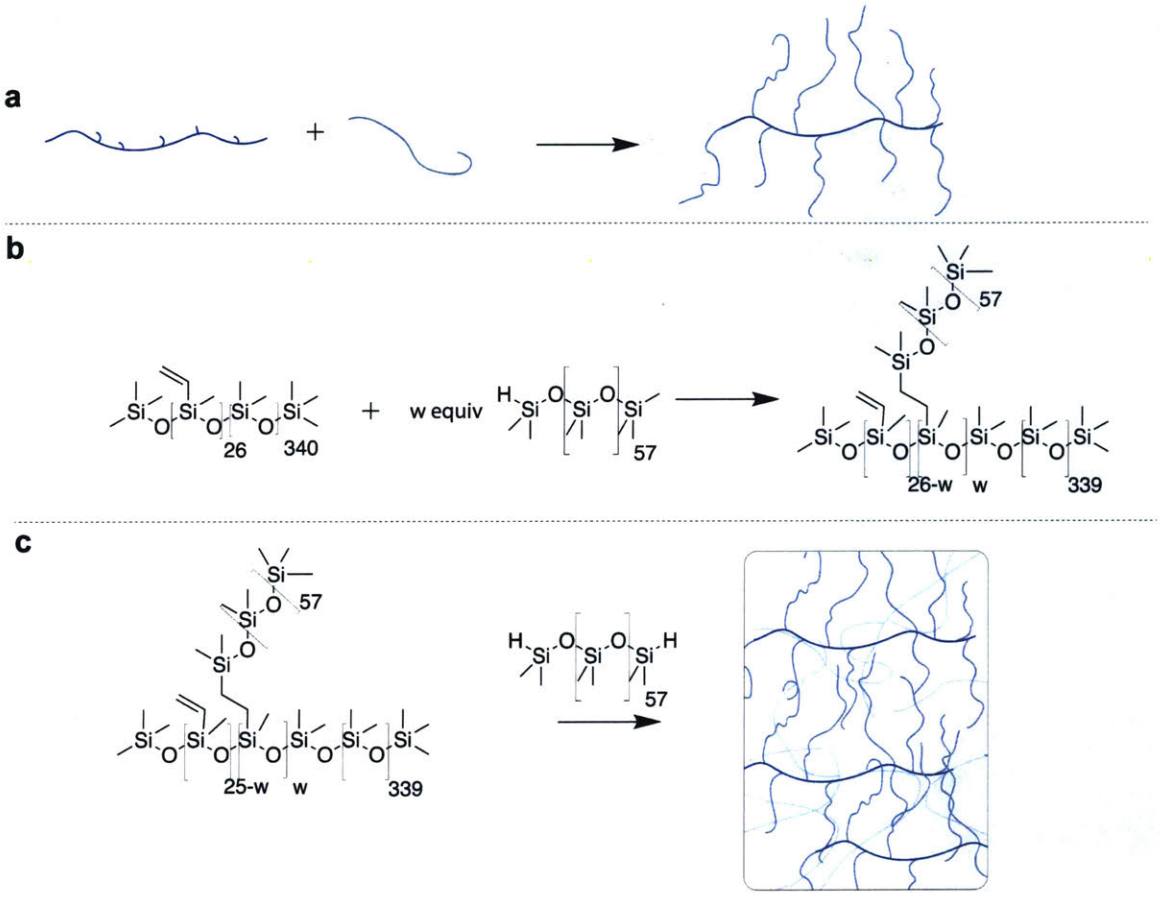


**Figure 5-5:** a) A graphic of the formation of a standard brush is shown here. 28k vinylmethylsiloxane dimethylsiloxane with 7-8% vinyl functionality (shown in dark blue), was combined under dilute conditions with a monofunctionalized PDMS hydride(shown in blue) and a platinum hydrosilylation catalyst to form 'loopy' brushes where loops are favored due to high dilution. b) Chemical structures for the formation of loopy brushes are shown here. Brushes were formed with the 28k vinyl methyl siloxane dimethyl siloxane and a 5k monohydride terminated PDMS (z=59). c) A 5k PDMS dihydride (z=59) was used for elastomer formation, forming series PDMS28kPDMSm5k. The quantity of monohydride terminated PDMS added under dilute conditions, 'w', varied with each elastomer within the series.

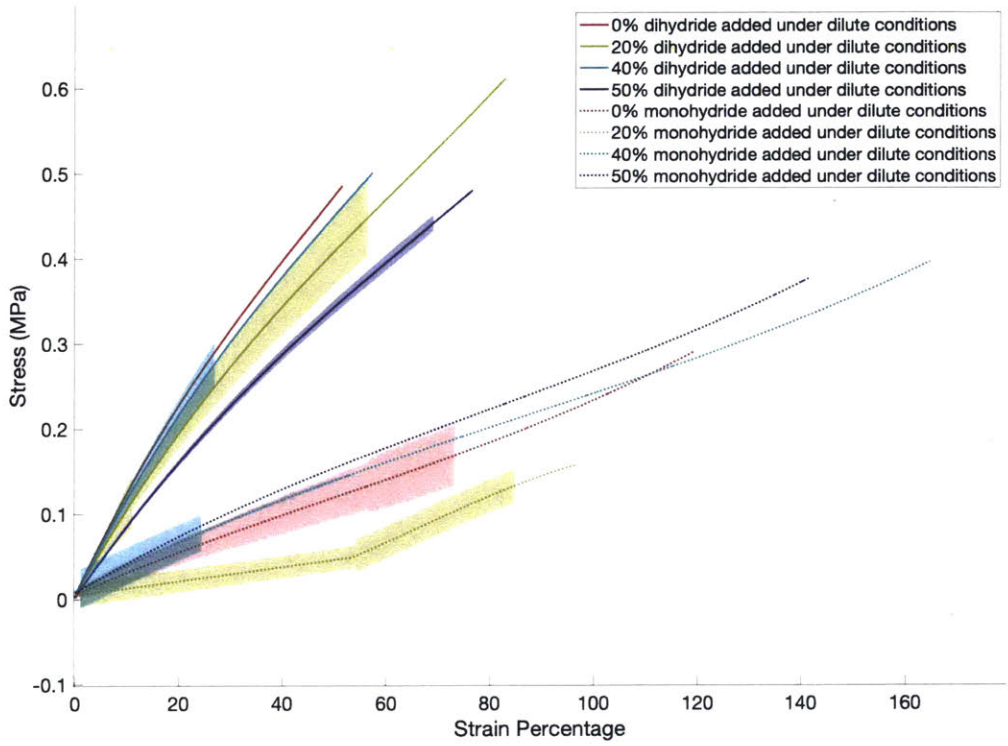


**Figure 5-6:** Tensile data is shown for two series of samples, PDMS28kPDMSm5k and PDMS28kPDMS5k, with differing percentages of PDMS added under dilute conditions. The samples containing monohydride terminated PDMS show a lower modulus and ultimate tensile strength then the samples made containing only dihydride terminated PDMS, suggesting that even the PDMS added under dilute conditions is elastically active.

composition of each elastomer within the two series remains constant. The 28k vinyl PDMS backbone remains constant. In all cases, the final stoichiometric functional group ratio between vinyl and hydride functional groups was kept at 0.5. Finally, a 1:1 molar ratio of 17,000 g/mol PDMS dihydride and 5,000 g/mol PDMS dihydride was used for each elastomer in both series. This resulted in a final stoichiometric functional group ratio of 0.25:0.25:1 5k PDMS hydride: 17k PDMS hydride: 28k vinyl PDMS. For each series, elastomers were made with 0%, 20%, 40%, and 50% of the total molar quantity of PDMS added under dilute conditions to form brushes. In series PDMS28kPDMS5k17k, 5,000 g/mol PDMS dihydride was added under dilute conditions, creating brushes with 'small loops'. In series PDMS28kPDMS17k5k, 17,000 g/mol PDMS dihydride was added under dilute conditions, creating brushes with 'large loops'.

The elastomers made from brushes with 'large loops' showed more extensibility than those made from brushes with 'small loops'. This trend was consistent through multiple batches of elastomer and with different loopy brushes used. The modulus was not strongly dependent upon either the percentage of PDMS added under dilute conditions nor whether brushes with 'large' or 'small' loops had been used for elastomer formation. Rheological data is available in the supporting information. The formation of an elastomer with enhanced extensibility without loss of modulus shows the reliance of mechanical properties upon network topology.

No evidence of hysteresis was seen in example elastomers from series PDMS28kPDMS5k17k and PDMS28kPDMS17k5k after seven cycles of extension and retraction. Similar results have been reported previously with topological networks.[12]

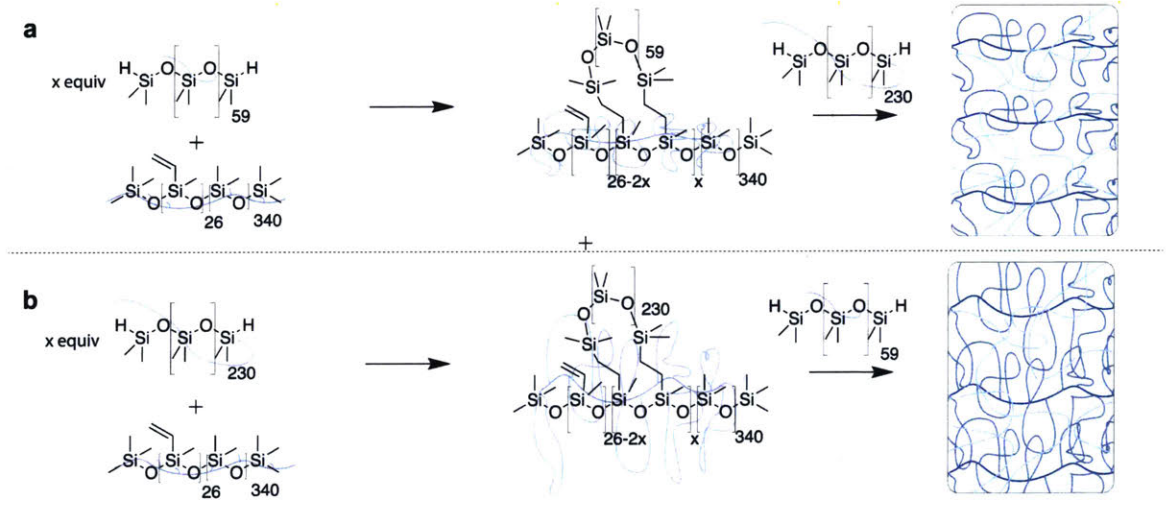


**Figure 5-7:** a) Chemical structures for the formation of loopy brushes are shown here. Brushes were formed with the 28k vinyl methyl siloxane dimethyl siloxane and a 5k hydride terminated PDMS (z=59). 17k PDMS dihydride (z=230) was used for elastomer formation, forming series PDMS28kPDMS5k17k. b) Chemical structures for the formation of loopy brushes are shown here. Brushes were formed with the 28k vinyl methyl siloxane dimethyl siloxane and a 17k hydride terminated PDMS (z=230). 5k PDMS dihydride (z=59) was used for elastomer formation, forming series PDMS28kPDMS17k5k.

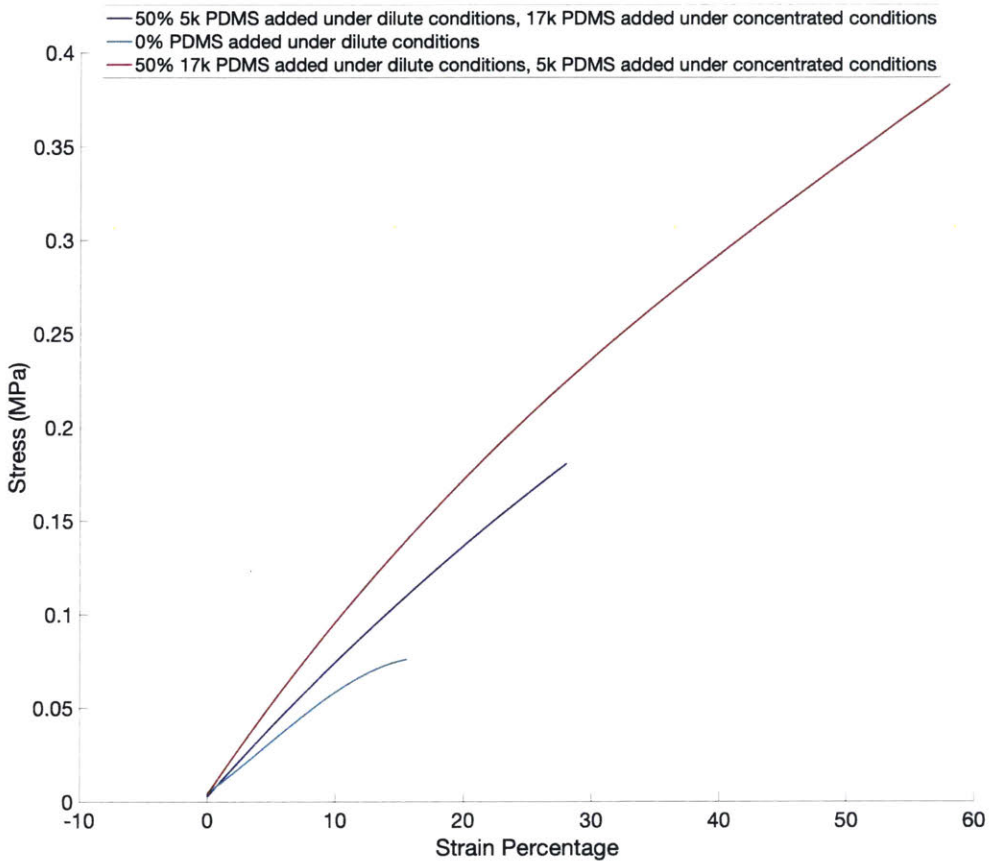


**Figure 5-8:** Tensile data is shown for select elastomers from series PDMS28kPDMS5k17k and PDMS28kPDMS17k5k. Data for other elastomers within the series are presented in the experimental section, following similar trends. The samples with 17k dihydride terminated PDMS added under dilute conditions show more extensibility than those with 5k dihydride terminated PDMS added under dilute conditions, suggesting a dependence upon the order of addition. (7.0-8.0% vinylmethylsiloxane) dimethylsiloxane copolymer, trimethylsiloxy terminated, 800-1200 cSt, 28,000g/mol, catalog number VDT-731, Hydride terminated polydimethyl siloxane, 100 cSt, 4,000-5,000g/mol, catalog number DMS-H21, and hydride terminated polydimethyl siloxane, 500 cSt, 17,200g/mol, catalog number DMS-H25 were used.

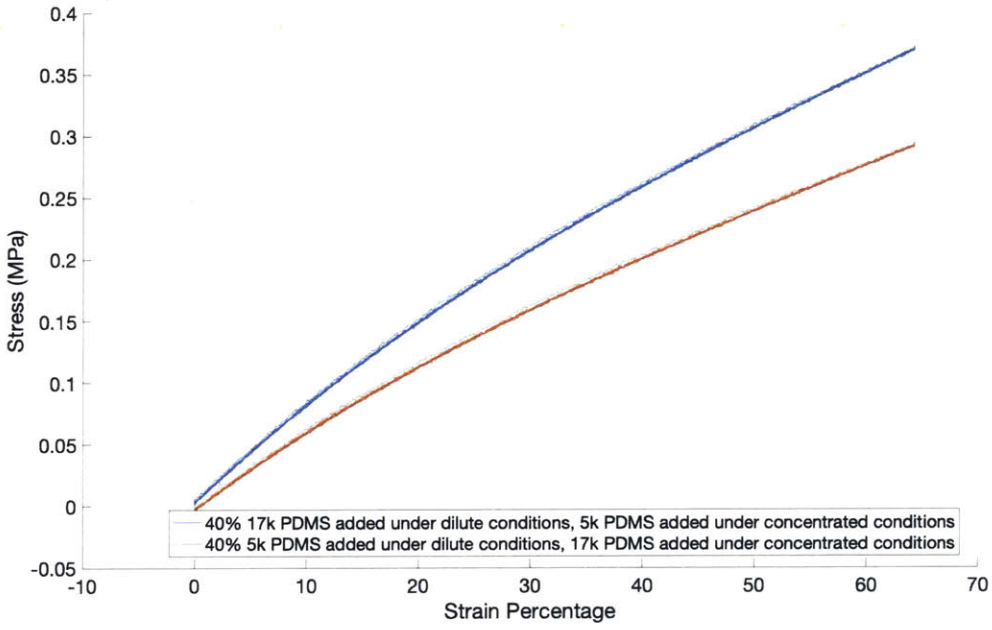


**Figure 5-9:** Tensile data is shown for select elastomers from series PDMS28kPDMS5k17k and PDMS28kPDMS17k5k. Neither elastomer showed evidence of hysteresis after seven cycles of extension and retraction. (7.0-8.0% vinylmethylsiloxane) dimethylsiloxane copolymer, trimethylsiloxy terminated, 800-1200 cSt, 28,000g/mol, catalog number VDT-731, Hydride terminated polydimethyl siloxane, 100 cSt, 4,000-5,000g/mol, catalog number DMS-H21, and hydride terminated polydimethyl siloxane, 500 cSt, 17,200g/mol, catalog number DMS-H25 were used.

## 5.3 Conclusions

Several series of elastomers were made with differing quantities of polydimethylsiloxane added under dilute conditions. These elastomers were evaluated primarily through tensile testing and rheology. The polydimethylsiloxane added under dilute conditions was shown to be elastically active through comparison with a control. Elastomers made with a single type of hydride terminated PDMS did not show mechanical properties dependent upon the concentration during addition of PDMS. Elastomers made with a combination of 17k hydride terminated polydimethylsiloxane and 5k hydride terminated polydimethylsiloxane showed tensile properties that varied with the polymer added under dilute conditions. When 17k hydride terminated PDMS was added under dilute conditions, more extensible, and thus tougher materials were observed.

## 5.4 Experimental

### 5.4.1 Materials

All reagents were purchased from commercial sources and used without further purification unless stated otherwise.

Hydride terminated polydimethyl siloxane, 500 cSt, 17,200g/mol, catalog number DMS-H25 was purchased from Gelest.

Hydride terminated polydimethyl siloxane, 100 cSt, 4,000-5,000g/mol, catalog number DMS-H21 was purchased from Gelest.

Mono-hydride terminated polydimethyl siloxane, 80-120 cSt, 4,500-5,000g/mol, catalog number MCR-H21 was purchased from Gelest.

Hydride terminated polydimethyl siloxane, 7-10 cSt, 1,000-1,100g/mol, catalog number DMS-H11 was purchased from Gelest.

Polybutadiene, 5,000g/mol, with 13.8% vinyl functionality was purchased from Sigma Aldrich, catalog number 383694.

Polybutadiene, 1,400g/mol, with 71% vinyl functionality was purchased from Polymer Source, catalog number P19292-Bd.

(7.0-8.0% vinylmethylsiloxane) dimethylsiloxane copolymer, trimethylsiloxy terminated, 800-1200 cSt, 28,000g/mol, catalog number VDT-731 was purchased from Gelest.

### 5.4.2 Instrumentation

Gel permeation chromatography (GPC) was performed on a Tosoh system equipped with a TSK guard column SuperHZ (4.6 mm ID x 3.5 cm, 4 $\mu$m) TSKgel SuperHZ 4000 (6.0 mm ID x 15 cm, 3 $\mu$m, TSKgel SuperHZ 3000 (6.0 mm ID x 15 cm, 3 $\mu$m),

and aTSKgel SuperHZ 2500 (6.0 mm ID x 15 cm, 3 $\mu$m) in series using 0.6 mL/min chloroform at 25 celsius as eluent.

Gel permeation chromatography with absolute molecular weight determination was performed on an Agilent 1260 instrument with two Shodex KD-806 M columns in series, a chloroform mobile phase run at 25 celsius, a Wyatt Optilab T-rEX detector, and a Wyatt Heleos II detector.

Column chromatography was carried out on silica gel 60F (EMD Millipore, 0.040-0.063 mm).

$^{1}$H nuclear magnetic resonance ($^{1}$H-NMR) and $^{13}$C nuclear magnetic resonance ($^{13}$C-NMR) spectra were recorded on Bruker AVANCE-400 NMR spectrometers in the Department of Chemistry Instrumentation Facility at MIT. Chemical shifts are reported in ppm relative to the signals corresponding to residual non-deuterated solvents: $CDCl_3$: $\delta$H = 7.26 ppm, DMSO-d6: $\delta$H = 2.50 ppm. Spectra were analyzed on MestReNova NMR software.

Dynamic Light Scattering (DLS) was taken with a Wyatt Möbius with a 660 nm laser. The average hydrodynamic diameter and aggregate molecular weight of a set of 20 readings was calculated with a regularization algorithm from Dynamics 7.3.1.15.

Preparative gel permeation chromatography (prep-GPC) was performed on a JAI Preparative Recycling HPLC (LaboACE-LC-5060) system equipped with 2.5HR and 2HR columns in series (20 mm ID x 600 mm length) with ethanol stabilized chloroform as the eluent running at 10 mL/minute.

Tensile testing was conducted on a Instron 8848 Microtester.

Rheological experiments were conducted on a TA instruments Discovery HR-2 with an 8mm Smart Swap Peltier Plate geometry (part number 511080.906).

Thickness measurements were taken with a Mitutoyo digimatic micrometer, manufacturer model number 293-832-30, with a friction thimble with a measuring range of 0- 25mm, resolution of 0.001mm, and accuracy of +/- 0.0025mm.

Length and width measurements were taken with General Tools 6" digital fractional calipers (manufacturer model number 147) with a measuring range of 0 -150 mm, resolution of 0.01mm, and accuracy of +/- 0.02mm.

### 5.4.3 Methods

#### Rheological experiments

8 mm round samples were prepared from an elastomer sheet with a typical thickness of 1.0 mm with a die cutter.

Amplitude strain sweep experiments were conducted on a TA instruments Discovery HR-2 with a parallel-plate geometry using an 8mm Smart Swap Peltier Plate geometry (part number 511080.906). Amplitude strain sweep experiments were performed at a 1.0 N load, 25 celsius, 10 rad/s frequency, from 0.0001 to 10 strain percent. This data was used to determine the linear viscoelastic regime and yield stress.

Frequency sweep experiments were conducted on a TA instruments Discovery HR-2 with a parallel-plate geometry using an 8mm Smart Swap Peltier Plate geometry (part number 511080.906). Frequency sweep experiments were performed from 0.1 rad/s to 100 rad/s at 1% strain, which had previously been confirmed to be in the linear viscoelastic regime. The shear modulus G' was determined based on G' values at 1 rad/s.

#### Tensile Testing

The standard sample preparations were as follows:

Elastomer strips were cut from an elastomer sheet with a typical thickness of 0.5 mm with a new razor blade using one fluid motion per side. These strips were cut with a typical length of 20mm and width of 3mm, then individually glued onto paper frames with 0.2 mL of Loctite clear silicone waterproof sealant applied in a layer between the paper and elastomer, and surrounding the upper 4 mm of the elastomer. The glue was allowed to cure for at least 24 hours. Care was taken to ensure that the glue reached the edges of the cardstock. Paper frames for tensile testing were laser

cut by myPonoko (http://www.ponoko.com) from 0.012" thick ivory cardstock into rectangles measuring 0.39" x 1.91" with a 0.25" x 0.48" rectangular cutout.

Tensile experiments were run at 1.0 mm/minute with a 10N load cell on an Instron 8848 Microtester unless otherwise specified.

### Gel Fraction

The gel fraction of all elastomers was determined by massing out a 10.0 mg cubic sample of elastomer. This elastomer was placed into a vial with 1.0 mL of dichloromethane, which was then tightly capped. After 1 hour and 2 hours from the initial swelling, the dichloromethane was removed and replaced with an equal volume dichloromethane. After allowing the sample to extract overnight, the final fraction of dichloromethane was removed. The swollen elastomer was then transferred into a National Appliance Company vacuum oven, model 5831 (room temperature, 66 mbar) connected to a Boc Edwards dual vacuum pump system cart (part number NGU515000) overnight, and then massed again. The gel fraction was taken as the final mass divided by the initial mass. At minimum, three samples were taken for each elastomer. The gel fraction of each elastomer sample shown here exceeded 0.95.

### Gel Swelling

Gel swelling data was obtained by massing out a 10.0 mg cubic sample of elastomer. This elastomer was placed into a vial with 1.0 mL of toluene, which was then tightly capped. The sample was allowed to equilibrate for a minimum of 24 hours. After equilibration, the toluene was carefully removed, and the sample surface lightly dried with a lab wipe. The swollen elastomer was massed, then transferred into a National Appliance Company vacuum oven, model 5831 (room temperature, 66 mbar) connected to a Boc Edwards dual vacuum pump system cart (part number NGU515000) for 48 hours, and then massed again. At minimum, three samples were taken for each elastomer. The density of toluene ($\rho_{toluene}$) was taken as 0.86g/mL, the molar volume of toluene ($V_{toluene}$) as 106.69mL/mol, the polymer solvent interaction parameter, $\chi$, as 0.48 and the density of PDMS as 0.98g/mL.[23] The equilibrium

swelling ratio $Q$ was taken as seen in Equation 5.1, where $V_{toluene}$ is the volume of toluene in the sample and $V_{PDMS}$ is the volume of PDMS in the sample. The Flory-Rehner equation was then used to determine the average molecular weight between crosslinks and the cross linking density.

$$Q = \frac{V_{toluene} + V_{PDMS}}{V_{PDMS}} \tag{5.1}$$

The equilibrium volume fraction of polymer, $v_{PDMS}$, was taken as the inverse of $Q$.

$$Q = \frac{1}{v_{PDMS}} \tag{5.2}$$

The Flory-Rehner equation was then used to determine the average molecular weight between crosslinks, $M_c$.[24,25]

$$-1[ln(1 - v_{PDMS}) + v_{PDMS} + \chi v_{PDMS}^2)] = \frac{\rho_{toluene}}{M_c} V_{toluene} v_{PDMS}^{1/3} \tag{5.3}$$

**Polybutadiene/PDMS mixed systems**

Example Elastomer Formation Conditions for Polybutadiene/Poly(dimethyl siloxane) mixed systems:

Here, an example with 60% of the total PDMS added under dilute conditions is shown.

Polybutadiene with 71% vinyl functionalization (1,4000 g/mol, 0.09g, 0.06mmol) was combined with hydride terminated polydimethylsiloxane (1,000 g/mol, 0.186 g, 0.18mmol) in 12.5 mL of dichloromethane under atmosphere. A solution of Karstedt's catalyst in xylenes (0.002 mmol, 65.8 $\mu$m) was added, and the scintillation vial sealed. After 18 hours, the reaction was left open to atmosphere overnight, then the solvent removed under vacuum at 20°C. Hydride terminated polydimethylsiloxane (1,000 g/mol, 0.124 g, 0.12mmol) was added to the concentrated mixture, and vortexed for 20 seconds. A second aliquot of Karstedt's catalyst in xylenes (0.002 mmol, 65.8 $\mu$m) was added. The combined materials were vortexed with a VWR analog vortex mixer

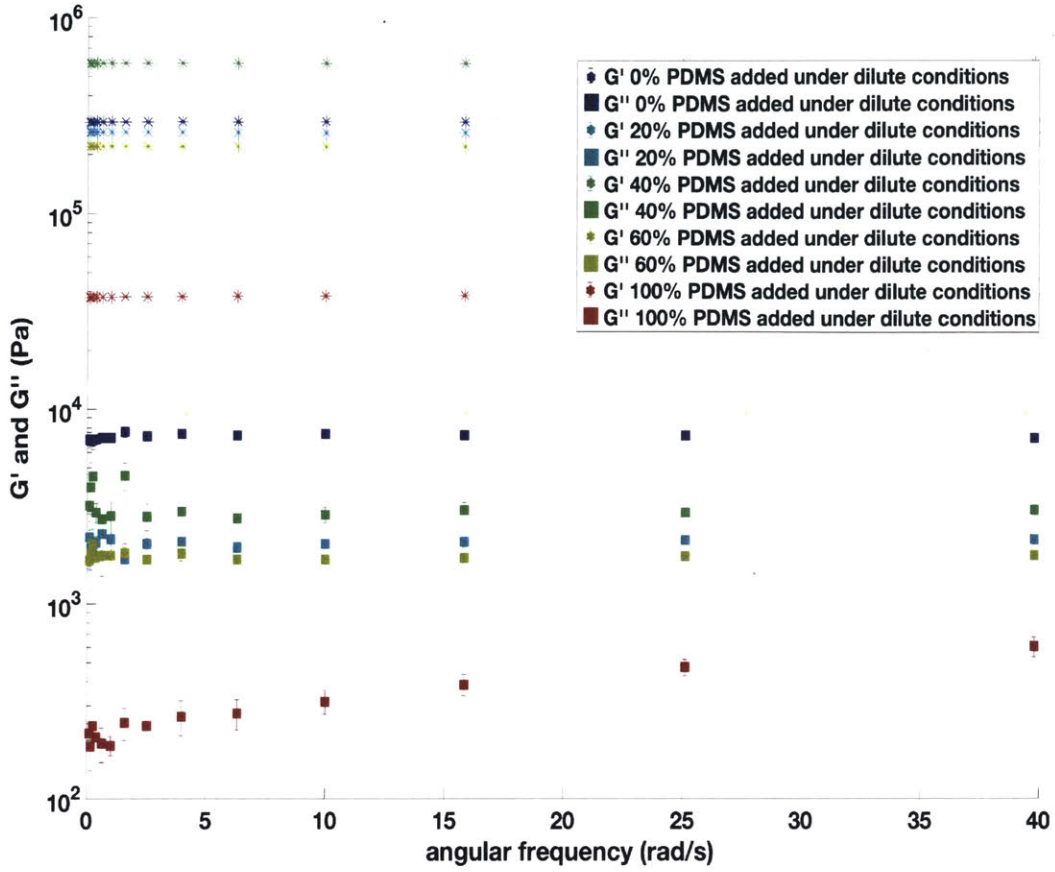


**Figure 5-10:** Polybutadiene (1,400g/mol, 71% vinyl functionality) was mixed with polydimethyl silioxane (1,000g/mol) under dilute conditions, then concentrated and combined with more 1k PDMS under neat conditions to form an elastomer. Although in all cases, the total amount of PDMS added remained consistent, the amount of PDMS added under dilute conditions varied in each elastomer in the series PBD1.4kPDMS1k. The storage modulus did not appear to depend strongly on the amount of PDMS added under dilute conditions.

at speed 10 for 10 seconds before being poured into a teflon mold. The elastomer was then transferred into a National Appliance Company vacuum oven, model 5831 (room temperature, 66 mbar) connected to a Boc Edwards dual vacuum pump system cart (part number NGU515000). After 24 hours, the samples were demolded with a metal spatula.

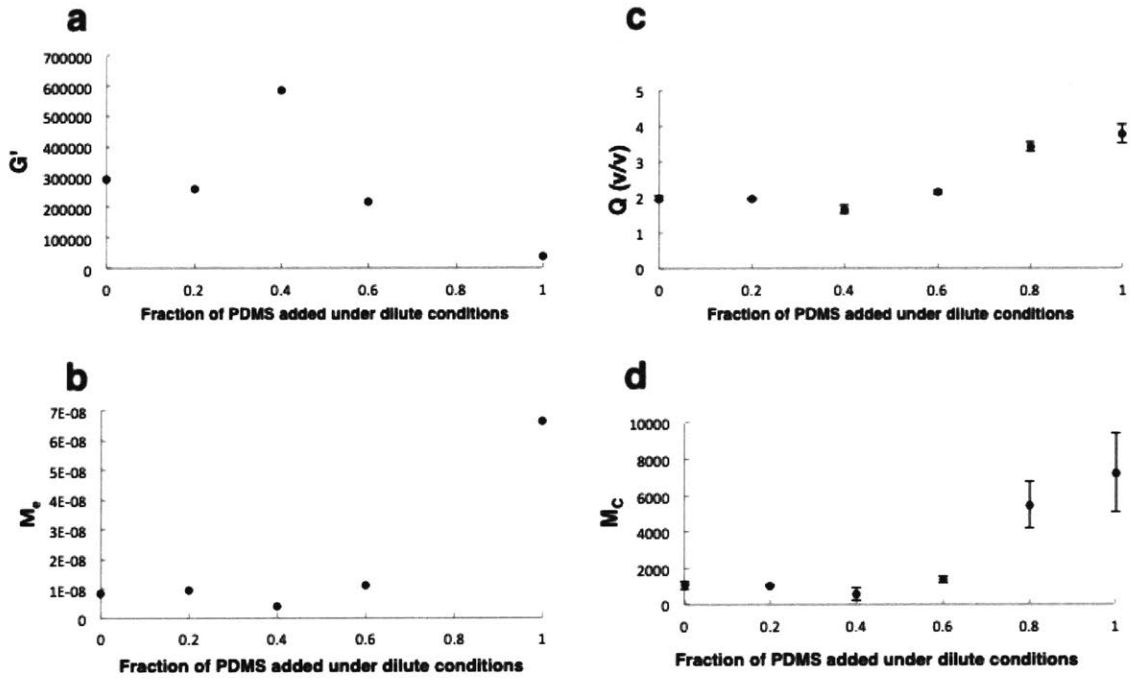


**Figure 5-11:** Polybutadiene (1,400g/mol, 71% vinyl functionality) was mixed with polydimethyl silioxane (1,000g/mol) under dilute conditions, then concentrated and combined with more 1k PDMS under neat conditions to form an elastomer. Although in all cases, the total amount of PDMS added remained consistent, the amount of PDMS added under dilute conditions varied in each elastomer in the series PBD1.4kPDMS1k. a) The storage modulus, G', was determined from rheological data in the above series, and used with the theory of rubber elasticity to determine b) $M_e$, a molecular weight between crosslinks where crosslinks encompass all polymer constrains such as chemical, physical, and topological crosslinks and entanglements.[26] The molecular weight between crosslinks tracked well with the molecular weight of PDMS used until 100% of PDMS was added under dilute conditions at which point Me increased, likely due to the increased fraction of elastically inactive loops. c) Samples were swollen in toluene to an equilibrium. Q, the ratio between the unswollen and swollen network was used to determine d) M, the molecular weight between crosslinks where here $M_c$ does not include entanglements.[24] $M_c$ increased with the fraction of PDMS added under dilute conditions, as expected due to the formation of loops.

### PDMS Loop Rich Brushes

Example Brush Formation Conditions for Poly(dimethyl siloxane) /Poly(dimethyl siloxane) systems:

Here, an example with 40% of the total PDMS added under dilute conditions is shown.

(7.0-8.0% vinylmethylsiloxane) dimethylsiloxane copolymer, trimethylsiloxy terminated (28,000 g/mol, 1.0g, 0.036mmol) was combined with polydimethylsiloxane dihydride (5,000 g/mol, 1.04 g, 0.31mmol) in 12.5 mL of dichloromethane under atmosphere. A solution of Karstedt's catalyst in xylenes (0.00052 mmol, 11.5 $\mu$m) was added, and the bottle sealed. After 48 hours, the reaction was left open to atmosphere overnight, Polydimethylsiloxane dihydride (5,000 g/mol, 1.56 g, 0.21mmol) was added to the mixture. The solvent was removed under vacuum at 20°C. A second aliquot of Karstedt's catalyst in xylenes (0.00052 mmol, 11.5 $\mu$m) was added. The combined materials were vortexed with a VWR analog vortex mixer at speed 10 for 10 seconds before being transferred to a 95x62x20 mm rectangular metal container with a hinged lid lined with a 0.005" polyethylene terephthalate release film purchased from McMaster-Carr (8567K95). Samples allowed to cure in a National Appliance Company vacuum oven, model 5831 (room temperature, 66 mbar) connected to a Boc Edwards dual vacuum pump system cart (part number NGU515000) for 24 hours, then post-cured at 120°C for 30 minutes.

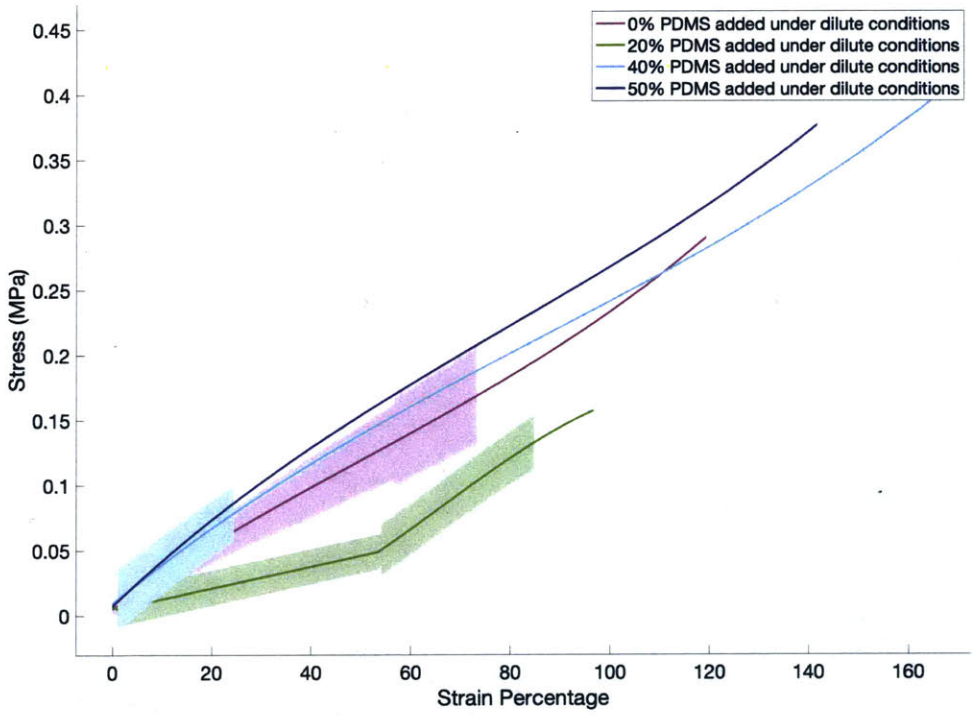


**Figure 5-12:** Instron data is shown for a series of samples, PDMS28kPDMS5k, with differing percentages of PDMS added under dilute conditions. No clear relationship is seen between the percentage of PDMS added under dilute conditions and the tensile properties of the elastomer. (7.0-8.0% vinylmethylsiloxane) dimethylsiloxane copolymer, trimethylsiloxy terminated, 800-1200 cSt, 28,000g/mol, catalog number VDT-731, and hydride terminated polydimethyl siloxane, 100 cSt, 4,000-5,000g/mol, catalog number DMS-H21 were used.

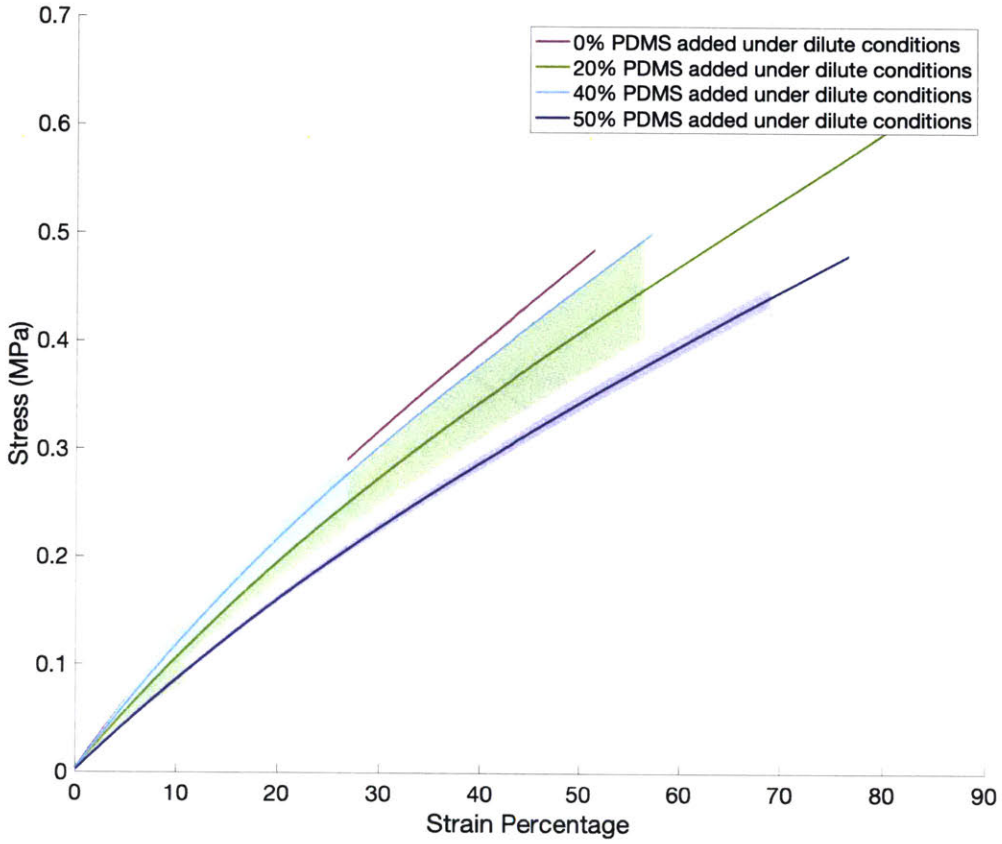


**Figure 5-13:** Instron data is shown for a series of samples, PDMS28kPDMSm5k, with differing percentages of PDMS added under dilute conditions. No clear relationship is seen between the percentage of PDMS added under dilute conditions and the tensile properties of the elastomer. (7.0-8.0% vinylmethylsiloxane) dimethylsiloxane copolymer, trimethylsiloxy terminated, 800-1200 cSt, 28,000g/mol, catalog number VDT-731, and mono-hydride terminated polydimethyl siloxane, 80-120 cSt, 4,500-5,000g/mol, catalog number MCR-H21 were used.

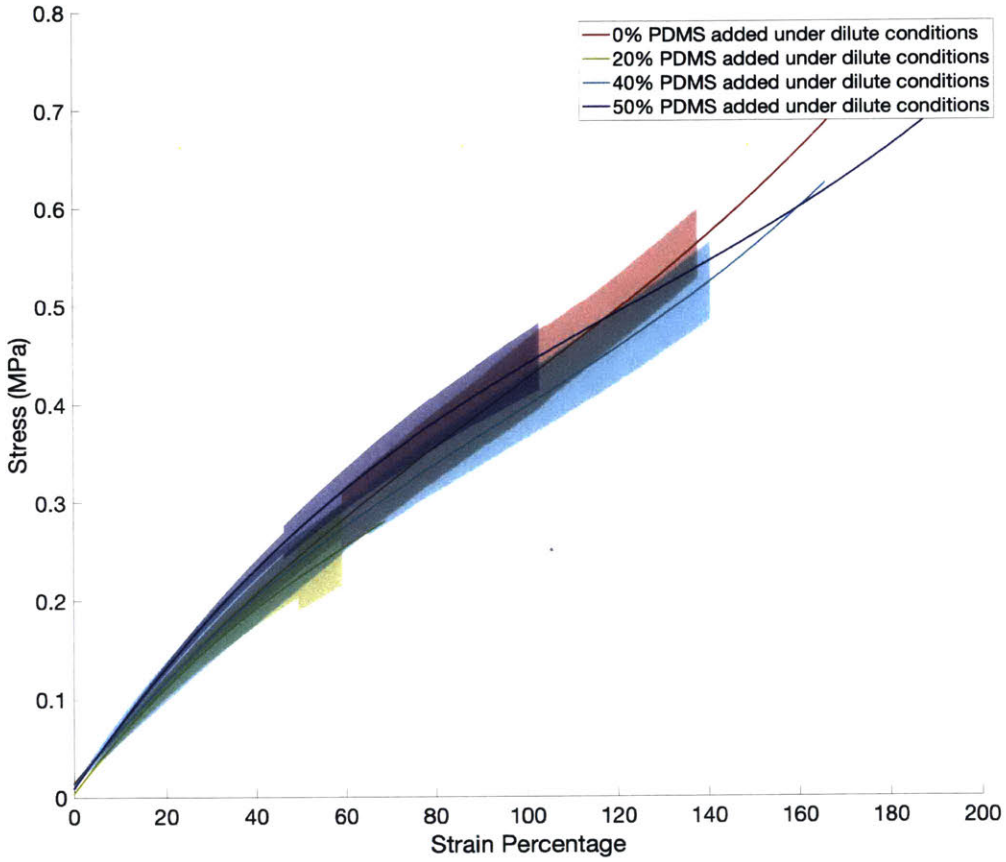


**Figure 5-14:** Instron data is shown for a series of samples, PDMS28kPDMS17k, with differing percentages of PDMS added under dilute conditions. No clear relationship is seen between the percentage of PDMS added under dilute conditions and the tensile properties of the elastomer. (7.0-8.0% vinylmethylsiloxane) dimethylsiloxane copolymer, trimethylsiloxy terminated, 800-1200 cSt, 28,000g/mol, catalog number VDT-731, and hydride terminated polydimethyl siloxane, 7-10 cSt, 1,000-1,100g/mol, catalog number DMS-H11 were used.

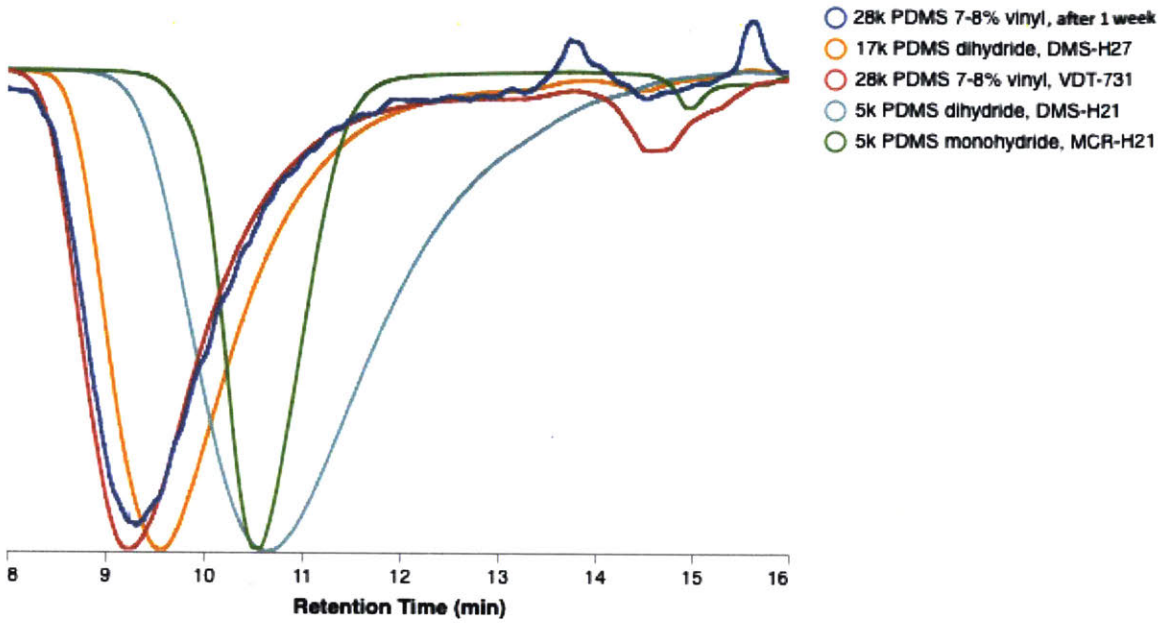


**Figure 5-15:** Gel permeation chromatograms are shown for all precursor polymers in addition to a sample of the 28k vinyl PDMS dissolved in chloroform with Karstedt's catalyst for a week with 0% PDMS dihydride added under dilute conditions. No change in the retention time of the 28k vinyl functionalized PDMS is seen after a week dissolved in chloroform with Karstedt's catalyst, as expected. This polymer is shown in blue, compared to the polymer directly after receipt from Gelest, and several other materials sourced directly from Gelest for reference.

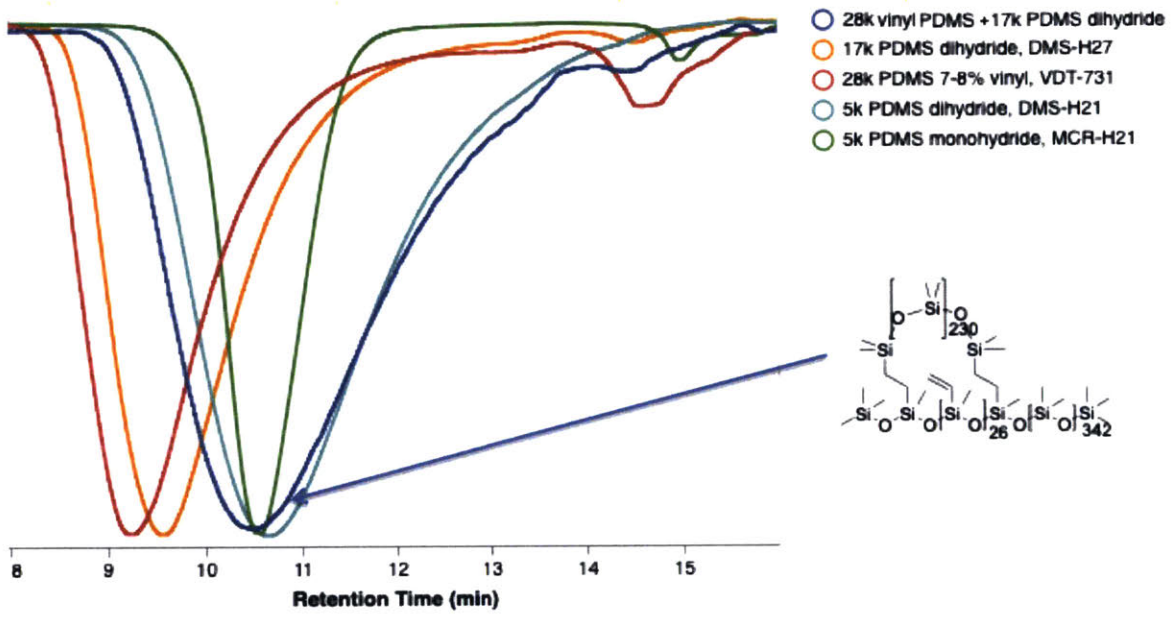


**Figure 5-16:** Gel permeation chromatograms are shown for all precursor polymers in addition to a sample of the 28k vinyl PDMS dissolved in chloroform under dilute conditions with 0.5 functional group equivalents of 17k PDMS dihydride and Karstedt's catalyst for a week. The retention time of this loopy brush increases relative to the 28k vinyl functionalized PDMS shown in red and the 17k dihydride terminated PDMS shown in orange, suggesting a reduced hydrodynamic volume.

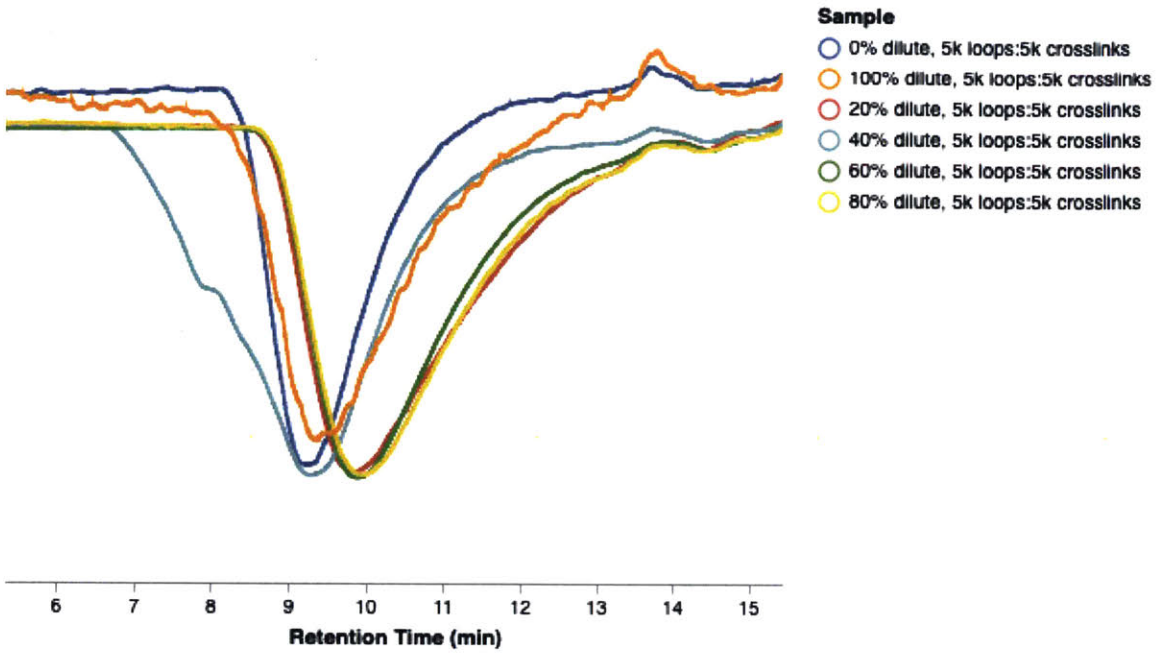


**Figure 5-17:** Gel permeation chromatograms are shown for a series of polymeric brushes. All brushes have the 28k vinyl functionalized PDMS with a variable amount of 5k hydride terminated PDMS added under dilute conditions. These materials were later crosslinked to form networks.

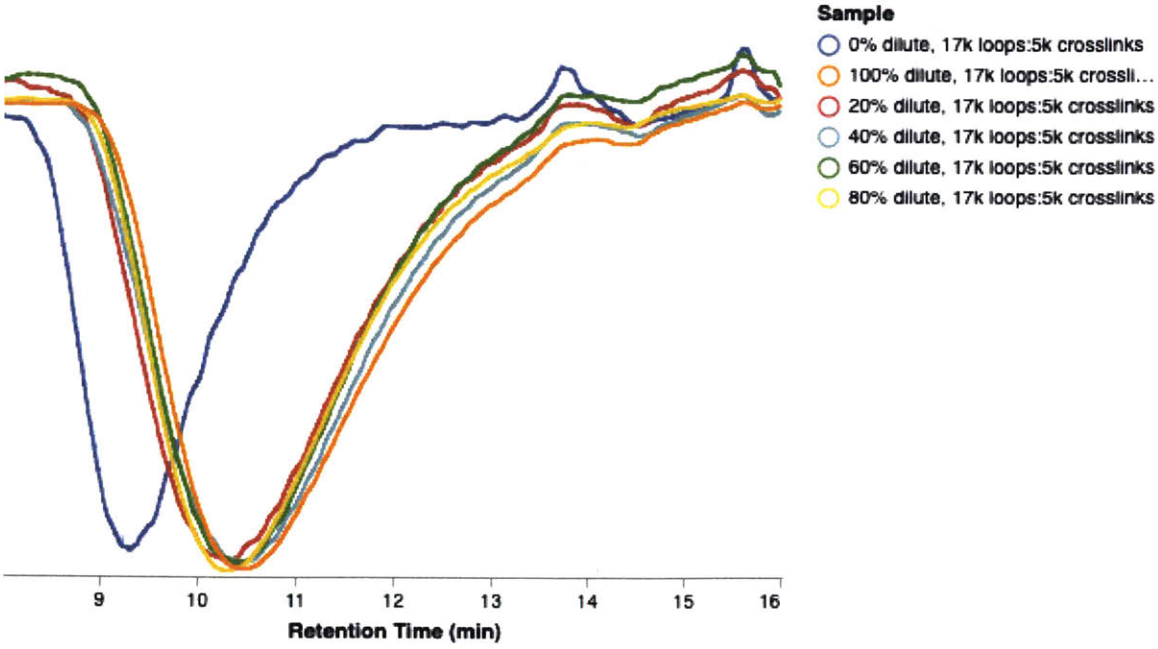


**Figure 5-18:** Gel permeation chromatograms are shown for a series of polymeric brushes. All brushes have the 28k vinyl functionalized PDMS with a variable amount of 17k hydride terminated PDMS added under dilute conditions. These materials were later crosslinked to form networks.

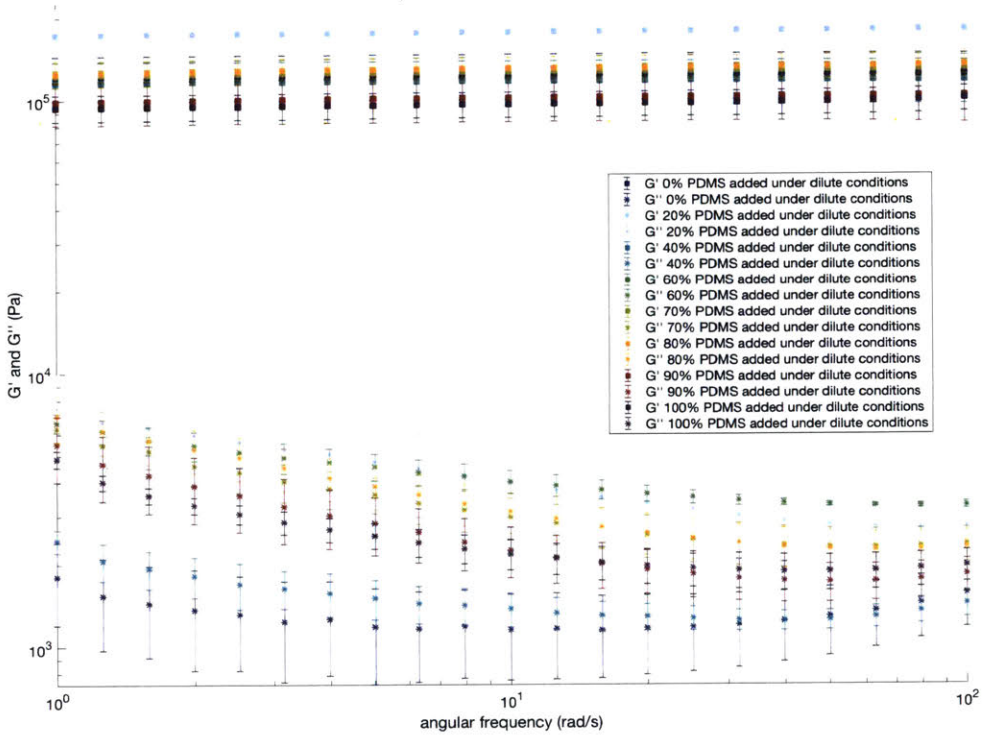


**Figure 5-19:** Rheology data is shown for a series of samples, with differing percentages of PDMS added under dilute conditions. Here, 5k PDMS was added under dilute conditions, and 17k PDMS added under concentrated conditions to form series PDMS28kPDMS5k17k. No significant different is seen in the moduli for these samples (7.0-8.0% vinylmethylsiloxane) dimethylsiloxane copolymer, trimethylsiloxy terminated, 800-1200 cSt, 28,000g/mol, catalog number VDT-731, Hydride terminated polydimethyl siloxane, 100 cSt, 4,000-5,000g/mol, catalog number DMS-H21, and hydride terminated polydimethyl siloxane, 500 cSt, 17,200g/mol, catalog number DMS-H25 were used.

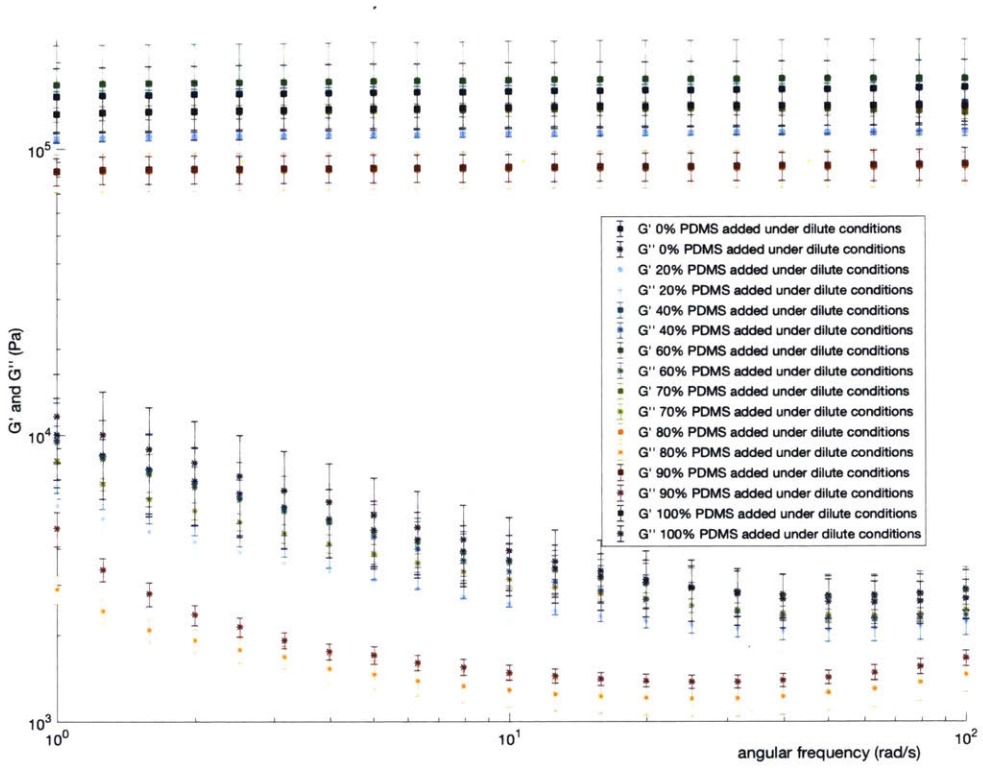


**Figure 5-20:** Rheology data is shown for a series of samples, with differing percentages of PDMS added under dilute conditions. Here, 17k PDMS was added under dilute conditions, and 5k PDMS added under concentrated conditions to form series PDMS28kPDMS17k5k.No significant different is seen in the moduli for these samples (7.0-8.0% vinylmethylsiloxane) dimethylsiloxane copolymer, trimethylsiloxy terminated, 800-1200 cSt, 28,000g/mol, catalog number VDT-731, Hydride terminated polydimethyl siloxane, 100 cSt, 4,000-5,000g/mol, catalog number DMS-H21, and hydride terminated polydimethyl siloxane, 500 cSt, 17,200g/mol, catalog number DMS-H25 were used.

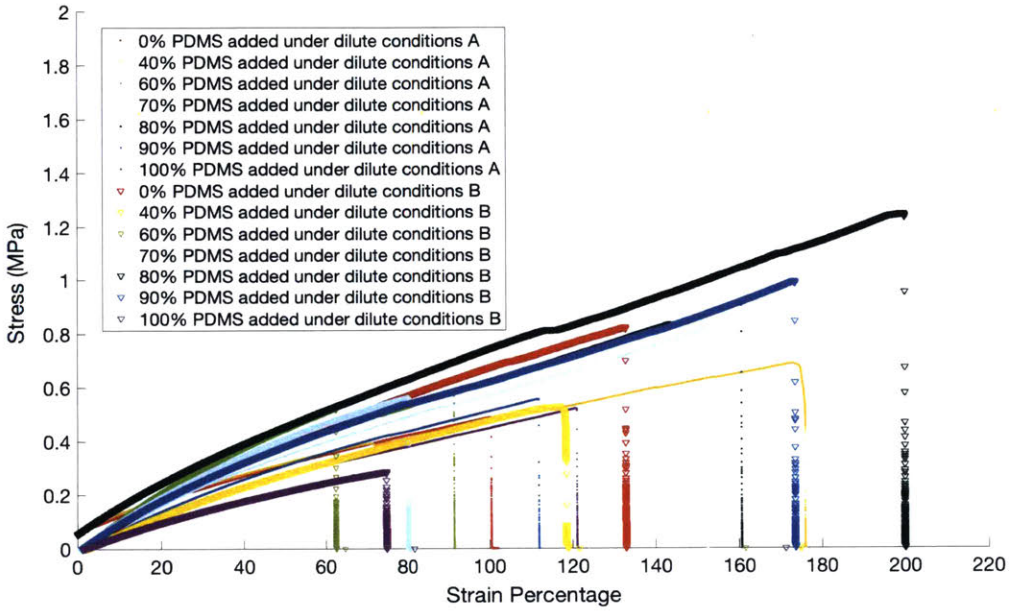


**Figure 5-21:** Instron data is shown for a series of samples, with differing percentages of PDMS added under dilute conditions. Condition A used 5k PDMS added under dilute conditions and 17k PDMS added under concentrated conditions to form series PDMS28kPDMS5k17k. Condition B used 17k PDMS added under dilute conditions and 5k PDMS added under concentrated conditionsto form series PDMS28kPDMS17k5k. Series PDMS28kPDMS17k5k show more extensibility than series PDMS28kPDMS5k17k, suggesting a dependence upon the order of addition. (7.0-8.0% vinylmethylsiloxane) dimethylsiloxane copolymer, trimethylsiloxy terminated, 800-1200 cSt, 28,000g/mol, catalog number VDT-731, Hydride terminated polydimethyl siloxane, 100 cSt, 4,000-5,000g/mol, catalog number DMS-H21, and hydride terminated polydimethyl siloxane, 500 cSt, 17,200g/mol, catalog number DMS-H25 were used.

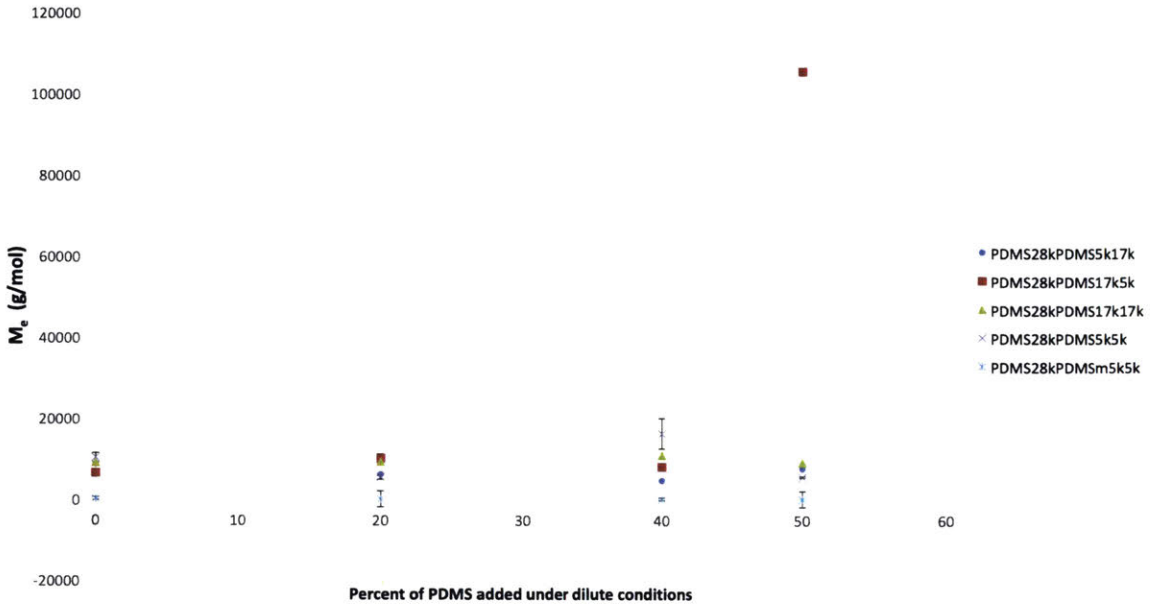


**Figure 5-22:** Gel swelling results are shown here for all entirely PDMS elastomer series discussed above. The calculated $M_e$ corresponded with tensile results, and did not vary with the percentage of PDMS added under dilute conditions.

## 5.5 References


(1) Kramer, E. J. Craze Fibril Formation and Breakdown. *Polym. Eng. Sci.* **1984**, *24*, 761–769.

(2) Song, L.; Ren, L.; Zhang, M.; Sun, S.; Gao, G.; Gui, Y.; Zhang, L.; Zhang, H. Effect of Entanglement Density on Mechanical Properties and Deformation Behavior of Rubber-Modified PVC/$\alpha$-MSAN Blends. *Ind. Eng. Chem. Res.* **2013**, *52*, 12567–12573.

(3) Huang, J. J.; Keskkula, H.; Paul, D. R. Rubber toughening of an amorphous polyamide by functionalized SEBS copolymers: morphology and Izod impact behavior. *Polymer* **2004**, *45*, 4203–4215.

(4) Delaviz, Y.; Gibson, H. Macrocyclic Polymers. 2.f Synthesis of Poly(amide crown ether)s Based on Bis(5-carboxy-l,3-phenylene)-32-crown-10. Network Formation through Threading. *Macromolecues* **1992**, *25*, 4859–4862.

(5) Gibson, H.; Nagvekar, D.; Powell, J.; Gong, C.; Bryant, W. Polyrotaxanes by In Situ Self Threading During Polymerization of Functional Macrocycles. Part 2*: Poly(ester crown ether)s. *Tetrahedron* **1997**, *53*, 15197–15207.

(6) Gong, C.; Gibson, H. Supramolecular chemistry with macromolecules: Macromolecular knitting, reversible formation of branched polyrotaxanes by self-assembly. *Macromol. Chem. Phys.* **1998**, *199*, 1801–1806.

(7) Ito, K. Novel entropic elasticity of polymeric materials: why is slide-ring gel so soft? *Polym. J.* **2011**, *44*, 38–41.

(8) Ito, K. Topological Gels. **2013**, 1–8.

(9) Karino, T.; Shibayama, M.; Ito, K. Slide-ring gel: Topological gel with freely movable cross-links. *Physica B* **2006**, *385-386*, 692–696.

(10) Kubo, M.; Hibino, T.; Uno, T.; Itoh, T. Synthesis and Copolymerization of Cyclic Macromonomer Based on Cyclic Polystyrene: Gel Formation via Chain Threading. *Macromolecules* **2002**, *35*, 5816–5820.

(11) Kubo, M.; Kato, N.; Uno, T.; Itoh, T. Preparation of Mechanically Cross-Linked Polystyrenes. *Macromolecules* **2004**, *37*, 2762–2765.

(12) Noda, Y.; Hayashi, Y.; Ito, K. From topological gels to slide-ring materials. *J. Appl. Polym. Sci.* **2014**, *131*, 40509.

(13) Oike, H.; Mouri, T.; Tezuka, Y. A Cyclic Macromonomer Designed for a Novel Polymer Network Architecture Having Both Covalent and Physical Linkages. *Macromolecules* **2001**, *34*, 6229–6234.

(14) Okumura, Y.; Ito, K. The polyrotaxane gel: A topological gel by figure-of-eight cross-links. *Adv. Mater.* **2001**, *13*, 485.

(15) Watanabe, J.; Ooya, T.; Nitta, K. H.; Park, K. D.; Kim, Y. H.; Yui, N. Fibroblast adhesion and proliferation on poly(ethylene glycol) hydrogels crosslinked by hydrolyzable polyrotaxane. *Biomaterials* **2002**, *23*, 4041–8.

(16) Zada, A.; Avny, Y.; Zilkha, A. Monomers for non-bond crosslinking of vinyl polymers. *Eur. Polym. J.* **1999**, *35*, 1159–1164.

(17) Zada, A.; Avny, Y.; Zilkha, A. Monomers for non-bond crosslinking of vinyl polymers II. Cyclic octaethylene glycol 5-methacrylamido- isophthalate. *Eur. Polym. J.* **2000**, *36*, 351–357.

(18) Johnson, J. A.; Lu, Y. Y.; Burts, A. O.; Lim, Y. H.; Finn, M. G.; Koberstein, J. T.; Turro, N. J.; Tirrell, D. A.; Grubbs, R. H. Core-clickable PEG-branch-azide bivalent-bottle-brush polymers by ROMP: grafting-through and clicking-to. *J. Am. Chem. Soc.* **2011**, *133*, 559–66.

(19) Johnson, J. A.; Lu, Y. Y.; Burts, A. O.; Xia, Y.; Durrell, A. C.; Tirrell, D. A.; Grubbs, R. H. Drug-Loaded, Bivalent-Bottle-Brush Polymers by Graft-through ROMP. *Macromolecules* **2010**, *43*, 10326–10335.

(20) Paturej, J.; Sheiko, S. S.; Panyukov, S.; Rubinstein, M. Molecular structure of bottlebrush polymers in melts. *Sci. Adv.* **2016**, *2*, e1601478.

(21) Cai, L. H.; Kodger, T. E.; Guerra, R. E.; Pegoraro, A. F.; Rubinstein, M.; Weitz, D. A. Soft Poly(dimethylsiloxane) Elastomers from Architecture-Driven Entanglement Free Design. *Adv. Mater.* **2015**, *27*, 5132–40.

(22) Baum, K.; Baum, J. C.; Ho, T. Side-loop polymers based on the hydrosilylation of polybutadiene. *J. Am. Chem. Soc.* **1998**, *120*, 2993–2996.

(23) Orwoll, R. A.; Arnold, P. A. In *Physical Properties of Polymers Handbook*, Mark, J. E., Ed.; Springer New York: New York, NY, 2007, pp 233–257.

(24) Flory, P. J.; Rehner, J. Statistical Mechanics of Cross-Linked Polymer Networks II. Swelling. *The Journal of Chemical Physics* **1943**, *11*, 521–526.

(25) Zhang, F.; Zhou, T.; Liu, Y.; Leng, J. Microwave synthesis and actuation of shape memory polycaprolactone foams with high speed. *Sci. Rep.* **2015**, *5*, 11152.

(26) Flory, P. J. Network structure and the elastic properties of vulcanized rubber. *Chem. Rev.* **1944**, *35*, 51–75.